Technische Universität München
TUM School of Natural Sciences

Expanding the Reaction Scope of Photochemically Active Chiral Phosphoric Acids

Max Lukas Stierle

Vollständiger Abdruck der von der TUM School of Natural Sciences der Technischen Universität München zur Erlangung eines Doktors der Naturwissenschaften genehmigten Dissertation.

Vorsitz: **Prof. Dr. Christopher Stein**

Prüfende der Dissertation:

1. **Prof. Dr. Thorsten Bach**
2. **apl. Prof. Dr. Wolfgang Eisenreich**

Die Dissertation wurde am 04.10.2025 bei der Technischen Universität München eingereicht und durch die TUM School of Natural Sciences am 10.11.2025 angenommen.

The presented PhD work was carried out at the Lehrstuhl für Organische Chemie I at the Technische Universität München between December 2021 and November 2025. The thesis was supervised by Prof. Dr. Thorsten Bach.

Part of this work has been published:

M. Stierle, C. Jaschke, D. Grenda, M. Peschel, T. Pickl, N. Gessner, P. Nuernberger, B. Fingerhut, C. Ochsenfeld, R. de Vivie-Riedle, T. Bach, *Angew. Chem. Int. Ed.* **2025**, *64*, e202501433.

M. Stierle, D. Bitterlich, J. Westermayr, T. Bach, *Chem. Sci.* **2025**, DOI: 10.1039/d5sc05356k.

In this thesis, the relative configuration of racemates is represented by straight lines (bold or hashed). The absolute configuration of enantiomerically pure or enriched compounds is represented by wedge-shaped lines (bold or hashed).

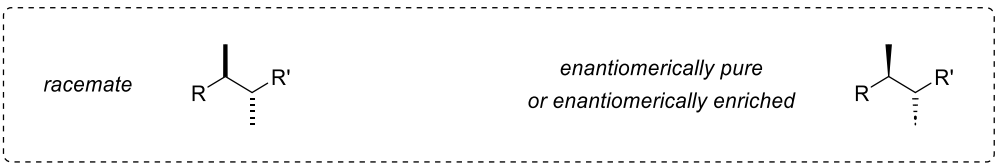

Danksagung

Ich danke an erster Stelle Prof. Dr. Thorsten Bach für das mir entgegengebrachte Vertrauen und die Möglichkeit, meine Doktorarbeit in seiner Gruppe anfertigen zu dürfen. Es war zwar nicht immer ein „Country Club“, aber ich habe die intensive Zeit des Lernens und des wissenschaftlichen Austauschs sehr genossen und bin persönlich daran gewachsen.

Hinsichtlich der Arbeitsbedingungen im Labor haben Dr. Stefan Breitenlechner und Dr. Simone Stegbauer durch ihre großartige Unterstützung dafür gesorgt, dass die Probleme weniger wurden und nicht mehr. Hierfür möchte ich mich herzlich bei ihnen bedanken.

Der Weltrekord für die Ermöglichung der schnellsten Erstattung von Reisekosten an der TUM geht wahrscheinlich an Kerstin Voigt, die bei allen administrativen und bürokratischen Problemen eine unersetzliche Hilfe war.

Ein großer Dank gilt auch Olaf Ackermann und Jürgen Kudermann, die mir durch ihre Expertise bei der Bestimmung so mancher *ees* zur Seite standen.

Durch den fleißigen Einsatz meiner Praktikanten Marcel Lippert, Manuel Reichel, Jan-Jonas Schneider und Robert Traber wurden mir einige Synthesen abgenommen, ihr wart super Leute!

Die im Rahmen dieser Arbeit entstandenen Publikationen haben sehr von der Kooperation mit einer Reihe an großartigen Gruppen profitiert und ich möchte an dieser Stelle allen Beteiligten danken.

Für das Korrekturlesen dieser Arbeit möchte ich Dr. Biki Ghosh und Johannes Hofer danken.

Ich habe in meiner Zeit am Lehrstuhl den Eindruck gewonnen, eine Arbeitsgruppe ist ein sich ständig verändernder, lebendiger Mikrokosmos. Die Erfahrungen und Erinnerungen, die man gewinnt, werden durch die Menschen, die dort arbeiten, geprägt. Ich möchte mich bei allen ehemaligen und gegenwärtigen Gruppenmitgliedern (und denen der Storch Gruppe) für die gemeinsame Zeit bedanken. Es ist so viel Witziges, Erstaunliches, Spannendes und Trauriges passiert, es war eine außergewöhnliche Zeit.

In dieser Flut an Erinnerungen gibt es als große Konstanten meine Mitbewohner aus Box 6, Christoph Buchelt und Johannes Hofer (Miau), denen ich für die gemeinsame Zeit danken möchte. Außerdem danke ich meinem quasi Nachbarn Maximilian Iglhaut für exzellente Fahrservices, magische Monsoon Besuche und viele anregende Diskussionen.

Den Freunden, die mich seit dem Bachelor begleiten, und denen, die ich kurz vor der Pandemie kennengelernt habe, Aoife, Corbi, Hubert, Simon und Werner, möchte ich herzlich danken. Außerdem danke ich meinen Freunden aus Hamburg, insbesondere Carl und Moritz, für eine Vielzahl unersetzlicher Erinnerungen.

Ohne den Rückhalt meiner Brüder und meines Vaters hätte ich es nie so weit geschafft, vielen Dank! Abschließend möchte ich meiner Freundin Mira danken, die mich durch alle Hochs und Tiefs der Promotion begleitet, und deren Unterstützung nie an Kraft verloren hat.

Abstract

Driven by the demand of the pharmaceutical industry for enantiomerically pure, complex organic molecules, asymmetric photocatalysis emerged in recent years as a powerful synthetic platform. Among several important classes of photocatalysts, photochemically active chiral phosphoric acids (PACPAs) gained notable attention. However, in the case of reactions mediated by triplet energy transfer, they have mainly been used for [2+2] photocycloadditions. In this work, the reaction scope of PACPAs was expanded to the enantioselective *cis-trans* isomerization of cyclohept-2-enone-3-carboxylic acid (up to 38% *ee*) as well as the photochemical deracemization of 2,3-allenoic acids (up to 71% *ee*).

Zusammenfassung

Angesichts der Nachfrage der pharmazeutischen Industrie nach enantiomerenreinen, komplexen organischen Molekülen hat sich die asymmetrische Photokatalyse in den letzten Jahren zu einer leistungsstarken synthetischen Plattform entwickelt. Unter den verschiedenen wichtigen Klassen von Photokatalysatoren haben photochemisch aktive chirale Phosphorsäuren (PACPAs) besondere Aufmerksamkeit erlangt, obwohl sie im Fall von Reaktionen, die durch Triplett-Energietransfer vermittelt werden, hauptsächlich für [2+2]-Photocycloadditionen verwendet wurden.

In dieser Arbeit wurde die Reaktionsbreite von PACPAs um die enantioselektive *cis-trans*-Isomerisierung von Cyclohept-2-enon-3-carbonsäure (bis zu 38% *ee*) sowie die photochemische Deracemisierung von 2,3-Allencarbonsäuren (bis zu 71% *ee*) erweitert.

Table of Contents

1. Synthetic Chemistry as a Driver of Innovation in Drug Discovery

Historically, pharmaceuticals beneficial to mankind were obtained from natural sources as plants or fungi and have been in use since thousands of years.[1] Only the development of the chemical industries around the world at the beginning of the 20th century gave rise to new and more efficient drugs: Synthetically modified, naturally occurring molecules, or by the means of organic synthesis *de novo* constructed scaffolds.[2] Since the early days of drug discovery, advancements have been sparked by innovations in synthetic methods.

In modern times (21st century) this is reflected by five Nobel Prizes awarded for the development of groundbreaking synthetic tools: The development of asymmetric hydrogenation and oxidation reactions in 2001,[3] the development of metathesis reactions awarded in 2005,[4] palladium-catalyzed cross couplings in 2010,[5] asymmetric organocatalysis in 2021[6] and most recently for the development of click chemistry and bioorthogonal chemistry in 2022.[7]

All these reactions significantly contributed to tackle the problems associated with the synthesis of new, more efficient drugs, although certain challenges remain. Among these, small-molecule drugs often contain heterocycles or unprotected, polar functional groups which are not well tolerated by many synthetic methods.[8] For example, highly desirable late-stage functionalization of already complex molecules (giving fast access to broad libraries of compounds) are only feasible, if specific functional groups are tolerated. Furthermore, medicinal chemists discovered that *Escaping from Flatland* (changing sp^2-rich, achiral aromatic molecules towards more three-dimensional compounds containing sp^3-hybridized carbon atoms) increases the chance of a drug candidate to become a marketed drug.[9] Due to the lack of commercially available building blocks, and the absence of suitable methods for the connection of these, *Escaping Flatland* still is considered a notable challenge.

Conclusively, in many cases molecules are investigated that chemists can synthesize, and not necessarily the most promising candidates they could think of.[10] Nevertheless, there are trends in the current research community to address these issues (Figure 1).

Maybe the most fundamental development of the last years is the rise of AI (*Artificial Intelligence*), which connects all areas of industry and has the potential to change the day-to-day life of everyone. More specifically, AI could help accelerating discovery timelines for example through faster target validation or fewer cycles of molecule design and optimization.[11]

One of the more synthetic trends observed over the past years is the use of bioisosteres ***a)*** to replace aromatic moieties through more sp^3-rich mimics.[12] This trend is fueled by a flow of publications addressing the synthesis of useful bioisostere building blocks.[13]

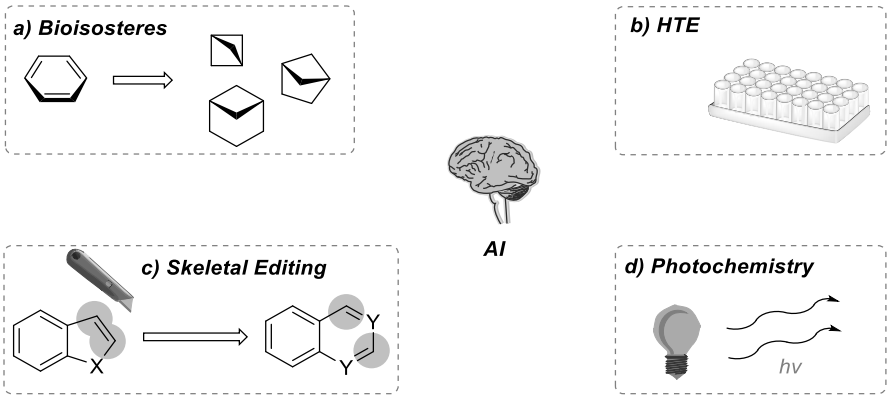

Figure 1. *Selection of synthetic and technological developments fueling innovation in drug discovery.*

HTE (*High Throughput Experimentation*) ***b)*** enables chemists to screen reaction conditions for a fraction of the cost and time of earlier days, allowing for rapid optimization of challenging synthetic steps. Furthermore, HTE facilitates the accelerated screening of compound libraries against therapeutical targets.[14]

Synthetically, another significant trend is skeletal editing ***c)***, which enables the modification of the core skeleton of a target molecule at a late-stage, allowing for rapid access to the chemical space around a lead compound. The *de novo* synthesis of each molecule is thereby circumvented.[15]

Photochemistry ***d)***, the main topic of the following chapters and this thesis, addresses synthetic challenges in many unique ways. Certainly, of special value for the pharmaceutical industry are novel methods for the formation of C-C bonds and other photoredox-mediated processes[16] but also processes involving singlet excited states[17] or triplet energy transfer[18] are of special interest. Considering the substantial need for homochiral compounds in the pharmaceutical industry, methods leading to enantiopure molecules are highly desirable.[19]

2. Principles of Enantioselective Photocatalysis

In contrast to conventional (thermal) enantioselective catalytic processes, enantioselective photocatalysis provides unique challenges, which often cannot be addressed by the same means as in the realm of thermal catalysis. Most importantly, upon irradiation with light, molecules gain a notable energy sufficient for fast subsequent reactions, which proceed without further catalysis. Therefore, it is crucial for a successful enantioselective photochemical reaction to ensure a chiral environment for the substrate molecule already in the excitation step.[20]

Some of the most important concepts to achieve this goal are summarized in Scheme 1.[21]

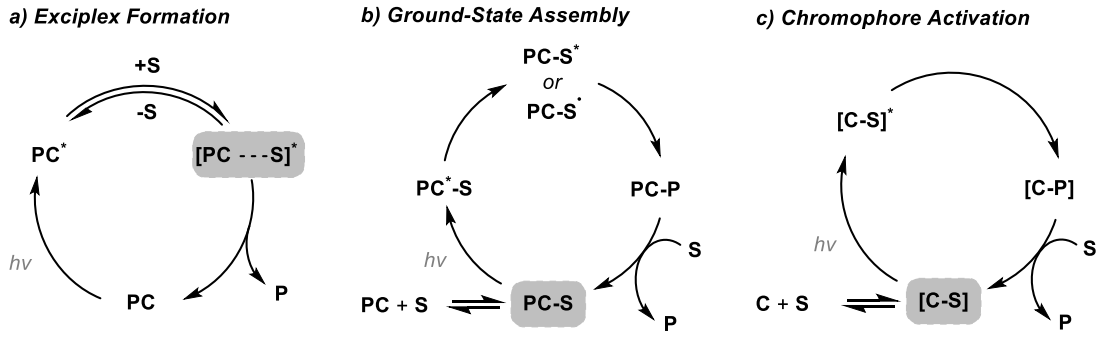

Scheme 1. *Selected mechanisms of enantiocontrol in photocatalytic processes. PC = photocatalyst, S = substrate, P = product, C = catalyst (without photocatalytic activity).*

While historically exciplex formation ***a)*** played an important role in the development of some of the first enantioselective photochemical reactions,[22] ground-state assembly ***b)***[23–25] and chromophore activation ***c)***[26] are the more widely applied principles today.

In general, it is important to prevent racemic background reactions by selective excitation of the substrate molecule (either by energy transfer or direct irradiation) within the vicinity of the chiral catalyst. If the rate of excitation is higher for substrate molecules bound to the catalyst than for non-complexed substrate and if the rate of the photoreaction is higher than the rate of dissociation of the catalyst-substrate complex, this is the case.

Along these lines, another key aspect to prevent racemic background reactions is the appropriate choice of the irradiation wavelength.

Figure 2 aims to give an overview of typical structures of chiral photocatalysts. They can be divided into three classes: ***a)*** organocatalysts (**1**-**4**),[22,27–29] ***b)*** semimetal and metal-based catalysts (**5**-**8**)[30,31,32] and ***c)*** macromolecular catalysts as **9**[33] which also include photocatalytically active enzymes.[34]

Apart from the distinction based on structural features, it is reasonable to further divide the most often applied catalytic systems into three groups:

i) Chiral, non-photochemically active catalysts

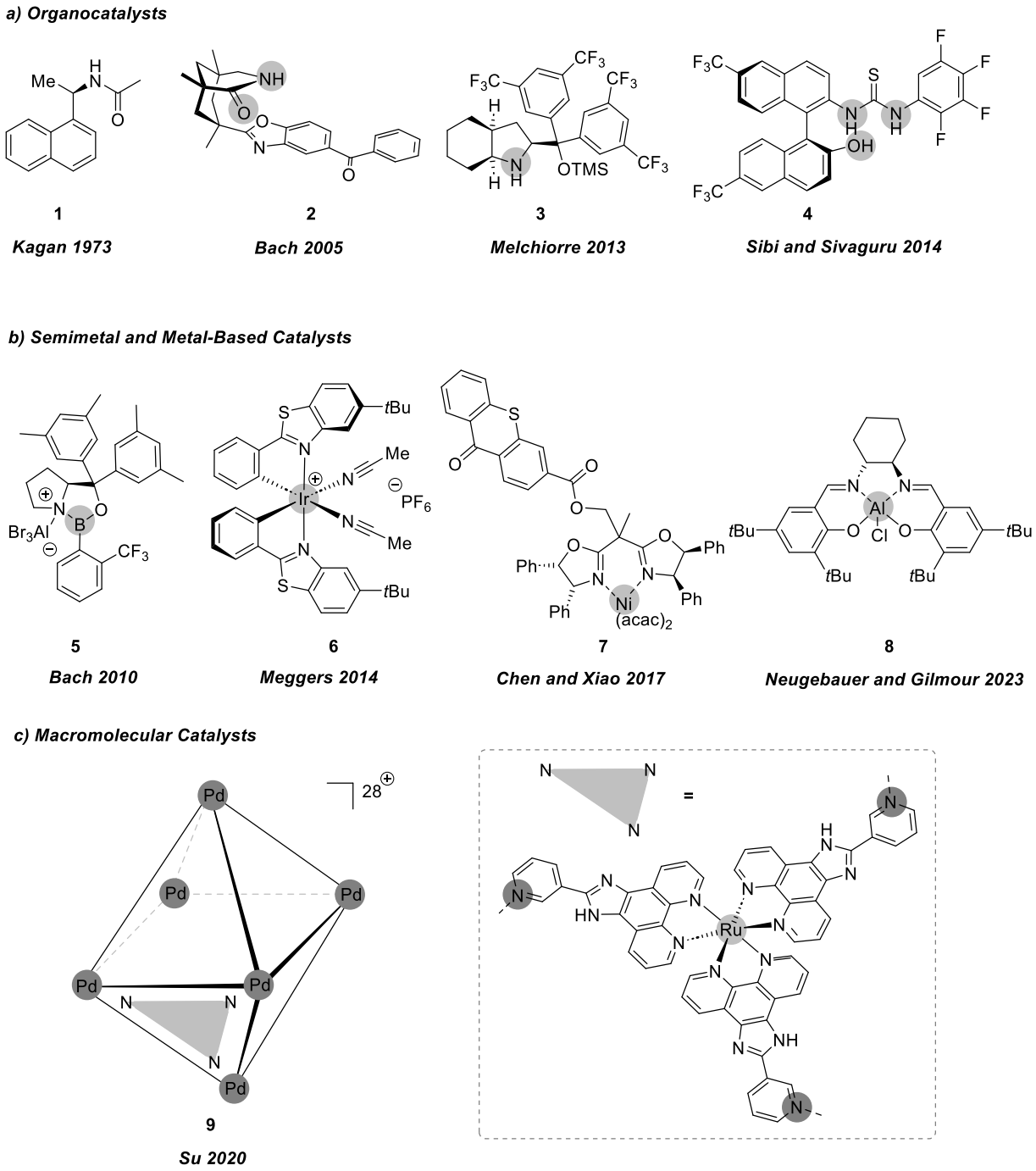

Figure 2. *Selected examples of catalysts used for enantioselective photochemical reactions across a plethora of structural diversity. Me = methyl, TMS = trimethylsilyl, tBu, = tert-Butyl, Ph = phenyl, acac = acetylacetonate.*

ii) Chiral, non-photochemically active catalysts in combination with achiral photocatalysts (*Dual Catalysis* approach)

iii) Chiral catalysts with photocatalytic activity

In the design of new catalysts for enantioselective photochemical transformations, thermal enantioselective chemistry has certainly been an inspiration in terms of available structural motives. In the design of a promising catalyst or catalyst class different factors play an

important role, but accessibility and price, as well as generality in terms of the reactions the catalyst can perform, are among the main points of interest. Given the overwhelming success of phosphoric acids and their derivatives in conventional enantioselective catalysis, it is little surprise that this class of catalysts also conquered the field of enantioselective photochemistry readily.

3. Chiral Phosphoric Acids as Privileged Catalysts for Enantioselective Photochemical Transformations

While the use of chiral *Lewis* acids for enantioselective photochemical transformations was established rather early,[30] the use of chiral *Brønsted* acids stayed underexplored for longer. An early example is the asymmetric aza-pinacol cyclization reported by *Knowles* in 2013 [see chapter 3.2 ***b)***],[35] operating in the regime of photoredox catalysis. Other pioneering contributions were made by *Sibi* and *Sivaguru* in 2014,[29] when they used a chiral thiourea derivative for an enantioselective intramolecular [2+2] photocycloaddition. Notably, in this work the concept of chromophore activation was extended from *Lewis* acids towards *Brønsted* acids, as the employed chiral catalyst led to a bathochromic shift in the absorption of the substrate coumarins, allowing for a selective direct irradiation of the substrate-catalyst complex. Other important seminal work by our group centered around the activation of dithianes by strong *Brønsted* acids, although in this case the reactions stayed racemic.[36]

The *Yoon* group showed in 2020, that a dual catalysis approach involving a *Brønsted* acid in combination with a ruthenium-based triplet sensitizer can lead to an improved racemic reaction. The findings in this study led to the conclusion that under certain circumstances *Brønsted* acid catalysts can lead to an improved rate of triplet energy transfer from a triplet sensitizer to an activated substrate.[37]

Based on these fundamental publications, the rapidly evolving field of enantioselective photochemistry relying on chiral *Brønsted* acids formed. The following chapters aim to describe the most recent developments with a focus on the most relevant chiral *Brønsted* acids, namely chiral phosphoric acids and their derivatives.

3.1. Non-Photochemically Active Chiral Phosphoric Acids

The *Yoon* group extensively exploited the principle of chromophore activation for a variety of highly enantioselective [2+2] photocycloadditions involving substrates like **10** (Scheme 2). The basic idea involves protonation of the 3-alkyl imidazole unit of **10** by the chiral *Brønsted* acid **CPA 1**, leading to a bathochromic shift of its absorption. By choosing a suitable irradiation wavelength of $\lambda > 400$ nm, the catalyst-substrate complexes are selectively excited leading to high enantioselectivities.

In the first publication of this series [Scheme 2 ***a)***], 2-acyl imidazole **10** was reacted with an excess of styrene (**11**) in the presence of 20 mol% of the acid catalyst leading to the corresponding enantioenriched cyclobutane **12** (33 examples, 37-85% yield, 62-99% *ee*).[38]

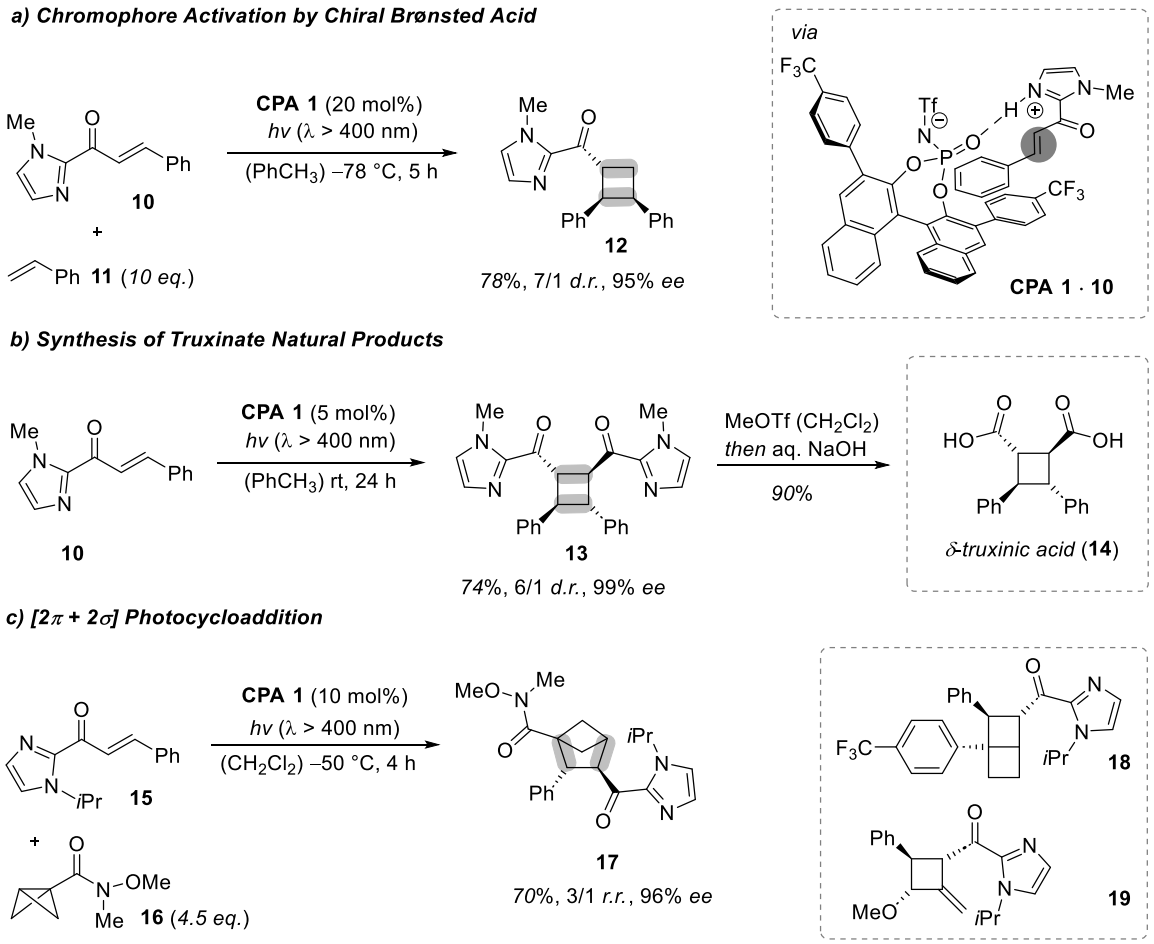

Scheme 2. *Synthetic work by the Yoon group:* ***a)*** *Chromophore activation by chiral Brønsted acid,* ***b)*** *Synthesis of Truxinate natural products,* ***c)****[2π + 2σ] photocycloaddition.*

In a follow-up project [Scheme 2 ***b)***], the same group elegantly demonstrated how the same 3-alkyl imidazole was homo-dimerized under similar reaction conditions to the cyclobutane **13** (12 examples, 48-81% yield, 93-99% *ee*).[39] In a single step, they accessed the natural product *δ*-truxinic acid (**14**) from **13**, underlining the synthetic utility of the developed methodology. Impressively, not only the problem of enantioselectivity was addressed, but the reactions proceeded also in a chemo-, regio- and diastereoselective fashion.

In the most recent synthetic study in this specific area [Scheme 2 ***c)***], *Plachinski et al.* used the closely related 3-alkyl imidazole **15** in a highly enantioselective [2π + 2σ] photocycloaddition with BCB (bicyclobutane) **16**.[40] The thereby generated bicyclo[2.1.1]hexanes such as **17** were afforded with exceptional enantioselectivities (22 examples, 35-87% yield, 88-98% *ee*). They are considered important building blocks for the development of new pharmaceutical and agrochemical active ingredients. Changing the substrate from 3-methyl imidazole **10** to 3-isopropyl imidazole **15** reportedly led do a decreased rate of unproductive homodimerization.

Utilizing slightly different reaction conditions, it was shown that also the medicinally relevant products **18** and **19** were accessible with excellent enantioselectivities (93% *ee* and 98% *ee*).
In a conceptually similar approach, the *Akiyama* group demonstrated the enantioselective [2+2] photocycloaddition between the alkenyl 2-pyrrole ketones **20** and **21** to the respective cyclobutane **22** upon irradiation with violet light (20 examples, 11-84% yield, 72-98% *ee*).[41] Key for the successful reaction was the use of 10 mol% of the BINOL (1,1'-bi-2-naphthol) based phosphoric acid **CPA 2**, which can interact in a two-point hydrogen bond with the substrates (Scheme 3).

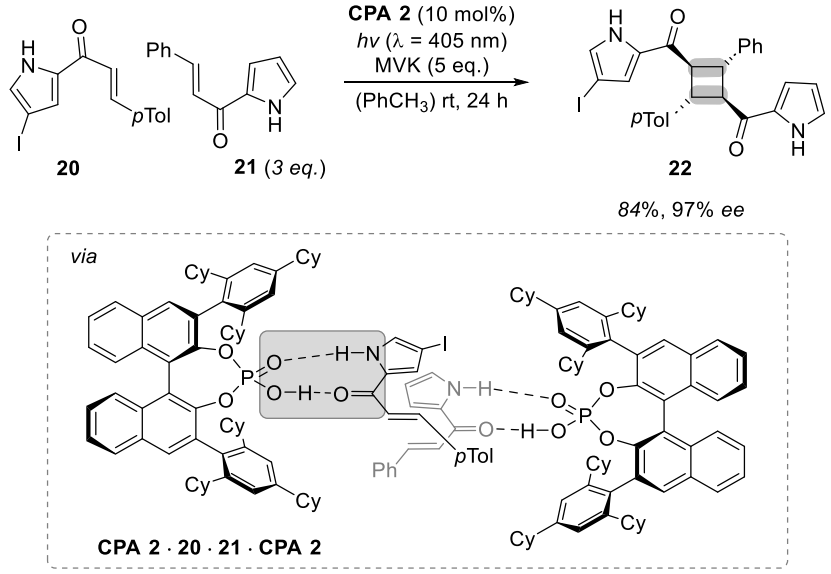

Scheme 3. *[2+2] photocycloaddition between the alkenyl 2-pyrrole ketones **20** and **21** catalyzed by **CPA 2** upon irradiation with purple light. pTol = para-tolyl, MVK = methyl vinyl ketone, Cy = cyclohexyl.*

This interaction leads to a bathochromic shift in the absorption of **20**, as previously described in the context of chromophore activation, facilitating a selective excitation of the substrate-catalyst complex. The authors proposed the formation of the shown dimer complex **CPA 2** · **20** · **21** · **CPA 2** involving two molecules of catalyst **CPA 2** in accordance with the results of a non-linear correlation study. Furthermore, it was suggested that the reaction proceeds from the singlet hypersurface, as it proceeds smoothly under oxygen.
In some cases, reactions are only possible or perform better, if the chiral phosphoric acid catalyst employed in the reaction is supported by an (achiral) photocatalyst which facilitates the photochemical reaction. Especially catalysts for triplet energy transfer (EnT) or photoredox catalysis are commonly used.

3.2. Chiral Phosphoric Acids in Combination with Photocatalysts

a) Reactions mediated by EnT

Photochemical reactions operating by EnT typically involve the transfer of triplet energy from a suitable sensitizer (which is directly excited) to a substrate molecule with a matching triplet energy. For successful sensitization it is beneficial if the sensitization process is exergonic, which is the case if the triplet energy (E_T) of the sensitizer is higher than the triplet energy of the substrate.[42]

The *Yoon* group showed in 2022 how the [2+2] photocycloaddition between vinylpyridine **23** and styrene (**11**) produces cyclobutane **24** (15 examples, 37-95% yield, 63-96% *ee*) in an efficient way (Scheme 4).[43]

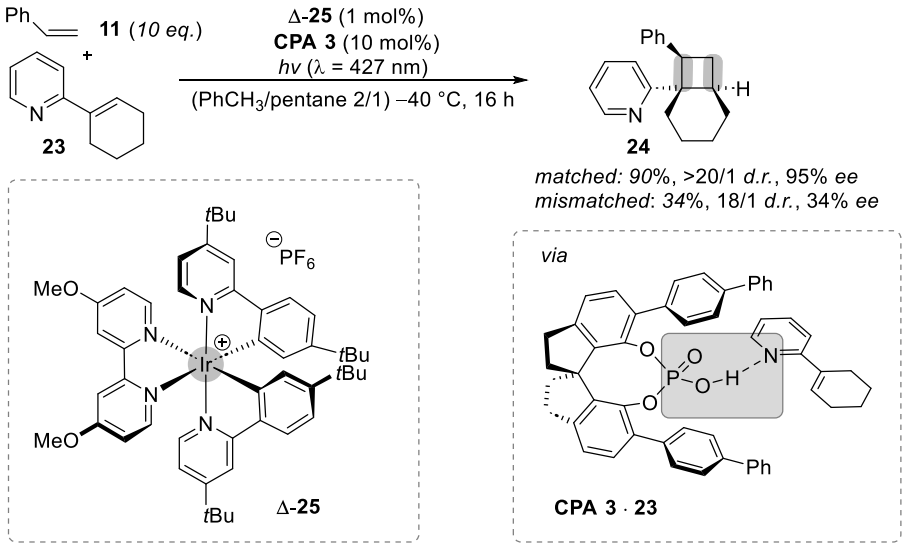

Scheme 4. *Cooperative stereoinduction in the [2+2] photocycloaddition between vinylpyridine **23** and styrene (**11**) mediated by a combination of chiral irrdium catalyst **Δ-25** and **CPA 3**.*

Key for the stereoselective reaction outcome was the combination of **CPA 3** and the chiral iridium-based sensitizer **Δ-25** in a matched fashion, meaning the right combination of the enantiomers of both sensitizer and acid (when **Δ-25** was used for the reaction, 95% *ee* were observed for **24**, while **Λ-25** only lead to 34% *ee*). **CPA 3** coordinates **23** *via* the nitrogen atom in its chiral cavity, presumably lowering the E_T of **23** and thereby generating a situation in which energy transfer towards the substrate is only feasible in the chiral environment of **CPA 3**. The authors explain the matching influence of the chiral sensitizer with the formation of a transient complex **Δ-25**^{3} · **CPA 3** · **23** between the triplet^3 excited sensitizer **Δ-25**^{3} and the pre-associated complex **CPA 3** · **23**, which reacts more efficiently with styrene than the respective diastereomeric complex **Λ-25**^{3} · **CPA 3** · **23**.

The same group, together with the *Mayer* group and the *Miller* group, demonstrated the utility of the vinyl pyridine binding motif in a similar study involving an enantioselective [2+2] photocycloaddition event.[44]

Furthermore, the *Yoon* group showed how enantioselective di-π-methane rearrangements are possible through the combination of a CPA and an achiral triplet sensitizer.[45]

The *Jiang* group made a notable contribution in the field using anthracene (**26**) in a dearomative [4+2] cycloaddition with alkenylazaarene **27** to afford the cycloadduct **28** with remarkable *ee* (62 examples, 43-99% yield, 66-99% *ee*). In this study, **CPA 4** was used in combination with the dicyano pyrazine based triplet sensitizer **29** (Scheme 5).[46]

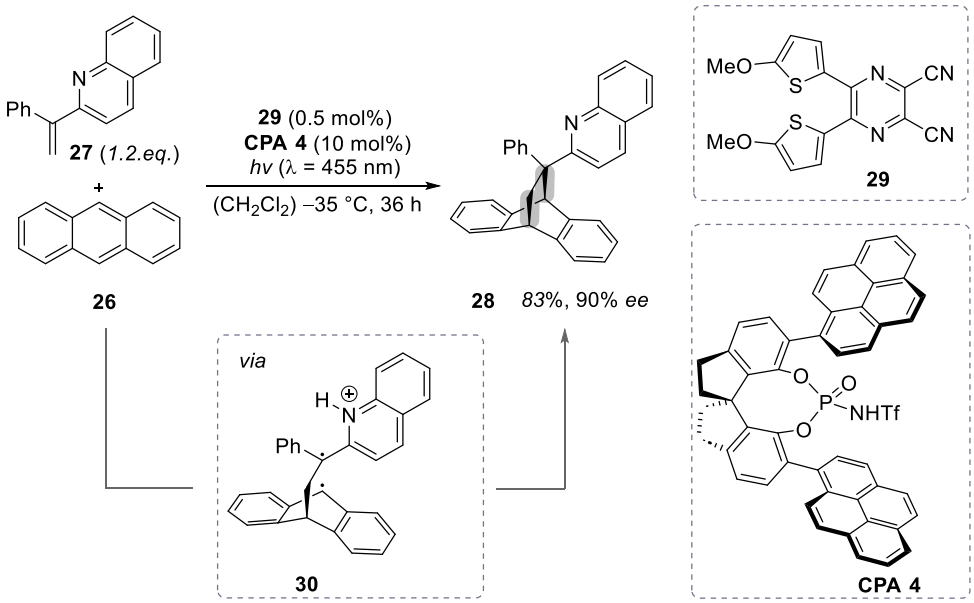

Scheme 5. *Dearomative [4+2] cycloaddition between anthracene (**26**) and alkenylazaarene **27** under visible light photocatalysis.*

Mechanistically, the authors propose triplet energy transfer from **29** towards anthracene (**26**), followed by addition of the resulting anthracene diradical to the ground state association complex between **CPA 4** and alkenylazaarene **27**. The formed diradical **30** undergoes intersystem crossing (ISC) and after radical recombination product **28** is formed.

Further important contributions from the *Jiang* group include the enantioselective formation of spirocyclic compounds,[47] as well as an enantioselective version of the *De Mayo* reaction,[48] although in this case a mechanism involving both triplet energy transfer as well as electron transfer is proposed. Furthermore, they showed very recently how the *Dual Catalysis* approach was used successfully for the deracemization of axially chiral azaarylidene cycloalkanes.[49]

b) Photoredox-mediated Reactions

Processes involving a catalyst which is able to undergo redox reactions in its excited state, in combination with a subsequent turnover step, resulting in a light-driven catalytic redox cycle are referred to as photoredox reactions.[50] As previously described, this reactions possess a significant synthetic potential for many applications and enantioselective variants have been excessively studied.

A seminal contribution by the *Knowles* group is the asymmetric aza-pinacol cyclization of hydrazone **31** to the alcohol **32** (14 examples, 45-96% yield, 77-95% *ee*) using HEH (*Hantzsch* dihydropyridine) as a stoichiometric reductant and employing **CPA 5** as well as photoredox catalyst **33** as the catalytic system (Scheme 6).[35]

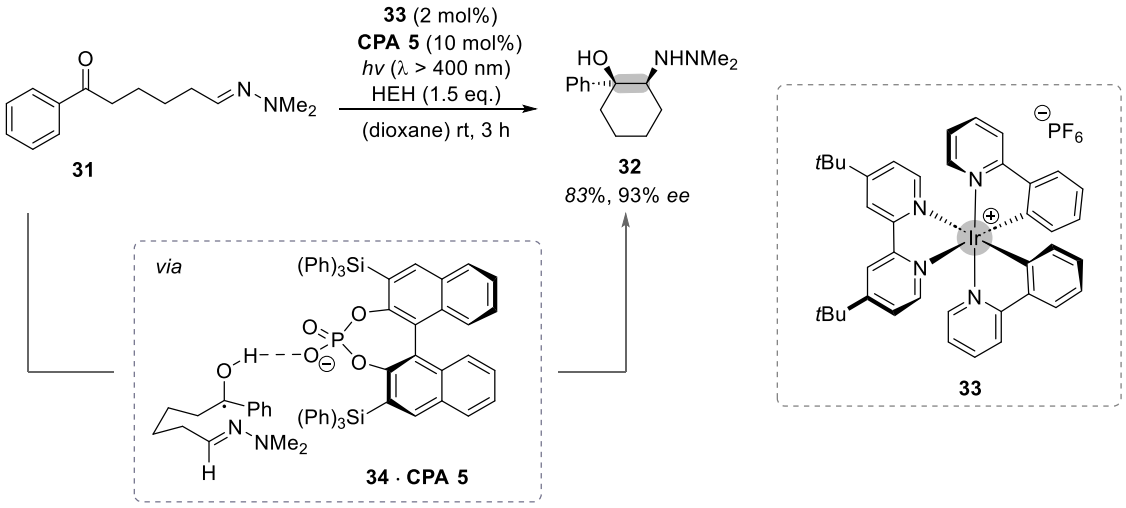

Scheme 6. *Aza-pinacol cyclization of hydrazone **31** to the alcohol **32** using enantioselective photoredox catalysis.*

Catalyst **33** becomes easily reducible by HEH in its excited state and the resulting Ir^{II} species forms key intermediate **34** by PCET (proton-coupled electron transfer). The obtained ketyl radical readily cyclizes in the chiral environment of **CPA 5**, determining the enantioselectivity of the overall process. After HAT (hydrogen atom transfer) from HEH, the product **32** is formed.

A few years later, the group of *Phipps* elegantly combined photoredox catalyst **35** with **CPA 6** to achieve a *Minisci*-type addition of the radical precursors **36** onto the heteroaromatic compound **37** yielding the chiral coupling product **38** (30 examples, 58-98% yield, 84-97% *ee*).[51] Mechanistically, the prochiral secondary radical **39** is formed from **36** in the usual way,[52] and **CPA 6** coordinates the respective radical as well as the quinolone electrophile **37**, facilitating the C-C bond formation. The authors suggested a reversible addition, making this step not the enantioselectivity determining step of the overall reaction. Instead, they assume the subsequent deprotonation step to be decisive for the observed enantioselectivity (Scheme 7).

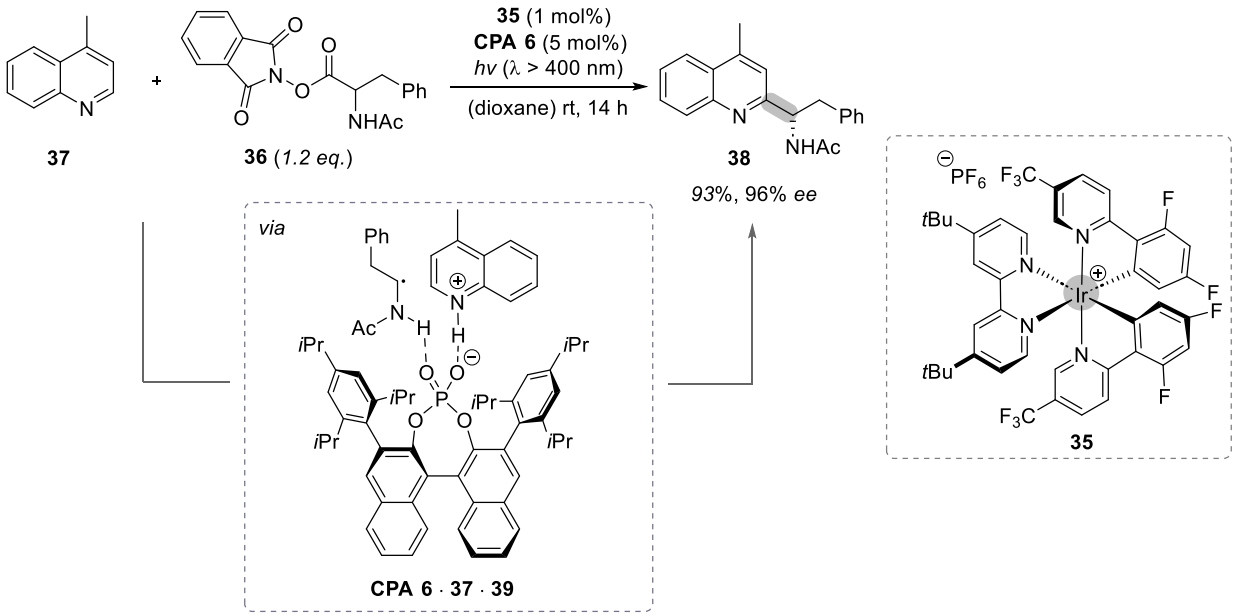

Scheme 7. *Photoredox mediated enantioselective Minisci reaction by the Phipps group.*

Apart from strategies involving separate CPA and photocatalyst, also single catalyst approaches combining both features are feasible. Research in this area is inspired by previous combinations of chiral fragments with photocatalysts by our group[27,53] and others.[32,54]

3.3. Photochemically Active Chiral Phosphoric Acids

The intriguing idea, to combine a CPA with a photocatalyst to form a bifunctional hybrid catalyst was sparked by the wide repertoire of available binding motifs known from thermal chemistry,[55,56] giving access to a wide range of potential substrates. Considering the somewhat limited number of available binding motifs for established photocatalytic systems, this seemed highly desirable.

a) Reactions mediated by EnT

The initial report in this field was published in 2020 by our group and exploited preliminary studies by the *List* group,[56] which demonstrated how carboxylic acids can form heterodimers with CPAs. The (*R*)-BINOL-based bifunctional **PACPA 1** (PACPA = photochemically active chiral phosphoric acid) catalyzed the reaction of carboxylic acid **40** with an excess of alkene **41** to afford, under irradiation with visible light and after benzylation of carboxylic acid **42**, the cyclobutane **43** (Scheme 8).[57]

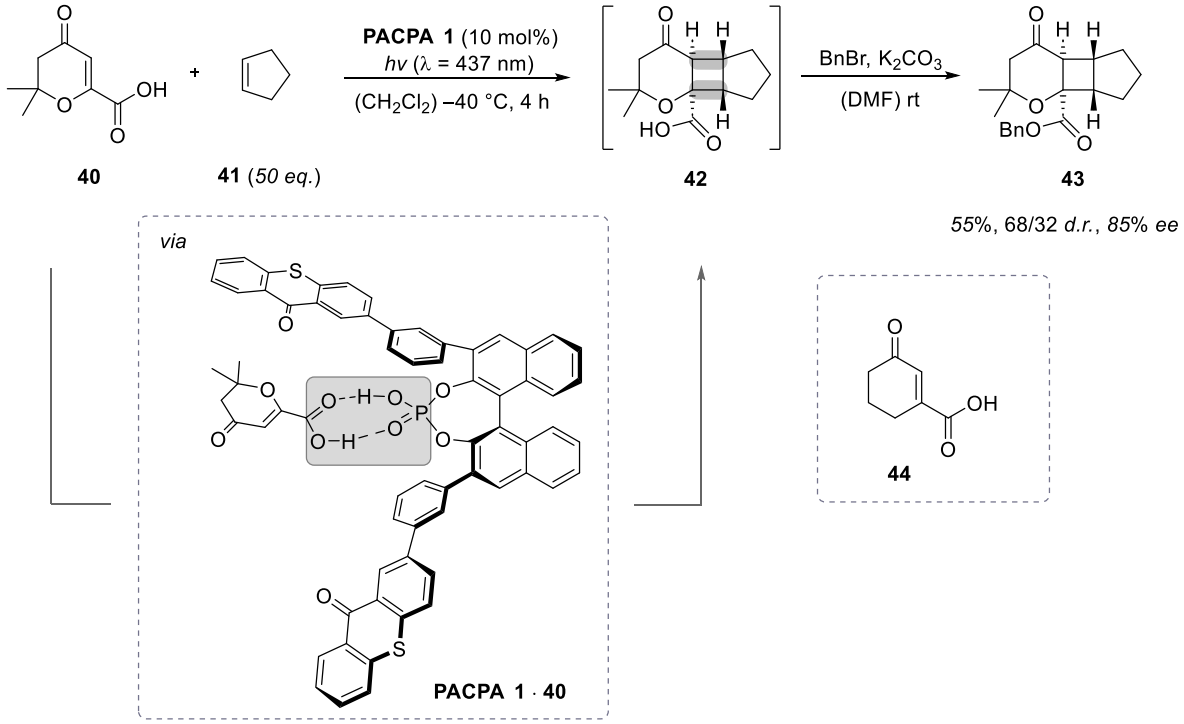

Scheme 8. *First example of a PACPA, employed in the intermolecular enantioselective [2+2] photocycloaddition between carboxylic acid **40** and alkene **41**.*

Mechanistically, a combination of NMR (nuclear magnetic resonance) spectroscopy studies and DFT (density functional theory) calculations suggest a two-point hydrogen bonding interaction between substrate **40** and **PACPA 1**, leading to a preferred EnT in the chiral environment of the catalyst, followed by a *Si* face attack of the respective alkene. The authors also used carboxylic

acid **44** in the scope study with different alkenes leading to a total of six examples with enantioselectivities of 45-85% *ee*.

The unique reactivity of **PACPA 1** was shortly after used in another synthetic study by our group, involving the reaction between the *N*,*O*-acetal **45** and 2,3-dimethylbuta-1,3-diene (**46**) to form the cyclobutane carbaldehyde **47** (19 examples, 54-96% yield, 84-98% *ee*).[58] The reaction proceeds *via* the in equilibrium formed imine **45'**, which associates with **PACPA 1** to form hydrogen bonding-assisted iminium ion pair **PACPA 1** · **45'** (Scheme 9).

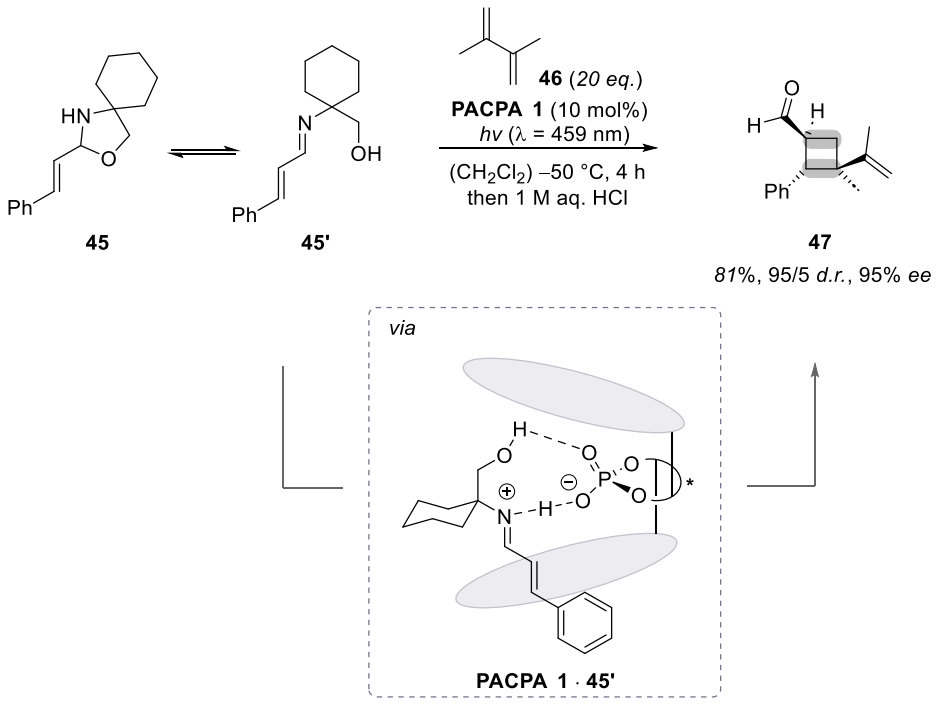

Scheme 9. *Enantioselective [2+2] photocycloaddition between N,O-acetal **45** and 2,3-dimethylbuta-1,3-diene (**46**) facilitated by **PACPA 1**.*

Upon irradiation, exergonic EnT from the sensitizing thioxanthone units of **PACPA 1** towards the bound iminium ion takes place, and after addition of the alkene from the *Si* face the product is formed.

The remarkable flexibility of PACPAs regarding the tolerance of different binding motifs was demonstrated by *Takagi et al.*. Following up on initial studies in which they used stochiometric amounts of a CPA as chiral complexing agent,[59] they showed how the C_1-symmetric H_8-BINOL (5,5',6,6',7,7',8,8'-octahydro-1,1'-bi-2-naphthol) -based **PACPA 2** can catalyze the [2+2] photocycloaddition of quinolone **48** to the cyclobutane **49** (9 examples, 24-95% yield, 73-98% *ee*).[60] Decisive for the stereoselective reaction outcome were the formation of a two-point hydrogen bond between the lactam moiety of **48** and the **PACPA 2**, as well as a π-π interaction between the aromatic substrate and the thioxanthone group of the catalyst (Scheme 10).

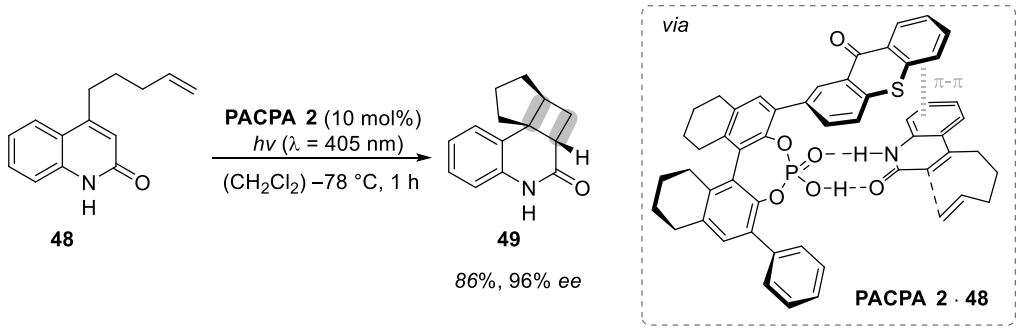

Scheme 10. *[2+2] photocycloaddition of* ***48*** *mediated by* ***PACPA 2****.*

b) Photoredox-mediated Reactions

Shortly after the initial report of a PACPA by our group, the *Masson* group used a similar catalyst (**PACPA 3**) for the enantioselective photoredox mediated amination of enecarbamate **50** with azodicarboxylate **51** to form diamine **52** with excellent enantioselectivity (15 examples, 30-95% yield, 91-99% *ee*, Scheme 11).[61,62]

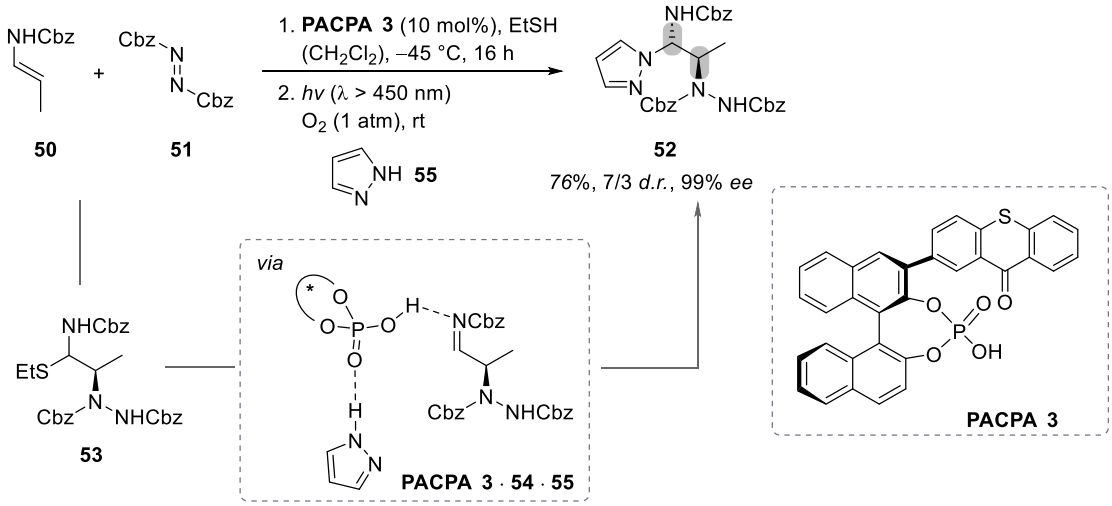

Scheme 11. *Enantioselective amination of enecarbamate* ***50*** *mediated by* ***PACPA 3*** *under irradiation with visible light.*

Mechanistically, the authors propose the thermal formation of α-carbamoylsulfide **53** followed by a subsequent photocatalytic oxidation mediated by **PACPA 3** to form the imine **54**. Similar to traditional CPA-catalyzed reactions, pyrazole (**55**) subsequently adds in a thermal reaction to the imine, generating product **52**.

A few years later, the *König* and the *Toste* group showed in a proof-of-principle study how the cyanoarene-based **PACPA 4** can act as a photoredox catalyst as well as a catalyst for EnT.[63] To test their catalyst they used it in the already known[64] *Minisci* reaction between 5-arylpyrimidine **56** and amino acid derived redox-active ester **57** to afford *Minisci* product **58**

(33% yield, 21% *ee*, Scheme 12) with a notable although lower enantioselectivity as previously reported (64% yield, >99% *ee*).

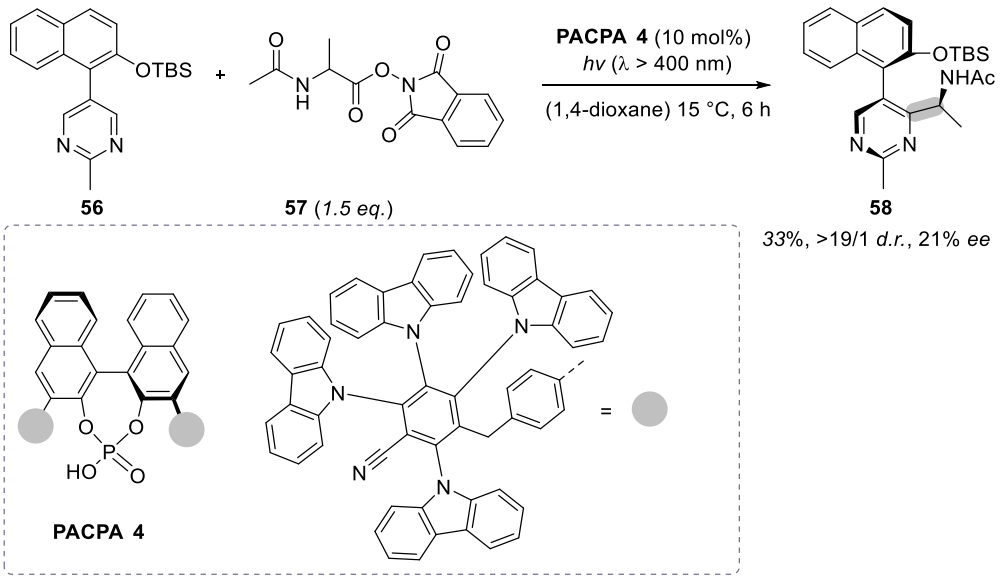

Scheme 12. *Enantioselective Minisci reaction mediated by the bifunctional cyanoarene-based* ***PACPA 4****.*

As a proof-of-concept for a reaction mediated by EnT, they repeated *Yoon's* [2+2] photocycloaddition [Scheme 2 ***a)***] with **PACPA 4** (5 mol% catalyst, 63% yield, 54% *ee*, with a slightly modified PACPA they obtained 80% yield and 65% *ee*).

Another study centering around the synthesis of bicyclo[2.1.1]hexanes was presented by the *Jiang* group in 2024.[65] They used 2-vinylpyridine (**59**) in the [2π + 2σ] photocycloaddition with BCB **60** employing the photoredox active **PACPA 5**, leading to the bicyclic product **61** with high enantioselectivity (52 examples, 46-99% yield, 83-99% *ee*, Scheme 13).

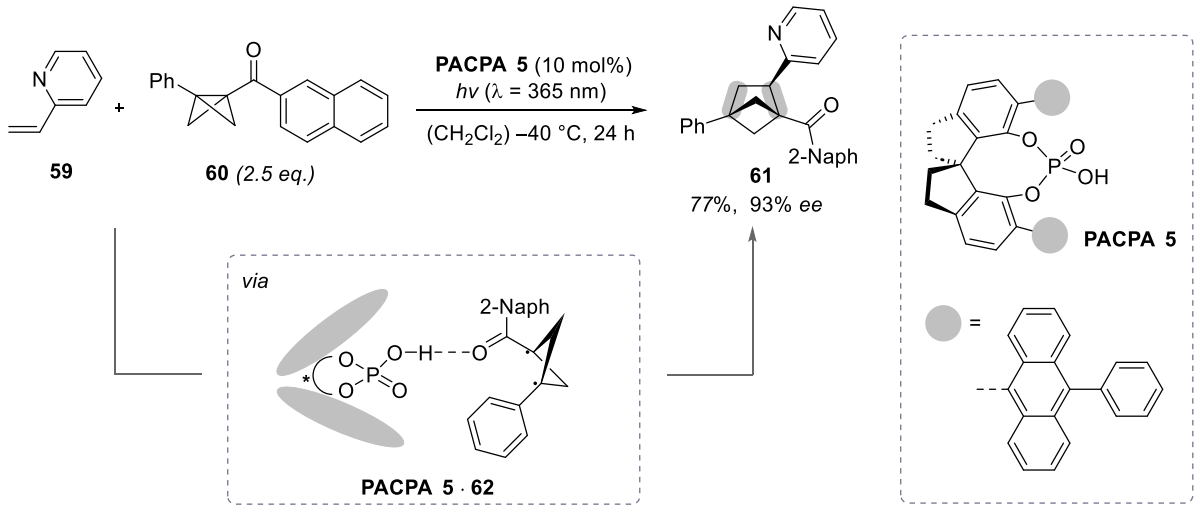

Scheme 13. *Synthesis of bicyclo[2.2.1]hexane* ***61*** *through enantioselective [2π + 2σ] photocycloaddition mediated by* ***PACPA 5****. 2-Naph = 2-naphthyl.*

Mechanistically, the authors propose excitation of the polycyclic aromatic moiety of **PACPA 5**, which undergoes PCET towards the ketone moiety of BCB **60**. Subsequent ring opening and electron back-transfer to the catalysts lead to the triplet intermediate **62**, and upon addition of alkene **59** in the vicinity of the chiral catalyst, the product is formed.

Considering the wide range of photochemical reactions unattained in an enantioselective fashion, as well as the considerable interest of our group in reactions mediated by EnT, we were deeply interested in further exploring the synthetic abilities of PACPAs in subsequent synthetic studies.

4. Expanding the Reaction Scope of Photochemically Active Chiral Phosphoric Acids

Inspired by work from our group[57,58] and others[60] we envisioned that by careful design of the respective PACPA catalyst also EnT mediated enantioselective reactions other than the photochemical [2+2] cycloaddition should become feasible.

On a structural level, modifications of different key features of the PACPA are proposed to lead to an improved performance in the desired enantioselective photochemical transformations (Figure 3).

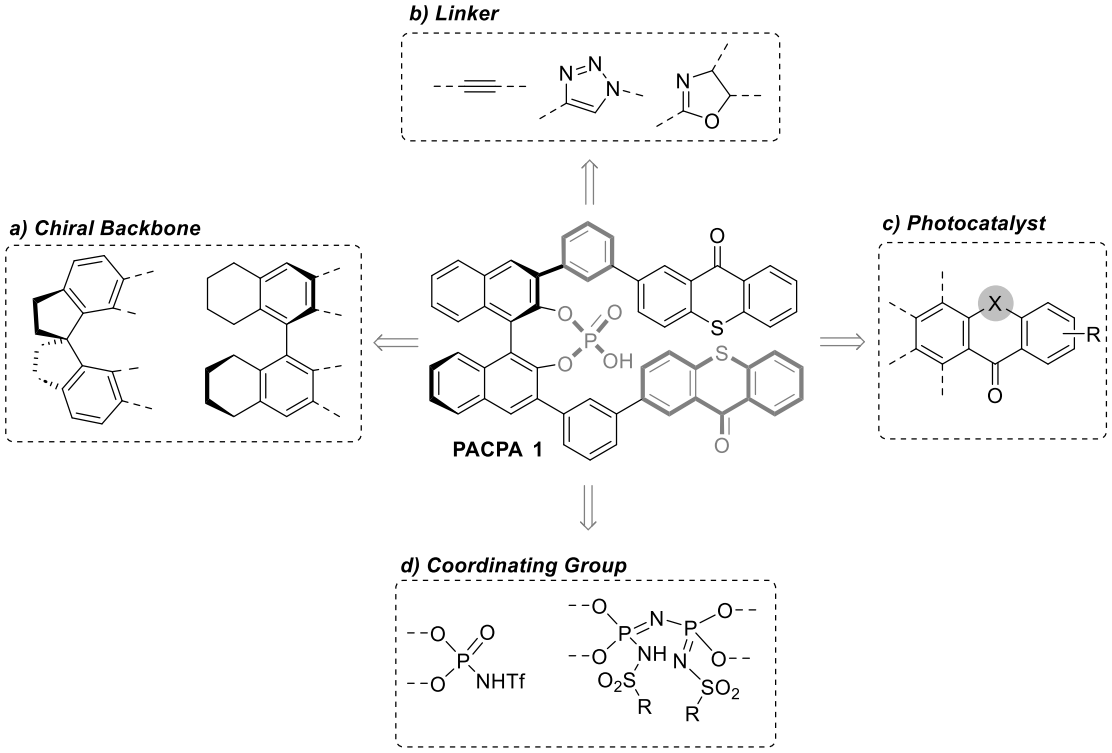

Figure 3. *Possible sites of structural modification of* ***PACPA 1****,* ***a)*** *Chiral Backbone,* ***b)*** *Linker,* ***c)*** *Photocatalyst,* ***d)*** *Coordinating Group. Tf = trifluoromethanesulfonyl, R = rest.*

Chiral Backbone ***a)*** as well as the *Linker* ***b)*** and the *Photocatalyst* ***c)*** influence the exact nature of the chiral pocket of the PACPA, which is decisive for a high degree of enantiodifferentiation. The *Linker* also strongly influences the distance between the chromophore of the catalyst and the substrate chromophore, which has been reported to be decisive especially in deracemization reactions.[23,66] The *Photocatalyst* (or photocatalytically active group) is highly tunable regarding steric demand, and most importantly, its triplet energy. The nature of the *Coordinating Group* ***d)*** decides over the binding mode of the respective substrate (hydrogen-bonding vs. ionic interaction), which is strongly dependent on its acidity.

Regarding possible reactions to test our new catalysts, seminal work by *Corey*[67] and *Eaton*[68] caught our attention. They had shown that cyclohept-2-en-1-one (*cis*-**63**) isomerizes upon excitation with light to the respective *trans*-isomer (*trans*-**63**). The highly reactive species can

be trapped by a suitable diene in a thermal *Diels-Alder* reaction. Along these lines our group investigated the racemic reaction,[69] with the idea in mind to develop an enantioselective version, intrigued by the inherent planar chirality of *trans*-**63**. We envisioned that a PACPA could coordinate a suitable cycloheptenone derivative and facilitate the isomerization by EnT in an enantioselective fashion. Stereospecific trapping of the enantiomerically enriched highly strained alkene in a thermal *Diels-Alder* reaction should lead to the enantiomerically enriched cycloaddition products [Scheme 14 ***a)***].

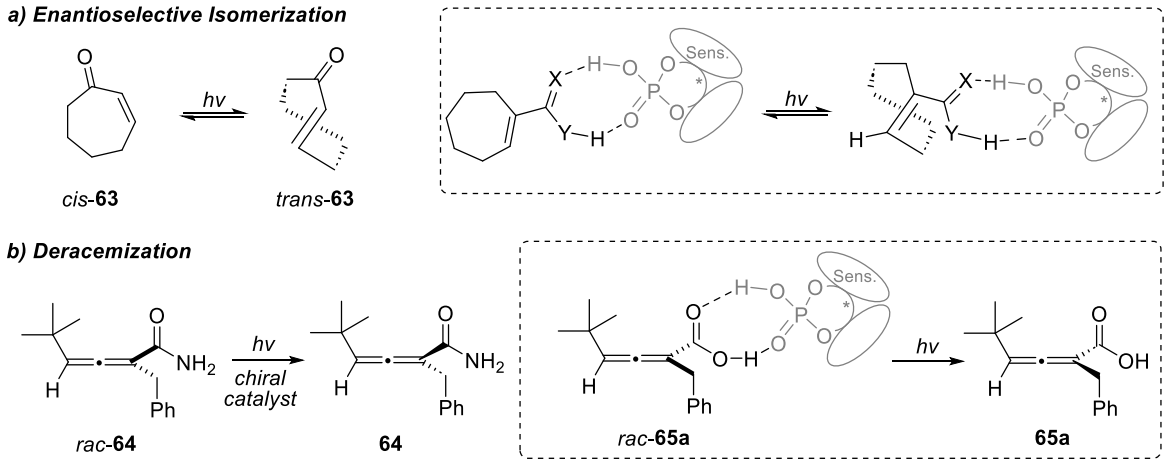

Scheme 14. a) *Left: Seminal work on the isomerization of cyclohept-2-en-1-one, Right: PACPA catalyzed enantioselective isomerization* ***b)*** *Left: Photochemical deracemization of primary allene amides by our group, Right: Envisioned PACPA catalyzed deracemization of allene carboxylic acids. Sens. = sensitizer.*

Recently, photochemical deracemization reactions gained a lot of attention,[23,24,70] and our group reported the photochemical deracemization of primary allene amide *rac*-**64** by a chiral lactam catalyst.[66] Inspired by this reaction, we anticipated a similar deracemization reaction, using the respective axially chiral allene carboxylic acid *rac*-**65a** in combination with a PACPA [Scheme 14 ***b)***].

By the synthesis of structurally optimized PACPA catalysts, we aimed to unlock exciting new reaction modes to expand the synthetic utility of bifunctional photochemically active chiral phosphoric acids.

5. Enantioselective Photochemical Generation of a Short-Lived, Twisted Cycloheptenone Isomer: Catalytic Formation, Detection and Consecutive Chemistry

Title:	"Enantioselective Photochemical Generation of a Short-Lived, Twisted Cycloheptenone Isomer: Catalytic Formation, Detection and Consecutive Chemistry"
Status:	Research Article, published online April 21, 2025
Journal:	*Angew. Chem. Int. Ed.* **2025**, *64*, e202501433
Publisher:	John Wiley and Sons
DOI:	doi.org/10.1002/anie.202501433
Authors:	Max Stierle, Constantin Jaschke, Daniel J. Grenda, Martin T. Peschel, Thomas Pickl, Niklas Gessner, Patrick Nuernberger, Benjamin P. Fingerhut, Christian Ochsenfeld, Regina de Vivie-Riedle, Thorsten Bach

Content: Cyclohept-2-enone-3-carboxylic acid was found to undergo a photochemical isomerization to its strained *trans*-form either under direct irradiation or under sensitizing conditions. The isomerized *trans*-form was detected by step-scan FTIR and a lifetime of 130 µs (r.t. CH_2Cl_2) was measured. Trapping of the strained alkene in a thermal *Diels-Alder* reaction led to *trans*-fused cycloaddition products (14 examples, 24-98% yield). When a bifunctional chiral phosphoric acid with a sensitizing group was used for the reaction, enantioselectivity was induced in the isomerization to the planar chiral *trans*-form of the substrate. The subsequent *Diels-Alder* reaction and benzylation sequence led to chiral products (seven examples, up to 38% *ee*). Extensive computational studies suggest that the observed enantioselectivity is indeed the product of an enantioselective isomerization reaction, although the phosphoric acid catalyzes the ground state *Diels-Alder* reaction preferentially to the opposite enantiomer, leading to an erosion of the overall observed enantioselectivity.

M. Stierle and T. Bach developed the project. M. Stierle planned and executed all synthetic experiments. C. Jaschke and M. T. Peschel performed all computational work. D. J. Grenda and N. Gessner were responsible for step-scan FTIR measurements. Thomas Pickl performed X-ray crystallographic analyses. P. Nuernberger, B. P. Fingerhut, C. Ochsenfeld, R. de Vivie-Riedle and T. Bach supervised the research and acquired funding. The manuscript was written with contributions from all authors.

GDCh Research Article Angewandte International Edition Chemie www.angewandte.org

Check for updates

How to cite: *Angew. Chem. Int. Ed.* **2025**, *64*, e202501433
doi.org/10.1002/anie.202501433

Photochemistry

Enantioselective Photochemical Generation of a Short-Lived, Twisted Cycloheptenone Isomer: Catalytic Formation, Detection, and Consecutive Chemistry

Max Stierle, Constantin Jaschke, Daniel J. Grenda, Martin T. Peschel, Thomas Pickl, Niklas Gessner, Patrick Nuernberger, Benjamin P. Fingerhut, Christian Ochsenfeld, Regina de Vivie-Riedle†, and Thorsten Bach**

Abstract: Cyclohept-2-enone-3-carboxylic acid undergoes a photochemical isomerization from its *cis*- to its *trans*-form either upon direct irradiation ($\lambda = 366$ nm) or in the presence of a triplet sensitizer ($\lambda = 459$ nm). The intermediate chiral *trans*-isomer was detected by step-scan FTIR, displaying a lifetime of 130 µs (r.t., CH_2Cl_2). Ensuing Diels–Alder reactions of the *trans*-isomer occurred smoothly and produced chiral *trans*-fused cycloaddition products (14 examples, 24%–98% yield). Benzylation led to esters, which were separated by chiral HPLC and which were employed to evaluate a possible enantioselective reaction course. It was discovered that a chiral phosphoric acid with a pendant sensitizing group induces a notable enantioselectivity in the photoisomerization step. The planar chirality of the *trans*-cycloheptene translates into point chirality in the Diels–Alder reaction (seven examples, up to 38% *ee*). Computational studies suggest that the chiral conformation of the *cis*-isomer adopted within the assembly to the chiral phosphoric acid induces the enantioselectivity in a one-bond flip (OBF) toward the *trans*-isomer. Trajectory surface hopping (TSH) simulations showed exemplarily how a chiral *trans*-cyclohept-2-enone is formed from a chiral *cis*-conformer. For the Diels–Alder reaction, a weak ground state selectivity was found to attenuate the enantioselectivity achieved in the photochemical step.

Introduction

Olefins can reach their first excited singlet state (S_1) by direct excitation or their first excited triplet state (T_1) by sensitization. Since either state is typically $\pi\pi^*$ in character, the olefin loses its configurational stability, and an out-of-plane rotation of its substituents becomes feasible. While the dihedral angle θ of two *trans*-positioned, vicinal substituents R is typically approx. 180° in the ground state, the substituents move away from each other in the excited state and adopt a conformation in which the dihedral angle approaches 90°. Once the olefin returns to the ground state, the planar arrangement is restored, and the two substituents can be either *cis*- ($\theta = 0°$) or *trans*-positioned ($\theta = 180°$). For acyclic olefins, it has been shown that a counter-thermodynamic[1–3] isomerization from a *trans*- to a *cis*-olefin is feasible either by choosing an irradiation wavelength at which the *trans*-isomer is excited but the *cis*-isomer is not or by selecting a sensitizer (sens.) with a triplet energy which is between the triplet energy of the *trans*- and the *cis*-isomer (Scheme 1).[4–7]

For cyclic olefins with a ring size $n = 4$–10, the *cis*-isomer is typically more stable than the *trans*-isomer[8] and the ring restricts free rotation even in an excited $\pi\pi^*$ state. Starting from cyclohexenes ($n = 6$), the *trans*-isomer is sufficiently stable to be detected and to be trapped in consecutive reactions (vide infra).[9–13] An intriguing fact pertinent to *trans*-cycloalkenes is their chirality, with the plane of chirality defined by the carbon atoms and the substituents of the olefin. It should, thus, be possible to create *trans*-cycloalkenes enantioselectively and to perform consecutive reactions which ideally occur with a high degree of chirality transfer. Pioneering work by Inoue and co-workers[14–17] has established the enantioselective formation of *trans*-cycloheptene by singlet energy transfer from chiral menthyl- and bornyl-derived catalysts (20 mol%). Although

[a] M. Stierle, M.Sc., T. Pickl, M.Sc., T. Bach
Department Chemie and Catalysis Research Center (CRC), School of Natural Sciences, Technische Universität München D-85747, Garching, Germany
E-mail: thorsten.bach@ch.tum.de

C. Jaschke, M.Sc., M. T. Peschel, B. P. Fingerhut, C. Ochsenfeld, R. de Vivie-Riedle†
Department of Chemistry, Ludwig-Maximilians-Universität München D-81377, München, Germany
E-mail: benjamin.fingerhut@cup.lmu.de

D. J. Grenda, M.Sc., N. Gessner, M.Sc., P. Nuernberger
Institut für Physikalische und Theoretische Chemie, Universität Regensburg D-93053, Regensburg, Germany

[†] Deceased on June 20, 2024.

Group Bluesky (student run account):
https://bsky.app/profile/bach-lab.bsky.social

Additional supporting information can be found online in the Supporting Information section

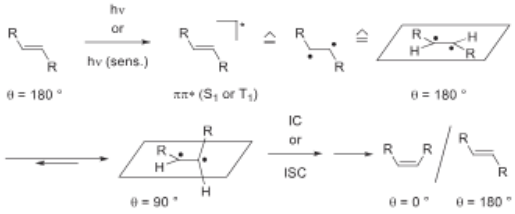

Scheme 1. Photochemical isomerization of olefins either by direct excitation to S_1 or sensitization to T_1 (IC = internal conversion; ISC = intersystem crossing).

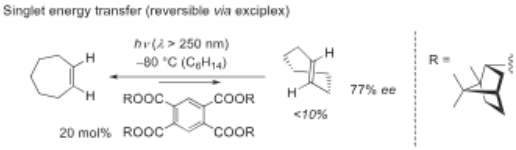

Scheme 2. Singlet energy transfer as a vehicle to achieve an enantioselective photoisomerization:[15] Low yield of enantioenriched *trans*-cycloheptene.

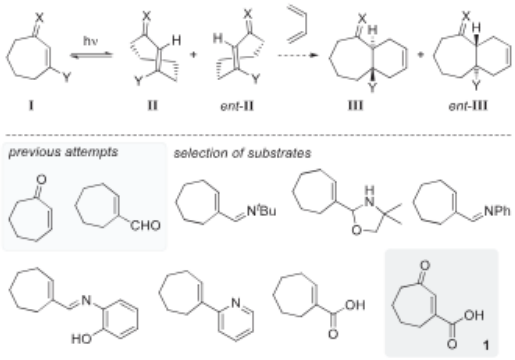

Scheme 3. Top: The isomerization of cycloheptenes **I** leads to chiral twisted *trans*-isomers **II** and ***ent*-II**, which should be competent to undergo a subsequent Diels–Alder reaction leading to **III** (from **II**) and to ***ent*-III** (from ***ent*-II**). Bottom: Previously studied cycloheptenes and a selection of alternative substrates from which cyclohept-2-enone-3-carboxylic acid (**1**) evolved as a suitable isomerization precursor.

the enantioselectivity of the process reached up to 77% *ee* (enantiomeric excess), it suffered from the fact that the *trans*-isomer remained the minor diastereoisomer formed in a ratio of *trans*/*cis* = 10/90 at best (Scheme 2). A yield of 6% was recorded in a preparative run in which racemic *trans*-cycloheptene was trapped by 1,3-diphenylisobenzofuran in a Diels–Alder reaction.[15]

While the enantioselectivities achieved by singlet energy transfer catalysis are notable, the intrinsic issue that the catalyst also promotes the reverse reaction to the *cis*-cycloalkene has not been overcome. In situ trapping of the *trans*-isomer is difficult due to the low reaction temperature and the short wavelength employed in the transformation. Triplet energy transfer could offer a solution to this challenge since it occurs under more suitable conditions and is strongly distance dependent. Geometric and thermodynamic constraints might be favorably employed to steer the directionality of the isomerization. However, there has been no conceptual proof that triplet energy transfer can be successfully employed for the enantioselective photoisomerization of *cis*-cycloalkenes.

Our group has for some time studied the photoisomerization of substituted cycloheptenes **I** and their subsequent Diels–Alder reactions (Scheme 3).[18,19] The key idea was to enforce the enantioselective formation of the strained *trans*-isomer **II** from the *cis*-isomer **I** by employing either a chiral Lewis acid[20] or a chiral triplet sensitizer.[21] A Diels–Alder reaction, schematically shown for 1,3-butadiene, would deliver with high chirality transfer *trans*-fused product **III**. Accordingly, enantiomer ***ent*-II** would deliver the mirror image ***ent*-III**. Although we could show that the reaction of the *trans*-isomers with various dienes proceeds in very good yields both for cyclohept-2-enones[18] and for cyclohept-1-ene-1-carbaldehydes,[19] attempts to render the reactions enantioselective remained futile. In the present study, we have attempted to identify cycloheptene substrates that would display a binding motif suitable for association with a chiral phosphoric acid. If the latter compound displayed a sensitizing substituent, an energy transfer would be possible, which in turn would populate one of the enantiomeric *trans*-isomers selectively. Several cycloheptenes were evaluated in racemic reactions from which cyclohept-2-enone-3-carboxylic acid (**1**) evolved as a suitable candidate.

It was found that the in situ generated *trans*-isomer reacts with a variety of dienes, forming intriguing tricyclic lactones. A comprehensive computational study suggests that a conformational bias prior to the photoisomerization was responsible for the formation of either enantiomeric *trans*-isomer. The experiments culminated in the first enantioselective cascade of a sensitized *cis*/*trans* isomerization and a Diels–Alder reaction. A full account of the details of our study is presented in this research article.

Results and Discussion

Nature of the excited state and racemic reactions. There are several techniques available to determine the lifetime of twisted *trans*-cycloheptenes. Early studies with UV illumination at temperatures of 113 K or lower showed the formation of *trans*-cyclohepten-2-one, which was stable for more than an hour.[22,23] Transient studies by Bonneau and co-workers revealed a lifetime of hours for *trans*-1-phenylcycloheptene at low temperatures as well and could even demonstrate light-induced back-isomerization; at ambient temperature, a lifetime of 250 s was reported in cyclohexane.[24] For *trans*-cyclohept-2-enone ($c \approx 100$ μM), room-temperature studies yielded lifetimes of 45 s in cyclohexane, but much lower values in polar protic solvents, e.g., 33 ms in methanol.[25] Inoue and his group determined the lifetime of *trans*-cycloheptene by

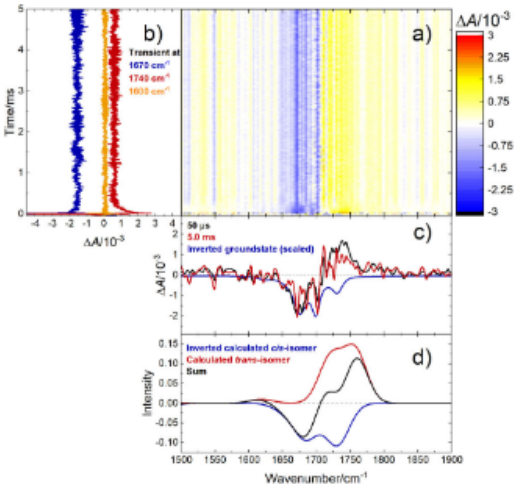

Figure 1. a) Step-scan FTIR data for **1** in CH_2Cl_2 ($c = 71.8$ mM) at room temperature. b) Evolution of bleached *cis*-isomer **1** at 1670 cm^{-1} and transiently formed *trans*-isomer (*rac*-**2**) at 1740 cm^{-1}, as well as the baseline at 1600 cm^{-1}. c) Spectra directly after excitation (black), toward the end of the measurement (red), and the steady-state spectrum of **1** (blue, inverted and scaled). d) Calculated spectra {[CPCM(CH_2Cl_2)]-R^2SCAN-3C/def2-mTZVPP, see the Supporting Information for details} for **1** (blue, inverted), *rac*-**2** (red), and their difference mimicking the difference spectra after excitation (black). Note that oscillatory signals of electronic origin had to be removed from the raw data (see Supporting Information for details).

trapping experiments with methanol at various temperatures (c = 0.01 M), which was extrapolated to 45 s at ambient temperature.[26,27] A lifetime of 7.1 min at −78 °C was determined for *cis*,*trans*-cycloheptadiene by Inoue and co-workers from transient UV–vis data (c = 0.12 mM) in isopentane-methylcyclohexane (3:1).[28] We investigated cycloheptene **1** in CH_2Cl_2 at room temperature by step-scan FTIR spectroscopy with a ns pump laser.[29–31] The transient IR data showed the ground-state bleach of *cis*-configured **1** together with a newly formed absorption associated with *trans*-isomer *rac*-**2** (Figure 1). While the former remained constant, the latter decayed with a lifetime of about 130 µs toward yet another carbonyl signal, which may be attributed to the [2+2] photocycloaddition product (see the Supporting Information for details). The relatively short lifetime appears to be testimony to the higher strain induced by the additional substitution, but it also suggests that the transient intermediate was sufficiently long-lived to participate in trapping studies.

Preliminary synthetic experiments were performed with various cycloheptenes and 1,3-cyclopentadiene as the diene component. It was found that some imine-derived cycloheptenes (see Scheme 3) suffered from stability issues and that pyridyl- and hydroxylcarbonyl-substituted derivatives were not sufficiently reactive. In notable contrast, irradiation of cyclohept-2-enone-3-carboxylic acid (**1**) at λ = 366 nm resulted in clean product formation, supporting the notion that the lifetime of the transient isomer *rac*-**2** allows for a successful bimolecular reaction. Optimization revealed dichloromethane as the superior solvent and a 1 M concentration of the diene (50 equiv.) as optimal (Scheme 4). The Diels–Alder product[32–37] *rac*-**3a** displayed the expected *trans*-configuration at the ring conjunction, and the *endo*-isomer was clearly preferred, i.e., the approach of the diene double bond had occurred *endo* to the carbonyl carbon atom. The diastereomeric ratio (d.r. = *endo*/*exo*) was 91/9 in favor of the *endo*-product, with the total yield being 90%. Due to the *trans* ring fusion, the carboxylic acid group gets into the proximity of the carbonyl group, enabling the formation of a lactone-type hemiacetal, which was, for compound *rac*-**3a**, the only detectable species. Single-crystal structure analysis confirmed the constitution and relative configuration of the compound.[38]

The novel structural feature of the products from the isomerization/Diels–Alder reaction/lactonization cascade warranted a more extensive exploration of the reaction scope. Several other dienes were employed in the sequence, and the respective products *rac*-**3** fully characterized. Six-membered dienes reacted well and displayed—like 1,3-cyclopentadiene—a preference for the *endo* product (products *rac*-**3b** and *rac*-**3c**). Furans were found to be suitable dienes, and the parent compound produced a mixture of two diastereoisomers, with the *endo*-product *rac*-**3e** prevailing. 2,5-Disubstituted furans gave in full analogy to the parent compound, the cascade products *rac*-**3e**-*rac*-**3h** in high yields as single isomers. For representative product *rac*-**3e**, it was shown by single-crystal X-ray crystallography that the Diels–Alder reaction proceeded in an *endo*-fashion.[39] 2,3-Dimethylfuran resulted in an inseparable product mixture with the shown isomer *rac*-**3i** being predominant (r.r. = regioisomeric ratio). The two regioisomeric products *rac*-**3j** and *rac*-**3j'** stemming from the reaction of 3-bromofuran could be separated and were free from any diastereoisomers. 2-Substituted furans also underwent the cascade reaction, but the regioselectivity was less pronounced. For 2-acetoxymethylfuran, only a single product isomer, *rac*-**3k** was isolated, but the low yield indicated that the other regioisomer was likely lost during work-up or was too unstable to be isolated. 2-Methylfuran delivered both conceivable regioisomers as an inseparable mixture with a preference for the shown isomer *rac*-**3l**. Acyclic dienes (2,3-dimethylbuta-1,3-diene, 1,2-bismethylene-cyclohexane) were competent reaction partners, but the respective products *rac*-**3m** and *rac*-**3n** delivered poorly resolved NMR spectra. It appeared as if there was an equilibrium between the lactone and the free carboxylic acid form, which led to line broadening of the NMR signals. To facilitate the isolation of single compounds from Diels–Alder products *rac*-**3m** and *rac*-**3n**, a consecutive benzylation of the carboxylic acid was pursued. In addition, it was desirable to convert the weakly UV-active compounds *rac*-**3** into better detectable products for HPLC analysis. In fact, racemic samples were required for unequivocal *ee* determination in the projected enantioselective reactions. Taking Diels–Alder product *rac*-**3a** (d.r. = 76/24) as a test case, we found treatment with benzyl bromide and potassium carbonate in DMF to be an operationally simple benzylation protocol (Scheme 5).

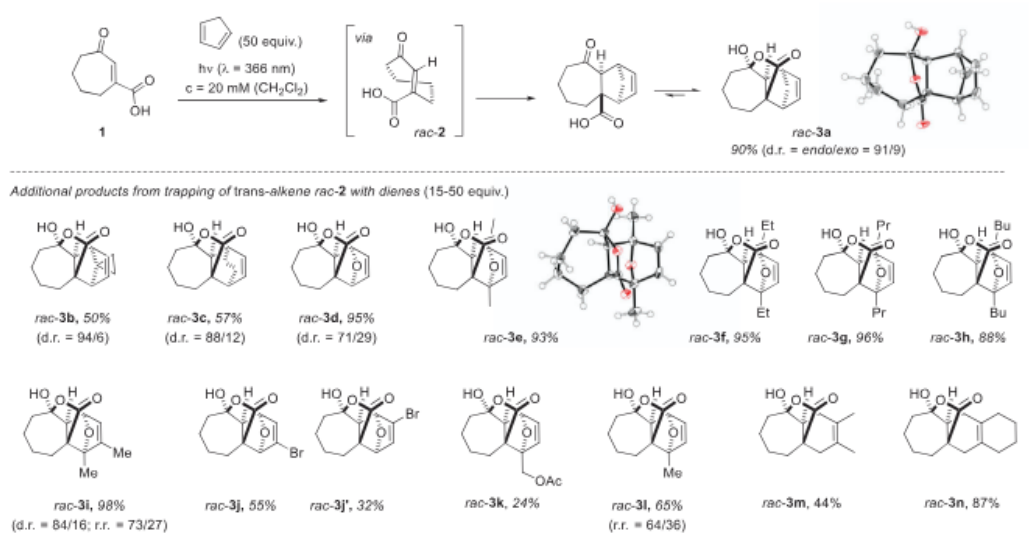

Scheme 4. Scope and limitations of the photochemical isomerization of cyclohept-2-enone-3-carboxylic acid (**1**) and subsequent trapping of the racemic *trans*-isomer *rac*-**2** by various dienes. In most cases, a lactonization/hemiacetal formation occurs, and this structure is depicted for the racemic products *rac*-**3**.

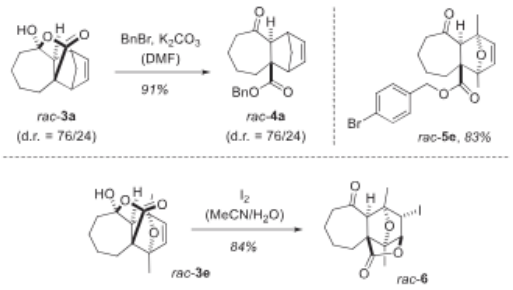

Scheme 5. Consecutive reactions of the Diels–Alder products *rac*-**3**. Top: Benzylation leads to products *rac*-**4a** and *rac*-**5e**, which can be detected and are separable by chiral HPLC. Bottom: Iodolactonization of compound *rac*-**3e** provides iodide *rac*-**6** in diastereomerically pure form.

The desired ester *rac*-**4a** was obtained in 91% yield (d.r. = 76/24). The reaction **3** → **4** is also applicable to the other lactones, and the relative configuration of product *rac*-**4e** was confirmed by single-crystal X-ray crystallography (see the Supporting Information for details).[40] The *para*-bromobenzyl ester *rac*-**5e** was obtained from Diels–Alder product *rac*-**3e** by benzylation with *para*-bromobenzyl bromide. The heavy atom was considered useful in the enantioenriched series (vide infra) for determining the absolute configuration. The same starting material, *rac*-**3e**, delivered upon treatment with iodine[41] the halolactonization product *rac*-**6**. The reaction confirmed the *endo* position of the double bond in product *rac*-**3e** since an *exo*-positioned double bond would not be available for halolactonization. The tetracyclic skeleton so generated has not been previously reported.

Enantioselective reactions employing a sensitizing phosphoric acid. Our group[42,43] and others[44–54] have for some time studied chiral phosphoric acids with pendant sensitizing groups as chiral catalysts for enantioselective photochemical reactions. So far, the focus has been on the discrimination of enantiotopic faces upon substrate binding to the phosphoric acid. To the best of our knowledge, there have not been any studies devoted to enantioselective photochemical isomerization reactions.[55–58] In this regard, there was no clear rationale as to the structure of a potential catalyst nor to its mode of action. Since the known C_2-symmetric acid **7** had shown promising results in [2+2] photocycloaddition chemistry,[42,43] it was taken as a blueprint for catalyst design (Figure 2).

The thioxanthone chromophore was considered suitable for energy transfer to cyclohept-2-enone-3-carboxylic acid (**1**). Starting from (*R*)-(+)-5,5′,6,6′,7,7′,8,8′-octahydro-1,1′-bi-2-naphthol (octahydrobinol) and from (*R*)-2,2′,3,3′-tetrahydro-1,1′-spirobis[indene]-7,7′-diol (spinol), the analogous C_2-symmetric catalysts **8a** and **9** were prepared (see the Supporting Information for details). Another C_2-symmetric phosphoric acid **8b**, lacking the phenyl spacer, was prepared from octahydrobinol. In addition, a fifth catalyst, **8c**, was added to the selection, which lacked C_2-symmetry but rather displayed a lipophilic aryl group at position C3'. Spectral features for catalysts **8a**, **8b**, and **9** were similar in that all three of them showed an absorption maximum around $\lambda = 400$ nm in their UV–vis spectrum with a tail extending in all cases far into the visible range ($\lambda \leq 470$ nm). The triplet energies (E_T) determined from their phosphorescence spectra (77 K, CH_2Cl_2) were found to be almost identical, with E_T varying

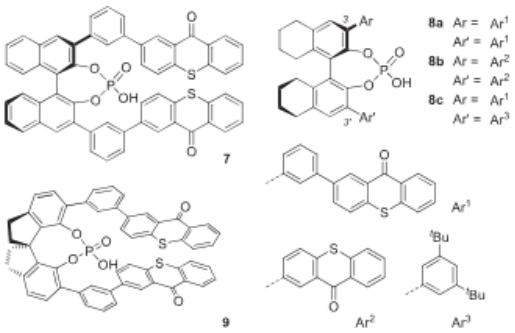

Figure 2. Structure of chiral phosphoric acids **7**–**9** used for triplet energy transfer to cyclohept-2-enone-3-carboxylic acid (**1**) in an attempted photochemical isomerization to the twisted isomer **2**.

between 252 and 253 kJ mol^{-1} (±2 kJ mol^{-1}). The values are higher than the previously determined triplet energy of catalyst **7** (E_T = 235 ± 2 kJ mol^{-1}).[42] The red-shifted emission is in line with a lower singlet state (S_1) energy of the latter compound as compared to thioxanthenes **8a**, **8b**, and **9**. The energy for the 0–0 transition determined from the crossing point of absorption and fluorescence emission was $E(S_1)$ = 286 kJ mol^{-1} for **7**, $E(S_1)$ = 288 kJ mol^{-1} for **8a**, $E(S_1)$ = 292 kJ mol^{-1} for **8b**, and $E(S_1)$ = 290 kJ mol^{-1} for **9**.

Studies toward an enantioselective photochemical isomerization followed by a Diels–Alder reaction were performed with 2,5-dimethylfuran as the diene component. Although enone **1** displays no distinct absorption at a wavelength $\lambda > 400$ nm, there was some notable background reaction upon irradiation with light-emitting diodes (LEDs) emitting at $\lambda_{em} \leq 437$ nm. Thus, we selected an irradiation source with an emission maximum (λ_{em} = 459 nm) that barely touched the long-wavelength absorption of the catalyst. Not surprisingly, the reaction **1** → **3e**/*ent*-**3e** was significantly slower than in the racemic case. The primary cascade products were directly taken into the benzylation reaction, and the ratio of benzyl esters **4e** and *ent*-**4e** was quantified by chiral HPLC after isolation. We were delighted to see that already at ambient temperature, there was a notable preference for one enantiomer over the other when employing 10 mol% of catalyst **7** (Table 1, entry 1). The enantioselectivity improved when decreasing the temperature to −20 °C (entry 2), but no improvement was recorded when further lowering the reaction temperature (entry 3) or when increasing the catalyst loading (entry 4). Although the product yield increased slightly when using other solvents (DCE = 1,2-dichloroethane) but dichloromethane (entries 5 and 6), the loss in selectivity made a solvent switch unattractive. Among the octahydrobinol- and spinol-derived catalysts (entries 7–10), catalyst **8a** clearly outperformed the others in terms of yield while the enantioselectivity remained similar throughout the series. The switch in the preference of *ent*-**4e** over **4e** for spinol-derived catalyst **9** was no surprise given the fact that its axis of chirality has an opposite direction than the stereogenic axis of catalysts **7** and **8**. The absolute configuration of the

Table 1: Optimization of reaction conditions for a sequence of enantioselective *E*/*Z*-isomerization, Diels–Alder reaction, and benzylation to generate enantioenriched product **4e** from cyclohept-2-enone-3-carboxylic acid (**1**).

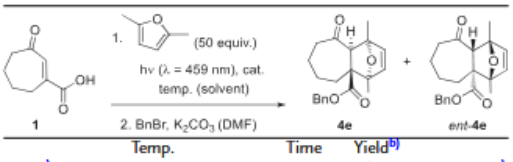

Entry[a]	Cat.	Temp. [°C]	Solvent	Time [h]	Yield[b] [%]	4e/*ent*-4e[c]
1	**7**	r.t.	CH_2Cl_2	21	33	55/45
2	**7**	−20	CH_2Cl_2	19	40	61/39
3	**7**	−40	CH_2Cl_2	23	33	58/42
4[d]	**7**	−20	CH_2Cl_2	19	33	58/42
5	**7**	−20	DCE	21	53	56/44
6	**7**	−20	PhCl	19	42	55/45
7	**8a**	−20	CH_2Cl_2	19	83	60/40
8	**8b**	−20	CH_2Cl_2	17	19	53/47
9	**8c**	−20	CH_2Cl_2	17	34	60/40
10	**9**	−20	CH_2Cl_2	16	45	41/59

[a] Optimization experiments were conducted on a 100 µmol scale under the indicated conditions with 10 mol% catalyst in a previously described set-up.[60] Irradiation was performed with an LED displaying an emission maximum at λ = 459 nm. (See Supporting Information for additional information). [b] Yield of isolated product after chromatography. [c] The ratio **4e**/*ent*-**4e** was determined by HPLC on a chiral stationary phase. [d] The reaction was conducted with 20 mol% of the catalyst.

major enantiomer was deduced from the reaction **1** → **3e**/*ent*-**3e** in the presence of catalyst **8a**. Instead of derivatizing the primary product with benzyl bromide as done in entry 7, the reaction mixture was treated with *para*-bromobenzyl bromide, delivering a mixture of products **5e**/*ent*-**5e** (vide infra). Separation of the enantiomeric bromo compounds by chiral HPLC delivered enantiomerically pure samples of both enantiomers. The minor enantiomer *ent*-**5e** gave crystals that were suitable to determine its absolute configuration by anomalous X-ray diffraction (see the Supporting Information for further details).[59]

After extensive futile experiments with other cycloheptenes (see Scheme 3) in an enantioselective sensitized photochemical isomerization, the reaction **1** → **3e** mediated by catalyst **8a** (entry 7) was a major breakthrough. It validated the so far unproven hypothesis that triplet energy transfer is a suitable vehicle to drive the reactions toward a single enantiomer. It allowed for a quantitative photochemical isomerization as opposed to previous work employing singlet energy transfer. Although the enantiomeric excess was low (20% *ee*), it seemed warranted to verify with other dienes the generality of the approach (Scheme 6). The experimental approach included the cascade reaction to compound **3** followed by benzylation of the crude mixtures. Yields and enantioselectivities were determined for benzyl esters **4**, with the former depending to some extent on the success of the benzylation reaction. 1,3-Cyclopentadiene gave product **4a** as an inseparable *endo*/*exo* mixture with a comparably high enantioselectivity for the *endo* product *endo*-**4a** (38% *ee*). The enantioselectivity

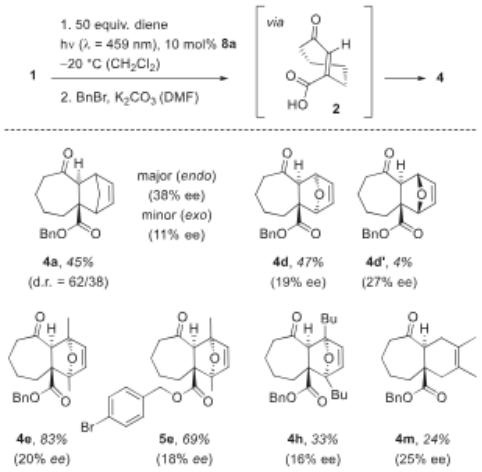

Scheme 6. Enantioselective *cis-trans* isomerization of cyclohept-2-enone-3-carboxylic acid (**1**) mediated by chiral catalyst **8a** and subsequent trapping of enantioenriched *trans*-isomer **2** by various dienes. The enantiomeric excess (*ee*) was determined after derivatization to the respective benzyl esters **4** by chiral HPLC analysis.

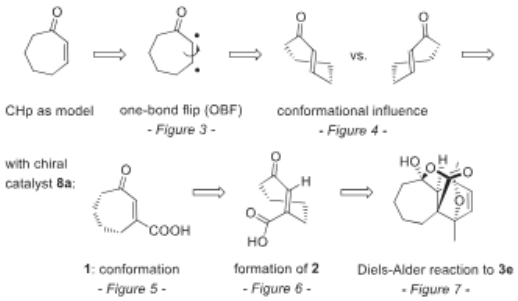

Scheme 7. Workflow of the quantum chemical studies: Cyclohept-2-enone (CHp) served as a model system to visualize the motion of substrate **1** in the complex with chiral catalyst **8a**.

of the furan cycloaddition reactions (products **4d**, **4d'**, **4e**, **5e**, **4h**) varied around the 20% *ee* previously recorded for product **4e**. The final example with 2,3-dimethylbuta-1,3-diene proceeded smoothly (product **4m**, 25% *ee*) but suffered from lower yields in the benzylation reaction.

A few additional experiments were performed to investigate the nature of the catalysis (see the Supporting Information for details). With the benzyl ester of cyclohept-2-enone-3-carboxylic acid and 2,5-dimethylfuran as the substrate, product *rac*-**4e** was obtained upon direct irradiation at $\lambda = 366$ nm (91% yield). However, a reaction of the same substrate under the optimized conditions of the sensitized irradiation (10 mol% **8a**) did not lead to any product, indicating the importance of the binding interaction exerted by the carboxylic acid but not by its ester. In the same vein, the reaction of cyclohept-2-enone-3-carboxylic acid (**1**) and 2,5-dimethylfuran proceeded cleanly upon direct irradiation in the presence of chiral phosphoric acid 3,3′-bis(2,4,6-triisopropylphenyl)-1,1′-binaphthyl-2,2′-diylhydrogenphosphat (TRIP, 50 mol%). However, upon benzylation, only the racemic Diels–Alder product *rac*-**4e** was isolated (83% yield), emphasizing the role of the pendant thioxanthone in catalyst **8a**.

While these experiments clearly supported the importance of both coordination and sensitization for a successful reaction, we felt that a deeper understanding of the photochemical isomerization could only be obtained by having a closer look at its progress by computational chemistry.

Computational results: General considerations and cyclohept-2-enones as model substrates. In order to maximize precision and to minimize computation time, we initially performed a more elaborate study with cyclohept-2-enone (CHp) as a model compound before turning toward cyclohept-2-enone-3-carboxylic acid (**1**) in the chiral setting of phosphoric acid **8a**. The goal of the computational study was to develop a comprehensive model of the reaction cascade. We focused on the high-yielding, *endo*-selective reaction **1** → **3e** mediated by catalyst **8a** to rationalize the experimentally observed enantioselectivity. While the photoinduced *cis*/*trans* isomerization of alkenes is well understood,[61] ring strain and the presence of catalyst **8a** increase the complexity of the reaction. We pursued a reductionist approach:

(a) Building on the experimental evidence (Scheme 4), the total reaction coordinate for the transformation of cycloheptene **1** to product **3e** was decomposed into an excited state coordinate (**1** to **2**/*ent*-**2**) and a ground state (S_0) coordinate (**2**/*ent*-**2** to **3e**/*ent*-**3e**), both of which were treated separately.

(b) Comparing the bond topologies of **1**, **2**/*ent*-**2**, and **3e**/*ent*-**3e**, we were able to partition the net enantioselectivity into three consecutive contributions: (i) The excited state dynamics, where two chiral depletion channels (one-bond flip [OBF]) compete directly. (ii) Non-equilibrium ground state dynamics after excited state depletion: Population, in separate enantiomeric channels, can branch between productive conversion into the *trans*-configured photoproduct **2**/*ent*-**2** or return non-productively to **1** with a *cis*-configuration. (iii) Equilibrium ground state dynamics (Diels–Alder reaction), describing the productive conversion into product **3e** or back-isomerization into **1**. Once formed, *trans*-configured species are non-interconverting, such that the relative effect of the factor (i) is expected to be larger than that of (ii) and (iii). These factors can be addressed separately, and results are presented along the order of elementary steps from **1** to **3e**.

(c) To keep the computational cost tractable, we commenced with a high-accuracy, unconstrained investigation of a non-catalyzed subsystem reaction, revealing dominant reaction pathways and identifying critical parameters modulating enantioselectivity. Subsequently, we used this knowledge to increase the system size while narrowing the full system's degrees of freedom to the essential stages only.

The presentation of computational results (Scheme 7) starts by presenting explicit dynamic simulations on the photoisomerization of the CHp model compound. The dynamic

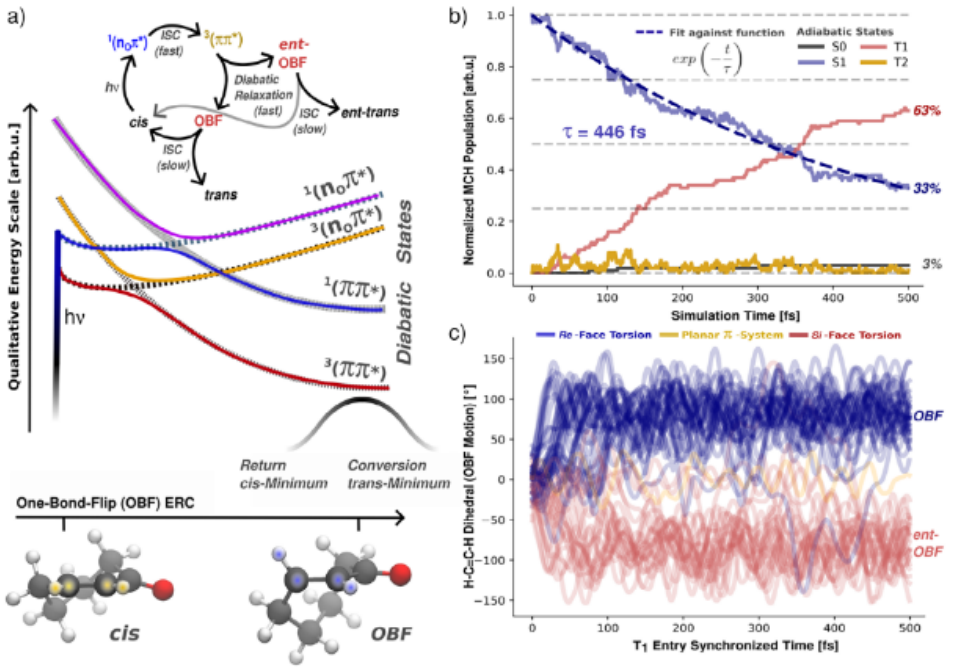

Figure 3. Results of the TSH simulations of the model system CHp. a) Sketch of the excited states T_1, S_1, T_2, and S_2 (solid-colored lines) and respective diabatic state character (dashed lines) along the ERC of OBF motion toward the dominant enantiomer in OBF-configuration. The scheme (top) illustrates the overall photoreaction cycle, which produces either the *trans* photoproduct or its enantiomer (*ent-trans*). Colored dots in the molecular structure highlight the H-C=C-H dihedral angle used to characterize the OBF motion. b) Population dynamics of TSH simulations from the initially populated S_1 state together with a global exponential fit of the dynamics. The timescale τ characterizes the ISC process toward a long-lived triplet species on T_1 via a transient, short-lived T_2 population. Population dynamics was averaged over an ensemble of 100 trajectories; all trajectories that violated various energy conservation criteria have been discarded in the analysis (for technical details, see Supporting Information). c) Evolution of the OBF motion, characterized via the H-C=C-H dihedral angle as a geometric parameter. Shown are the 66 trajectories populating the T_1 state within 500 fs. The time evolution of OBF motion is synchronized with respect to entry into the T_1 state. Trajectories were extended for an additional 500 fs after population of the T_1. The color scheme characterizes each individual trajectory according to the sign of the dihedral at the end of the simulation time. Interconversion between the faces was a rare event (two instances) and short-lived.

simulations reveal the interdependence of the dynamics along an OBF reaction coordinate and the alkyl backbone (Figures 3 and 4). This is followed by an investigation of the photoreaction of compound **1** in the presence of catalyst **8a**, rationalizing the influence exerted by hydrogen bonding (Figures 5 and 6). Finally, the catalyzed Diels–Alder ground state reaction leading to **3e** is discussed (Figure 7) and compared to the uncatalyzed reaction.

Photochemical reaction dynamics of cyclohept-2-enone (CHp). In the following, we aim to construct a model which explains the selectivity (i) from a static perspective. As we will demonstrate, this objective is met by a conformer-specific projection of the photo-reactive $^3(\pi\pi^*)$ state along an essential motion twisting the C=C double bond (OBF reaction coordinate, cf. Scheme 7). We start by introducing the electronic structure of cycloalk-2-enones. CHp was chosen as the model system for **1** due to the smaller π-system allowing for a significant reduction of computational cost. As detailed in the Supporting Information, CHp is able to recover the relevant aspects of the electronic structure and conformational distribution of **1**. The latter is relevant as we will show that interactions between the chromophore and the alkyl fragment induce *conformer-specific* asymmetry.

Cycloalk-2-enones display a complex photoreactivity, which is strongly influenced by ring size and substituent effects.[62–66] Yet, the electronic structure in the Franck–Condon (FC) region of the *cis*-configuration remains largely unaltered (Figure 3a).[67–69] Highly accurate, wave function-based XMS-CASPT2/cc-pVTZ calculations showed that the lowest singlet excited state (S_1) is always spectroscopically dark and has $^1(n_O\pi^*)$ character, followed by a bright $^1(\pi\pi^*)$ state (S_2) (see Supporting Information for the choices of active spaces).[70,71] Higher-lying states are of $^1(\pi\pi^*)$ character with significant contributions from double excitations. The energetically lower-lying triplet excited states (T_n) show the same ordering [$^3(n_O\pi^*)$ followed by $^3(\pi\pi^*)$]. For the following discussion, the nuclear motion in the excited states is expressed through *essential reaction coordinates* ([ERCs];

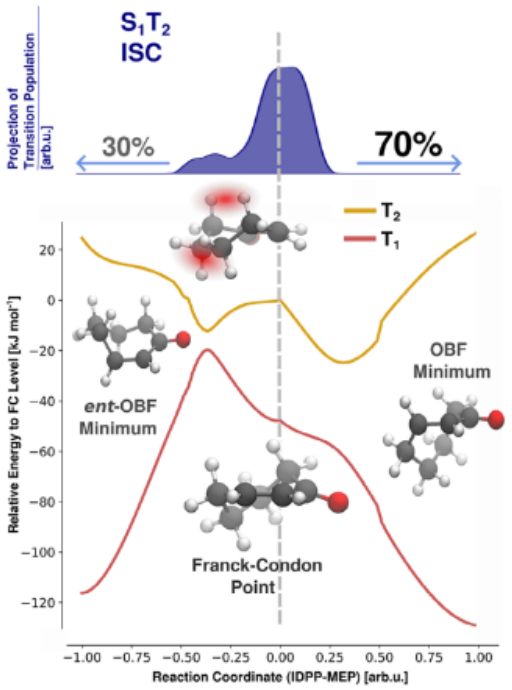

Figure 4. Fate of the chiral conformer CHp-2 formed by ISC during the surface hopping trajectories dynamics of cyclohept-2-enone (CHp). Top: Gaussian-broadened distribution of geometries at the time point of the S_1-T_2 surface hop, projected onto a vector capturing the essential motions along the *ent*-OBF/OBF reaction coordinate (see Supporting Information). The two maxima correspond to the position of the S_1T_2 crossing seam on either side. Bottom: Excited state energy landscape along an IDPP-MEP reaction coordinate from the FC geometry to either the **OBF** or ***ent*-OBF** T_1 minima. Adiabatic surfaces T_1 (red) and T_2 (yellow) are evaluated at the XMS-CASPT2 level of theory. The red shading of methylene groups (molecular inlay) highlights intramolecular repulsion between the reorganizing aliphatic methylene groups.

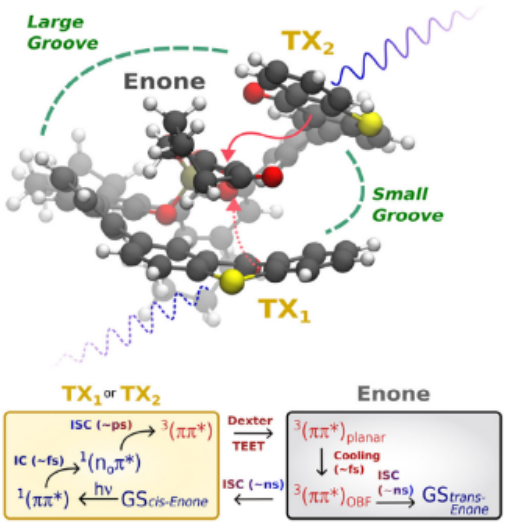

Figure 5. Model for excitation energy relaxation within the complex of cyclohept-2-enone-3-carboxylic acid (**1**) and catalyst **8a**. Top: Lowest free energy conformation of the substrate-catalyst complex, depicted at a perspective looking into the binding pocket of the sandwich motif. The asymmetric confinement forces compound **1** to adopt a chiral conformation, which predetermines the direction of the OBF. Bottom: Proposed relaxation model, starting from an initially excited state (indicated by the blue wave) on either the TX_1 or TX_2 sides of catalyst **8a** and subsequent triplet excitation energy transfer ([TEET], indicated by the red arrows) into the reactive triplet state of the enone fragment.

see the Supporting Information for a detailed description). While a Norrish type I cleavage pathway[69] is not observed for CHp, torsion about the C=C bond leads toward two chiral one-bond flip (**OBF**/*ent*-**OBF**) channels (OBF-ERC). They are responsible for *cis*-*trans*-isomerization reactions in flexible cycloalk-2-enones and were investigated in closer detail for both CHp and **1**:

Figure 3a illustrates the excited-state reaction scheme along the OBF coordinate. Starting in the *cis*-configuration of CHp (left), the bright state S_2 has $^1(\pi\pi^*)$ character, and the S_1 state has $^1(n_O\pi^*)$ character. Two triplet states, T_1 and T_2 ($^3(n_O\pi^*)$ and $^3(\pi\pi^*)$ character, respectively), are found close to S_1. Elongation of the C=O bond leads to local minima of the S_1 and T_1 states of $^1(n_O\pi^*)$ and $^3(n_O\pi^*)$ character. Close by, interaction among S_1 and T_2 states forms an energetically accessible intersection, suggesting the importance of intersystem crossing (ISC). According to El-Sayed's rules, transitions between S_1 $^1(n_O\pi^*)$ and T_2 $^3(\pi\pi^*)$ are allowed, which can subsequently lead to relaxation dynamics within the triplet manifold. In the OBF-configuration (right), minima of $^1(\pi\pi^*)$ and $^3(\pi\pi^*)$ states are found at low energies.

The role of vibrational modes in guiding the excited state relaxation cascade along these paths is essential, necessitating explicit dynamical treatment. Trajectory surface hopping (TSH) simulations allow to follow the nonadiabatic excited state dynamics in full coordinate space while retaining some quantum aspects, like the branching of population between electronic states. We performed TSH dynamics within the SHARC program suite on the XMS-CASPT2 level of theory using a cc-pVDZ basis set. Validation of the basis was performed via comparison of the energetics of stationary points to the superior cc-pVTZ basis set and via a systematic basis set expansion in static simulations to the aug-cc-pV5Z basis (a detailed description of the workflow and a validation of the basis set is provided in the Supporting Information).[72] The simulations treated the full conformer space of CHp within a *chiral* standard orientation chosen to match the chiral frame within the constraints of catalyst **8a**. The dynamics simulations were expected to allow insight into two questions: First, we needed to track electronic relaxation to discern whether the singlet or triplet manifold is the decisive relaxation channel (see Supporting Information). Second, we sought to quantify the competition of excited state depletion to S_0 and **OBF**/*ent*-**OBF** channel interconversion. With this, we discerned if

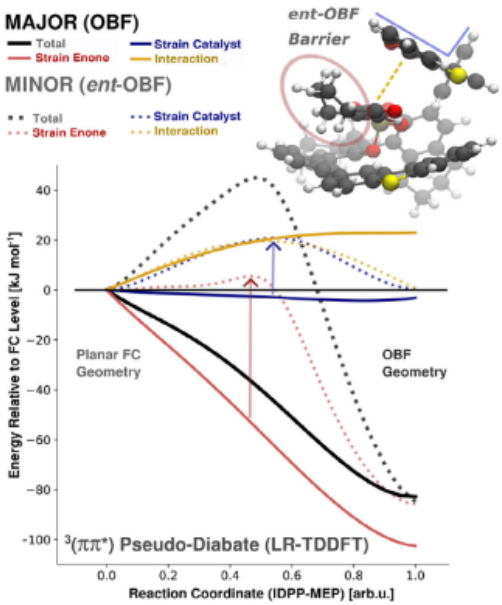

Figure 6. Excited state distortion-interaction energy decomposition analysis of the dominant chiral conformer of the **1**·**8a** complex along the IDPP-MEP reaction coordinate linking the FC geometry (planar enone configuration) with the related enone-**OBF** and enone-*ent*-**OBF** configurations. In the top right corner, the *ent*-**OBF** geometry with the highest barrier at the center of the pathway is shown. Total (black) denotes the total energy, strain enone (red) denotes repulsive contributions due to Pauli repulsion, strain catalyst (blue) denotes destabilization due to deconjugation of the π-system, and interaction (yellow) denotes van der Waals interactions in the complex.

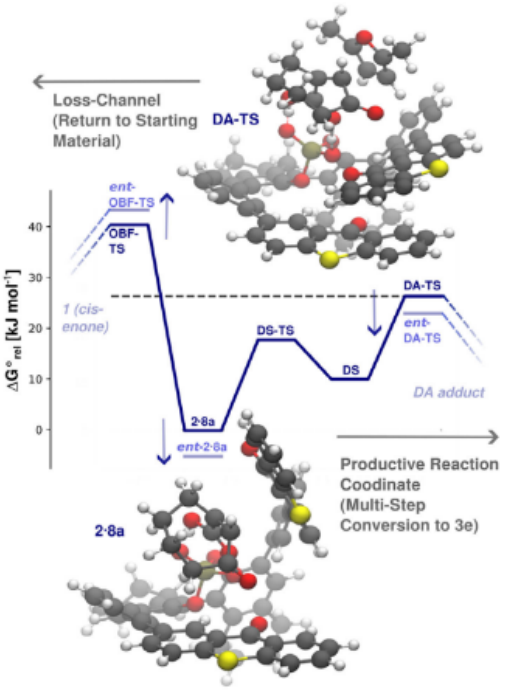

Figure 7. Computed ground state reaction pathways relative to the photochemically generated *trans*-isomers **2**/*ent*-**2** with 2,3-dimethylfuran as the reaction partner. The productive reaction coordinate describes the Diels–Alder (DA) reaction to product **3e**, whilst the loss channel describes the back-isomerization to **1**. The energy diagram presents the critical section along the reaction coordinates for the catalyzed reaction. The catalyst **8a** adds complexity due to the interconversion between a shielded conformation **2**·**8a** and a de-shielded (DS) conformation as a local minimum; the main barrier is the **DA-TS**. Comparing the major (dark blue) with the minor enantiomers (faint blue), a weak ground state selectivity is suggested that opposes the photochemical selectivity.

either the initial branching of population or the Boltzmann distribution of the OBF-conformers is relevant for estimating the enantioselectivity from the excited state dynamics [cf. factor (i)]. An ensemble of 106 independent trajectories was simulated of which 100 trajectories fulfilled all energy conservation criteria during the propagation time of 500 fs and were further employed for data analysis. Initial conditions were obtained from sampling a Wigner distribution using a restricted excitation window ($\lambda \geq 300$ nm) that reflects direct excitation conditions (cf. Scheme 4). Under these conditions, a probabilistic assignment of the initial electronic state via transition dipole moments yielded the exclusive population of the S_1 state with $^1(n_O\pi^*)$ character (see the Supporting Information for technical details). Transferred to the catalytic experimental conditions (cf. Scheme 6), where the reaction dynamics are presumably initiated by triplet energy transfer from the catalyst (see below), we consider initiating the dynamics in S_1 more realistic than initiating the dynamics in the S_2 state, which would involve substantial vibrational excess energy. Electronic relaxation commences immediately after initiation, as is evident from the evolution of state populations (Figure 3b). The S_1 state shows, after population, an exponential decay on the few hundred femtosecond timescale. The decay of S_1 is associated with the population of the T_2 state, which almost immediately relaxes into the lowest triplet T_1 state. The lifetime of the S_1 state was determined to be 446 fs (exponential fit), which is slightly faster than the previously reported value of 746 fs for cyclohexen-2-enone.[68] OBF-mediated internal conversion (IC) into S_0 is observed as a minor pathway (3%). Instead, ISC within the planar configuration space accounts for the majority of the observed S_1 population decay (IC:ISC = 5:95). The acceptor state in the triplet manifold was almost exclusively T_2, which quickly decayed into a long-lived T_1 as the end point of the excited state relaxation. Accordingly, we focused the attention on the fate of the triplet species. The simulation time for the 66 trajectories undergoing ISC was extended until a stable population of the T_1 was observed for 500 fs. This set of longer trajectories revealed that the OBF motion was the only active ERC, agreeing with the absence of Norrish type I side products (vide supra). To understand a possible preference toward

one enantiomer of *trans*-CHp, we tracked several well-defined geometric parameters. In particular, the chiral OBF-ERCs were monitored through the H–C=C–H dihedral evolution (Figure 3c; see Supporting Information for further details). Upon entry into T_1, the ensemble underwent rapid and irreversible differentiation into the **OBF** and *ent*-**OBF** channels (timescale 10 fs). This branching was observed to be asymmetric, favoring the **OBF** channel over the *ent*-**OBF** channel. In addition, the aliphatic reorganization was monitored through inversions of its dihedrals. While the conformer distribution of the S_0 was maintained throughout S_1 occupancy, it decayed toward the Boltzmann distribution of the OBF-space upon population of T_1 with an 80 fs delay on a timescale of 100 fs (see Supporting Information). The moderate timescale separation suggests an interaction between the chromophore and aliphatic fragments, investigated in the following.

Combining the observations of a very short-lived T_2 and immediate activation of the OBF-ERCs after population of T_1, the system dynamics follow the diabatic character of the $^3(\pi\pi^*)$ hypersurface (Figure 3a). As such, we suggest that the *early* branching on the $^3(\pi\pi^*)$ surface captures the excited state enantioselectivity. For the vibrationally hot **OBF** and *ent*-**OBF** channels, cross-channel interconversion was rare and the initially formed enantiomer ratio remarkably stable (Figure 3c). We thus assume that the initial T_1-branching ratio is upheld on the longer timescales of excited state depletion.[73] Intriguingly, the delay between the chromophore and response of the aliphatic skeleton indicates that the excited state dynamics may differ for each conformer. Indeed, we found large alterations for their intrinsic enantiomeric ratios (see Supporting Information).

A closer investigation was conducted for the most selective chiral conformer [CHp-2, **OBF**/*ent*-**OBF** = 70:30, corresponding to 40% *ee*], which is also dominant upon binding to the catalyst (vide infra). The critical pathway, interpolating from the S_0-FC to both T_1-**OBF** and T_1-***ent*-OBF** minima, was investigated along a reaction coordinate described as an image-dependent pair potential minimum energy path (IDPP-MEP)[74] (Figure 4; see Supporting Information for details).

Along the reaction coordinate, the surfaces of the T_1, T_2, and S_1 states (S_1 not shown) were evaluated at the XMS-CASPT2 level of theory (see Supporting Information for a detailed description).[75–77] We found that the T_1 and T_2 potential energy surfaces exhibit an asymmetry toward the **OBF** channel, which induces a biased branching of population via two mechanisms: First, a weak asymmetry on the S_1 surface shifts the population upon S_1-T_2 transition toward the ISC seam of the **OBF**-direction (Figure 4, top panel). Nevertheless, such biased preparation does not fully account for the observed ratio, as the majority of transitions occur fairly centered. Second, propagation toward the **OBF** minimum is favored via a steep gradient. The fraction of the population that moves toward this direction is rapidly steered away from the *cis*-configuration of the FC point and trapped in the **OBF** minimum (Figure 4, lower panel). In contrast, a barrier induces a slower evolution toward the *ent*-**OBF**-ERC, suggesting that the **OBF**/*ent*-**OBF** asymmetry is imposed by conformational constraints.

Overall, we deciphered the necessary conditions to explain the photochemical enantioselectivity in CHp: A time scale separation between the chromophore and alkyl reorganization is just close enough to prevent equilibration between the enantiomeric channels, such that the initial branching becomes decisive. It is, thus, sufficient to study the ground state conformer distribution and the properties of the $^3(\pi\pi^*)$ state toward the early-stage OBF-ERCs to explain the excited state selectivity. The model CHp and compound **1** vary by the COOH substitution of the enone fragment (cf. Scheme 7). Electronic structure simulations of excited states (see Supporting Information) allow to quantify the influence of the COOH group on the topology of the ERC and thus assess the influence on the initial reaction dynamics. We find that along the initial OBF reaction coordinate, the minima are preserved, but the OBF minima of **1** are slightly more stabilized. Also, the energy gap between the $^1(\pi\pi^*)$ minimum with OBF-configuration and associated S_0/S_1 crossing seams is widened, which suggests that nonradiative relaxation to the ground state is reduced. Both findings support the notion that cross-channel interconversion of the competing chiral OBF channels, found to be rare for the CHp model system, should be even more reduced in compound **1**. The model system CHp thus provides valuable insight into the early steps of the catalyzed photoreaction to be applied to a more complex substrate.

*Computational results: Isomerization of cyclohept-2-enone-3-carboxylic acid (**1**) in the chiral pocket.* In this section, we analyze the influence of the catalyst on the relaxation cascade toward an asymmetric photoproduct distribution, considering substrate **1**. The results on the model system CHp suggest the following important conditions for a high enantiomeric ratio of the **2**/*ent*-**2** intermediate: First, it is necessary to generate an asymmetric conformer distribution in the S_0. Yet, this is not sufficient for a satisfactory performance of the overall photoreaction, as a vibrationally hot ensemble could, in principle, undergo a random walk on the photoreactive surface. Thus, either vibrational cooling is required preceding the population transfer onto the enone or enhanced asymmetry along the enone's photoreactive state. To describe the complex interactions between **1** and catalyst **8a**, we follow an efficient yet accurate protocol to narrow the large conformer space. A previous study by Yepes et al. validated a combination of metadynamics sampling, ensemble optimization, and Boltzmann weight refinement for a C_2-symmetric, chiral catalyst with similarities to **8a**.[78–80] Extending beyond the work of Yepes et al., we conceived an iterative, dynamically constrained refinement of the initially obtained Boltzmann sum that succeeds in removing intruder conformers from the prescreening on the lower level of theory (see Supporting Information for a detailed description). In a similar manner to Bickelhaupt and Houk, we extended the IDPP-MEP reaction coordinate approach by a distortion-interaction energy decomposition analysis of the excited state that provides an intuitive explanation of the influence of the catalyst.[81] Comparing both the ground and excited state perspectives, our results suggest a crucial role of the flexibility of the linker segments in **8a**.

Calculations on the **1**·**8a** complex showed the clear dominance of a specific binding motif (termed the sandwich motif, top panel in Figure 5), which accounts for about 96% of the Boltzmann sum. In this motif, the substrate is bound to the phosphoric acid moiety via two hydrogen bonds. An asymmetric catalyst interaction is achieved if at least three binding anchors between the catalyst and the substrate are provided, and the hydrogen bonding interactions account for two. The third anchor is introduced by a key feature of the catalyst: The C_2-symmetry of **8a** is broken by an inward tilt of the TX_1-phenyl-linker, which allows for the thioxanthone groups (TX_1 and TX_2) to tightly fold around the binding site. Both thioxanthone groups adopt a relative perpendicular orientation, in turn generating a small and a large groove. Upon capture of **1**, the TX groups simultaneously engage in stabilizing π-π interactions with the enone moiety within the small groove (enone-TX_n-distance: ~0.35 nm), while forcing the alkyl fragment to bend into the large groove. This not only induces a chiral conformer distribution but also narrows it. Only for the CHp-2-like conformation of **1**, predicted to show an intrinsic selectivity, steric repulsion with the TX arms is minimized, and its relative Boltzmann weight increases substantially (from 56% in **1** to 94% in **1**·**8a**). Electronic excitation is spatially confined to either of the TX sites (see Supporting Information for natural transition orbital analysis). At the double-hybrid density functional level of theory (SCS-RI-ωPBEPP86), we found two nearly degenerate transitions to S_1 (359 nm, TX_1 site) and S_2 (357 nm, TX_2 site), both of which are spectroscopically accessible. Their local orbital symmetry resembles the optically allowed excited state of thioxanthone (TX). Previous studies on TX outlined an initial relaxation cascade (Figure 5, bottom right): Following excitation, a fast two-step process yields the lowest triplet state, likely via initial IC toward $^1(n_O\pi^*)$ (fs timescale) followed by ISC (ps timescale).[82] Similar timescales are expected for the complex **1**·**8a**. Accordingly, we assume that the excitation energy is transferred to the enone chromophore via short-range triplet energy transfer.[83,84] Such a mechanism is consistent with the loss of conversion upon *O*-benzylation of **1** (vide supra) and highlights the catalytic efficacy of the sandwich motif by bringing the donor and acceptor sites in close proximity. Since triplet energy transfer is an exchange-mediated process depending on orbital overlap, a transition is most likely to occur into the $^3(\pi\pi^*)$ state, preparing the substrate chromophore for photoisomerization. The potential surface of the full system (Figure 6) exhibits strong asymmetry between the enantiomeric channels, even more pronounced than observed for the CHp model (cf. Figure 4).

The favored enantiomer shows barrier-less relaxation toward the OBF channel, in agreement with the experimental outcome. Such selectivity is found to be a strain-mediated effect: Along the early OBF-ERCs (~ 0.4 Reaction Coordinate), the TX_n groups undergo a synchronous torsional motion about the C_{linker}–C_{TX} bond, maintaining π–π interactions. Hence, the interaction energies vary synchronously. The decomposition analysis suggests that the strongest contribution to the *ent*-**OBF** barrier stems from the enone fragment, and it is caused by the reorganization of the alkyl fragment. A minor contribution to the barrier further stems from a rearrangement of the catalyst. Rotation onto the **OBF** face allows the alkyl backbone of **1** to escape confinement by further bending into the large groove. In contrast, rotation onto the *ent*-**OBF** face induces a complete de-conjugation of the phenyl and TX_2 π-systems, as the latter evades the approaching, bulky alkyl fragment. These findings allow to rationalize the experimentally observed outcome: The origin of the systems' excited-state selectivity is the formation of the sandwich binding motif, which forces an asymmetric conformer space.

Computational results: Thermal Diels–Alder reaction inside the chiral pocket. What remained to be determined were selectivity effects of the equilibrium ground state dynamics [cf. factor (iii)]. In a first step, we ruled out that lactonization to **3e** occurs before the Diels–Alder reaction (see the Supporting Information for details). Rather, the lactonization is an ensuing step without any influence on the stereoselectivity. To identify critical reaction barriers for the cycloaddition, we performed a high-level assay on the achiral ground state reaction network of *trans*-isomers **2**/*ent*-**2** (see Supporting Information). The results identify productive reaction coordinates, which afford products **3e**/*ent*-**3e**, and nonproductive loss channels associated with the back-isomerization to **1**. It was found that the competition of the **OBF-TS** (TS = transition state) against the **DA-TS** is decisive at this stage of the reaction. The cycloaddition proceeds over a thermally accessible barrier and affords **3e**/*ent*-**3e** in a net exergonic cascade. In the reaction catalyzed by **8a** (Figure 7), the reorganization dynamics of both TX groups increase the complexity of the productive reaction coordinate compared to the uncatalyzed reaction. We identify decisive barriers (**DA-TS**/*ent*-**DA-TS**, **OBF-TS**/*ent*-**OBT-TS**) for both enantiomeric channels, for which the minor *ent*-**2**·**8a** network appears to be stabilized along the productive coordinate and destabilized along the loss channel.

While the calculated free energy differences of the barriers should be considered with some care, the findings suggest that the equilibrium ground state selectivity [cf. (iii)] is opposed to the photochemical selectivity of the reaction [cf. (i)]. This could explain the erratic trend observed for varying diene reaction partners (Scheme 4) and the relatively low overall enantioselectivity. The final product, **3e**/*ent*-**3e**, is sterically bulky and thus interacts poorly with the catalyst, such that it is readily exchanged for **1**. The event closes the catalytic cycle and guarantees a reasonable turnover. The prevalence of **3e** over *ent*-**3e** is a result of the excited state process.

Conclusion

In summary, we have shown for the first time that a *cis*-cycloalk-2-enone can be enantioselectively converted into its chiral *trans*-isomer. In a fundamental study employing *cis*-cyclohept-2-enone-3-carboxylic acid (**1**) as the substrate, the *trans*-isomer was identified by transient IR spectroscopy and trapped in a stereospecific Diels–Alder reaction. Proof of principle was obtained that a chiral thioxanthone with an appropriate binding cavity can induce a notable enantioselectivity. A suite of computational studies revealed the

enantioselective reaction course to be linked to a chiral recognition within the constraints of the catalyst-cycloalkenone assembly. The *cis*-isomer **1** is bound in a chiral conformation, which then translates upon energy transfer via an OBF to the chiral *trans*-isomer **2**. The computational results clearly associate the rotation around the former double bond with the first excited $^3(\pi\pi^*)$ triplet state of the enone and provide a clear picture of how the *trans*-isomer is formed. Since the reorganization of the aliphatic backbone is slower than the bond flip, the chirality transfer is high. The findings allowed access to the enantioselectivity of the process from the binding properties of various conformers of substrate **1** to the chiral phosphoric acid **8a** with two pendant thioxanthone groups. Triplet energy transfer was shown to be possible for a preferred conformation and triggers the consecutive reactions. The model so obtained (cf. Figure 6) can serve as guidance for the design of future photoisomerization mediated by chiral phosphoric acids. When studying the further course of the *trans*-isomers **2** and *ent*-**2** in the Diels–Alder reaction, it became evident that the chosen catalyst **8a** favors a preferred cycloaddition to the minor enantiomer *ent*-**2**. In other words, the enantioselectivity achieved in the photoisomerization erodes in the Diels–Alder reaction depending on which diene traps the chiral *trans*-isomer and which approach the diene takes (*endo* vs *exo*). This hypothesis is supported by the fact that the enantioselectivity varied between 16% and 38% *ee* for different dienes. *Vice versa*, it is safe to assume that the enantioselectivity obtained in the photoisomerization is at least 38% *ee*, which in turn provides an excellent reference point for further work in the area.

Acknowledgements

Financial support by the Deutsche Forschungsgemeinschaft (TRR 325; projects A5, B2, C5; 444632635) is gratefully acknowledged. The authors thank O. Ackermann, N. Pflaum, and P. Freund (all TU München) for their help with the HPLC analyses. They are grateful to Dr. S. Breitenlechner (TU München) for his advice on the preparation of the repository and to M. Lippert (TU München) for experimental assistance.

Open access funding enabled and organized by Projekt DEAL.

Conflict of Interests

The authors declare no conflict of interest.

Data Availability Statement

The data that supports the findings of this study are available in the supplementary material of this article. Primary research data are openly available in the repository RADAR4Chem at https://doi.org/10.22000/2pbrutk9aq6s1t0y.[85]

Keywords: Computational chemistry · Cycloaddition · Enantioselectivity · Isomerization · Photochemistry

[1] P. Wang, W. Xiao, J. Chen, *Nat. Rev. Chem.* **2023**, *7*, 35–50.
[2] J. S. DeHovitz, T. K. Hyster, *ACS Catal.* **2022**, *12*, 8911–8924.
[3] H. Wang, Y. Tian, B. König, *Nat. Rev. Chem.* **2022**, *6*, 745–755.
[4] T. Neveselý, M. Wienhold, J. J. Molloy, R. Gilmour, *Chem. Rev.* **2022**, *122*, 2650–2694.
[5] J. J. Molloy, T. Morack, R. Gilmour, *Angew. Chem. Int. Ed.* **2019**, *58*, 13654–13664.
[6] D. Cameron, S. Eisler, *J. Phys. Org. Chem.* **2018**, *31*, e3858.
[7] T. Arai, K. Tokumaru, *Chem. Rev.* **1993**, *93*, 23–39.
[8] S. E. Barrows, T. H. Eberlein, *J. Chem. Educ.* **2005**, *82*, 1334–1339.
[9] K. Singh, W. Trinh, J. D. Weaver III, *Org. Biomol. Chem.* **2019**, *17*, 1854–1861.
[10] P. Das, M. DeSpain, A. Ethridge, J. D. Weaver, *Org. Lett.* **2023**, *25*, 7316–7321.
[11] T. D. Schoch, J. D. Weaver, *J. Am. Chem. Soc.* **2023**, *145*, 14945–14951.
[12] M. R. J. Vallée, I. Inhülsen, P. Margaretha, *Helv. Chim. Acta* **2010**, *93*, 17–24.
[13] K. Schmidt, P. Margaretha, *Helv. Chim. Acta* **2012**, *95*, 423–427.
[14] Y. Inoue, T. Yokoyama, N. Yamasaki, A. Tai, *Nature* **1989**, *341*, 225–226.
[15] R. Hoffmann, Y. Inoue, *J. Am. Chem. Soc.* **1999**, *121*, 10702–10710.
[16] Y. Inoue, H. Ikeda, M. Kaneda, T. Sumimura, S. R. L. Everitt, T. Wada, *J. Am. Chem. Soc.* **2000**, *122*, 406–407.
[17] R. Maeda, T. Wada, T. Mori, S. Kono, N. Kanomata, Y. Inoue, *J. Am. Chem. Soc.* **2011**, *133*, 10379–10381.
[18] D. P. Schwinger, M. T. Peschel, C. Jaschke, C. Jandl, R. de Vivie-Riedle, T. Bach, *J. Org. Chem.* **2022**, *87*, 4838–4851.
[19] D. P. Schwinger, T. Pickl, T. Bach, *J. Org. Chem.* **2023**, *88*, 12844–12852.
[20] D. P. Schwinger, T. Bach, *Acc. Chem. Res.* **2020**, *53*, 1933–1943.
[21] J. Großkopf, T. Kratz, T. Rigotti, T. Bach, *Chem. Rev.* **2022**, *122*, 1626–1653.
[22] E. J. Corey, M. Tada, R. LaMahieu, L. Libit, *J. Am. Chem. Soc.* **1965**, *87*, 2051–2052.
[23] P. E. Eaton, K. Lin, *J. Am. Chem. Soc.* **1965**, *87*, 2052–2054.
[24] R. Bonneau, J. Joussot-Dubien, J. Yarwood, J. Pereyre, *Tetrahedron Lett. 18*, **1977**, 235–238.
[25] R. Bonneau, P. Forner de Violet, J. Joussot-Dubien, *Nouv. J. Chim.* **1977**, *1*, 31–34.
[26] Y. Inoue, T. Ueoka, T. Kuroda, T. Hakushi, *J. Chem. Soc., Chem. Commun.* **1981**, 1031–1033.
[27] Y. Inoue, T. Ueoka, T. Kuroda, T. Hakushi, *J. Chem. Soc., Perkin Trans. 2* **1983**, 983–988.
[28] Y. Inoue, S. Hagiwara, Y. Daino, T. Hakushi, *J. Chem. Soc., Chem. Commun.* **1985**, 1307–1309.
[29] G. V. Hartland, W. Xie, H.-L. Dai, A. Simon, M. J. Anderson, *Rev. Sci. Instrum.* **1992**, *63*, 3261–3267.
[30] J. Torres-Alacan, U. Das, A. C. Filippou, P. Vöhringer, *Angew. Chem. Int. Ed.* **2013**, *52*, 12833–12837.
[31] H. E. Wagner, P. Di Martino-Fumo, P. Boden, M. Zimmer, W. Klopper, F. Breher, M. Gerhards, *Chem. Eur. J.* **2020**, *26*, 10743–10751.
[32] For selected Diels-Alder reactions of trans-cyclohept-2-enones see: refs. [22, 23].
[33] H. Shinozaki, S. Arai, M. Tada, *Bull. Chem. Soc. Jpn.* **1976**, *49*, 821–822.
[34] H. Dorr, V. H. Rawal, *J. Am. Chem. Soc.* **1999**, *121*, 10229–10230.
[35] J. Nikolai, Ø. Loe, P. M. Dominiak, O. O. Gerlitz, J. Autschbach, H. M. L. Davies, *J. Am. Chem. Soc.* **2007**, *129*, 10763–10772.
[36] S. Ghosh, S. Bose, A. Jana, A. Nijamudheen, A. Datta, *Tetrahedron* **2014**, *70*, 9783–9790.

[37] R.-B. Wang, S.-G. Ma, C. S. Jamieson, R.-M. Gao, Y.-B. Liu, Y. Li, X.-J. Wang, Y.-H. Li, K. N. Houk, J. Qu, S.-S. Yu, *Chem. Sci.* **2021**, *12*, 7003–7011.
[38] Supplementary crystallographic data for *rac*-**3a** have been deposited with the Cambridge Crystallographic Data Centre (CCDC 2409855).
[39] Supplementary crystallographic data for *rac*-**3e** have been deposited with the Cambridge Crystallographic Data Centre (CCDC 2409858).
[40] Supplementary crystallographic data for *rac*-**4e** have been deposited with the Cambridge Crystallographic Data Centre (CCDC 2409856).
[41] F. M. Harvey, A. H. Heidecker, C. Merten, T. Bach, *Org. Biomol. Chem.* **2023**, *21*, 4422–4428.
[42] F. Pecho, Y.-Q. Zou, J. Gramüller, T. Mori, S. M. Huber, A. Bauer, R. M. Gschwind, T. Bach, *Chem. Eur. J.* **2020**, *26*, 5190–5194.
[43] F. Pecho, Y. Sempere, J. Gramüller, F. M. Hörmann, R. M. Gschwind, T. Bach, *J. Am. Chem. Soc.* **2021**, *143*, 9350–9354.
[44] J. Lyu, A. Claraz, M. R. Vitale, C. Allain, G. Masson, *J. Org. Chem.* **2020**, *85*, 12843–12855.
[45] R. Takagi, T. Tanimoto, *Org. Biomol. Chem.* **2022**, *20*, 3940–3947.
[46] For selected examples of chiral phosphoric acid derivatives in enantioselective photocatalysis see: R. S. J. Proctor, H. J. Davis, R. J. Phipps, *Science* **2018**, *360*, 419–422 and refs. [47–54].
[47] Z. C. Girvin, L. F. Cotter, H. Yoon, S. J. Chapman, J. M. Mayer, T. P. Yoon, S. J. Miller, *J. Am. Chem. Soc.* **2022**, *144*, 20109–20117.
[48] R. Takagi, C. Tabuchi, *Org. Biomol. Chem.* **2020**, *18*, 9261–9267.
[49] M. J. Genzink, M. D. Rossler, H. Recendiz, T. P. Yoon, *J. Am. Chem. Soc.* **2023**, *145*, 19182–19188.
[50] T. Uchikura, K. Takahashi, T. Oishi, T. Akiyama, *Org. Biomol. Chem.* **2023**, *21*, 9138–9142.
[51] Q. Fu, S. Cao, J. Wang, X. Lv, H. Wang, X. Zhao, Z. Jiang, *J. Am. Chem. Soc.* **2024**, *146*, 8372–8380.
[52] J. Wang, Q. Fu, S. Cao, X. Lv, Y. Yin, X. Ban, X. Zhao, Z. Jiang, *J. Am. Chem. Soc.* **2024**, *146*, 22840–22849.
[53] Y. Liu, M. Chu, X. Li, Z. Cao, X. Zhao, Y. Yin, Z. Jiang, *Angew. Chem. Int. Ed.* **2024**, *63*, e202411236.
[54] S. B. Cahoon, S. J. Chapman, T. A. Fiala, M. J. Genzink, T. P. Yoon, *J. Org. Chem.* **2024**, *89*, 17615–17620.
[55] T. Kratz, P. Steinbach, S. Breitenlechner, G. Storch, C. Bannwarth, T. Bach, *J. Am. Chem. Soc.* **2022**, *144*, 10133–10138.
[56] For general reviews on enantioselective photochemical reactions see: M. J. Genzink, J. B. Kidd, W. B. Swords, T. P. Yoon, *Chem. Rev.* **2022**, *122*, 1654–1716 and refs. [57, 58].
[57] C. Prentice, J. Morrisson, A. D. Smith, E. Zysman-Colman, *Beilstein J. Org. Chem.* **2020**, *16*, 2363–2441.
[58] M. Silvi, P. Melchiorre, *Nature* **2018**, *554*, 41–49.
[59] Supplementary crystallographic data for *ent*-**5** have been deposited with the Cambridge Crystallographic Data Centre (CCDC 2409857).
[60] D. Lenhart, A. Bauer, A. Pöthig, T. Bach, *Chem. - Eur. J.* **2016**, *22*, 6519–6523.
[61] A. Nenov, R. de Vivie-Riedle, *J. Chem. Phys.* **2011**, *135*, 034304.
[62] For selected early examples of photochemical transformations of strained cycloalk-2-enones see: P. E. Eaton, T. W. J. Cole, *J. Am. Chem. Soc.* **1964**, *86*, 3157–3158 and refs. [63–66].
[63] D. I. Schuster, A. C. Fabian, *Tetrahedron Lett.* **1966**, *7*, 4093–4098.
[64] L. L. Barber, O. L. Chapman, L. D. Lassila, *J. Am. Chem. Soc.* **1969**, *91*, 3664–3665.
[65] H. E. Zimmermann, K. G. Hancock, *J. Am. Chem. Soc.* **1968**, *90*, 3749–3760.
[66] W. C. Agosta, A. B. I. Smith, A. S. Kende, R. G. Eilerman, J. Benham, *Tetrahedron Lett.* **1969**, *10*, 4517–4520.
[67] X. Chen, Z. Rinkevicius, Y. Luo, H. Ågren, Z. Cao, *J. Chem. Phys. A* **2011**, *115*, 7815–7822.
[68] M. T. Peschel, P. Kabacinski, D. P. Schwinger, E. Thyrhaug, G. Cerullo, T. Bach, J. Hauer, R. de Vivie-Riedle, *Angew. Chem. Int. Ed.* **2021**, *60*, 10155–10163.
[69] N. Jeremias, M. T. Peschel, C. Jaschke, R. de Vivie-Riedle, T. Bach, *J. Org. Chem.* **2023**, *88*, 6294–6303.
[70] T. H. Dunning Jr., *J. Chem. Phys.* **1989**, *90*, 1007–1023.
[71] T. Shiozaki, W. Győrffy, P. Celani, H.-J. Werner, *J. Chem. Phys.* **2011**, *135*, 081106.
[72] S. Mai, P. Marquetand, L. González, *Int. J. Quant. Chem.* **2015**, *115*, 1215–1231.
[73] R. Bonneau, *J. Am. Chem. Soc.* **1980**, *102*, 3816–3822.
[74] S. Smidstrup, A. Pedersen, K. Stokbro, H. Jónsson, *J. Chem. Phys.* **2014**, *140*, 214106.
[75] F. Weigend, R. Ahlrichs, *Phys. Chem. Chem. Phys.* **2005**, *7*, 3297–3305.
[76] S. Grimme, A. Hansen, S. Ehlert, J.-M. Mewes, *J. Chem. Phys.* **2021**, *154*, 064103.
[77] M. Casanova-Pácz, L. Goerigk, *J. Chem. Theory Comput.* **2021**, *17*, 5165–5186.
[78] D. Yepes, F. Neese, B. List, G. Bistoni, *J. Am. Chem. Soc.* **2020**, *142*, 3613–3625.
[79] C. Bannwarth, S. Ehlert, S. Grimme, *J. Chem. Theory Comput.* **2019**, *15*, 1652–1671.
[80] S. Grimme, *J. Chem. Theory Comput.* **2019**, *15*, 2847–2862.
[81] F. M. Bickelhaupt, K. N. Houk, *Angew. Chem. Int. Ed.* **2017**, *56*, 10070–10086.
[82] R. Mundt, T. Villnow, C. T. Ziegenbein, P. Gilch, C. Marian, V. Rai-Constapel, *Phys. Chem. Chem. Phys.* **2016**, *18*, 6637–6647.
[83] D. L. Dexter, *J. Chem. Phys.* **1953**, *21*, 836–850.
[84] Z.-Q. You, C.-P. Hsu, *Int. J. Quantum Chem.* **2014**, *114*, 102–115.
[85] M. Stierle, C. Jaschke, D. J. Grenda, M. Peschel, T. Pickl, N. Gessner, P. Nuernberger, B. P. Fingerhut, C. Ochsenfeld, R. de Vivie-Riedle, T. Bach, Dataset for Publication "Enantioselective Photochemical Generation of a Short-Lived, Twisted Cycloheptenone Isomer: Catalytic Formation, Detection, and Consecutive Chemistry". RADAR4Chem; **2025**, https://doi.org/10.22000/2pbrutk9aq6s1t0y.

Manuscript received: January 17, 2025
Revised manuscript received: April 01, 2025
Accepted manuscript online: April 01, 2025
Version of record online: April 21, 2025

6. Photochemical Deracemization of 2,3-Allenoic Acids Mediated by a Sensitizing Chiral Phosphoric Acid Catalyst

Title:	"Photochemical deracemization of 2,3-allenoic acids mediated by a sensitizing chiral phosphoric acid catalyst"
Status:	Edge Article, published online September 22, 2025
Journal:	*Chem. Sci.* **2025**, DOI: 10.1039/d5sc05356k
Publisher:	Royal Society of Chemistry
DOI:	doi.org/10.1039/d5sc05356k
Authors:	Max Stierle, Daniel Bitterlich, Julia Westermayr, Thorsten Bach

Content: Seven photochemically active chiral phosphoric acids bearing a thioxanthone chromophore were synthesized and evaluated as catalysts in the photochemical deracemization of 2,4-disubstituted 2,3-allenoic acids. For the best performing catalyst 2-benzyl-4-*tert*-butyl-2,3-allenoic acids were obtained in 58-97% yield and with enantiomeric ratios between 71/29 and 85/15. The products were determined to be (*R*)-configured, and a mechanistic picture for the observed reaction outcome was developed based on quantum-chemical and experimental studies. The synthetic utility of the obtained axially chiral acids was demonstrated by consecutive reactions leading to products with point chirality.

M. Stierle and T. Bach developed the project. M. Stierle planned and executed all synthetic experiments. D. Bitterlich performed all computational work. T. Bach and J. Westermayr supervised the research and acquired funding. The manuscript was written with contributions from all authors.

Chemical Science

ROYAL SOCIETY OF CHEMISTRY

EDGE ARTICLE

View Article Online
View Journal

Cite this: DOI: 10.1039/d5sc05356k

All publication charges for this article have been paid for by the Royal Society of Chemistry

Photochemical deracemization of 2,3-allenoic acids mediated by a sensitizing chiral phosphoric acid catalyst

Max Stierle,[a] Daniel Bitterlich,[b] Julia Westermayr[bc] and Thorsten Bach*[a]

Photochemistry opens the possibility to convert a racemic mixture of a chiral compound into a distinct enantiomer in a single operation. Seven chiral phosphoric acids with a pendant thioxanthone chromophore were synthesized and evaluated as catalysts for the visible light-driven deracemization of 2,4-disubstituted 2,3-allenoic acids. A catalyst derived from 1,1′-spirobiindane-7,7′-diol (spinol) performed best and delivered 2-benzyl-4-*tert*-butyl-2,3-allenoic acids in 58–97% yield and with enantiomeric ratios (e.r.) varying between 71/29 and 85/15 depending on the benzyl substitution pattern. The major enantiomer was shown to be (*R*)-configured, and other 2,3-allenoic acids were also probed in the reaction. A mechanistic scenario for the observed enantioselectivity is provided that rests on experimental and quantum-chemical studies.

Received 18th July 2025
Accepted 22nd September 2025

DOI: 10.1039/d5sc05356k

rsc.li/chemical-science

Introduction

Since racemates of chiral compounds are typically available at a lower cost than enantiomerically pure compounds, extensive efforts have been undertaken to resolve racemic mixtures. A wide arsenal of separation techniques has become available to obtain the two enantiomers of a given chiral compound with high purity.[1] Alternatively, it is possible to differentiate two enantiomers in a racemic mixture by kinetic resolution. Typically, chiral catalysts, often enzymes,[2] are employed to involve one enantiomer in a chemical transformation while the other enantiomer remains unchanged. For the preparation of enantiopure carboxylic acid derivatives, a kinetic resolution reaction frequently involves either an esterification or an ester hydrolysis.[3] Since ester and carboxylic acid are easily interconvertible, the process can be iterated, eventually leading to a single enantiomer. Alternatively, kinetic resolution reactions can be performed under conditions which allow for an equilibration of the two enantiomers (dynamic kinetic resolution),[4] thus facilitating complete conversion of a racemic mixture into an enantioenriched or enantiopure product.

Allenes (1,2-propadienes) display an axis of chirality if they carry two sets of different substituents at their terminal carbon atoms. The compound class has received great interest due to its high synthetic utility and its potential for creating chiral structures with a defined absolute configuration.[5] In the latter context, 2,4-disubstituted 2,3-allenoic acids invite kinetic resolutions by enzyme catalysis starting from an ester precursor. Pioneering work by Jones and co-workers[6] revealed that enantioenriched 2,3-allenoic acids **1** can be obtained by hydrolysis of the respective allenoate (Scheme 1). Ethyl ester *rac*-**2a** was reported to deliver the (*S*)-configured allenoic acid in a low, yet detectable enantiomeric ratio (e.r.) of 53.5/46.5.

While subsequent work with wild-type enzymes delivered improved results,[7] major breakthroughs were not achieved

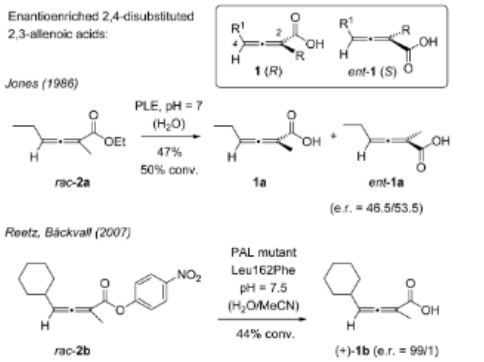

Scheme 1 Enantioenriched 2,4-disubstituted 2,3-allenoic acids (**1**) obtained by enzymatic kinetic resolution of racemic esters **2**. PLE = pig liver esterase. PAL = *Pseudomonas aeruginosa* lipase.

[a]*Technische Universität München, School of Natural Sciences, Department of Chemistry and Catalysis Research Center, Lichtenbergstrasse 4, 85747 Garching, Germany. E-mail: thorsten.bach@ch.tum.de; Web: https://www.ch.nat.tum.de/en/oc1/home/*

[b]*Leipzig University, Wilhelm-Ostwald-Institute for Physical and Theoretical Chemistry, Linnéstraße 2, 04103 Leipzig, Germany*

[c]*Center for Scalable Data Analytics and Artificial Intelligence (ScaDS.AI), Leipzig/Dresden, Humboldtstraße 25, 04105 Leipzig, Germany*

before directed evolution was applied to allenoate hydrolysis. The Reetz and the Bäckvall laboratories engineered a lipase by site-specific mutagenesis which processes almost exclusively one enantiomer of ester *rac*-**2b** to provide product (+)-**1b** with an excellent e.r.[8] Although a method for the racemization of allenoates had been previously reported,[9] a dynamic kinetic resolution was to the best of our knowledge never applied to the preparation of enantioenriched 2,4-disubstituted 2,3-allenoic acids. Despite the development of highly powerful alternative kinetic resolution methods,[10,11] there is no direct access to this compound class that allows for a complete conversion of the respective racemate to a single enantiomer.

Given our interest in photochemical deracemization reactions of allenes and related axially chiral compounds,[12,13] we considered possible catalyst designs to be applicable to chiral 2,3-allenoic acids. Deracemization promises the complete conversion of a racemic mixture to a given enantiomer under photochemical conditions.[14] A suitable photocatalyst requires a binding motif for the carboxylic acid group and needs to display chromophores that induce the desired deracemization event. From previous work, it was known that thioxanthones are competent to facilitate promotion of allenes into their triplet state,[12a,c] which in turn suggested that a catalyst with suitably placed thioxanthones[15] might enable the required differentiation of enantiomeric starting materials (*vide infra*). We now report on the synthesis of new chiral phosphoric acid-based[16] thioxanthone catalysts[17,18] and their application to the photochemical deracemization of 2,4-disubstituted 2,3-allenoic acids (**1**). A catalyst derived from 1,1′-spirobiindane-7,7′-diol (spinol) evolved as best suited for this purpose, and its mode of action was studied in more detail by mechanistic and quantum-chemical investigations.

Results and discussion

Preliminary experiments were performed with chiral allenoic acid *rac*-**1c**, which was irradiated with light of fluorescent lamps at an emission maximum of $\lambda = 420$ nm (for details see the SI). At this wavelength, the allenoic acid is transparent, while thioxanthones typically absorb visible light in the blue region of the electromagnetic spectrum ($\lambda \leq 450$ nm). Since separation of the two enantiomers of *rac*-**1c** by chiral HPLC was not feasible, the acid was converted into its methyl ester by treatment with trimethylsilyldiazomethane (TMS = trimethylsilyl). The methyl ester enantiomers **2c** and *ent*-**2c** were separable and allowed for an assessment of their relative ratio by chiral HPLC (Scheme 2). Initial experiments were performed with previously reported chiral phosphoric acids, which were derived from 1,1′-bi-2-naphthol (binol, **3a**),[18] 5,5′,6,6′,7,7′,8,8′-octahydro-1,1′-bi-2-naphthol (octahydrobinol, **3b** and **3d**)[19] or 1,1′-spirobiindane-7,7′-diol (spinol, **3c**).[19] At first sight, the outcome of the reactions was disappointing because there was no significant preference for one of the two enantiomers. Even prolonged irradiation did not lead to an improvement. On the positive side, we noted that the spinol-based catalyst **3c** outperformed the related catalysts **3a** and **3b**, and that it seemed beneficial to move the thioxanthone chromophore closer to the chiral

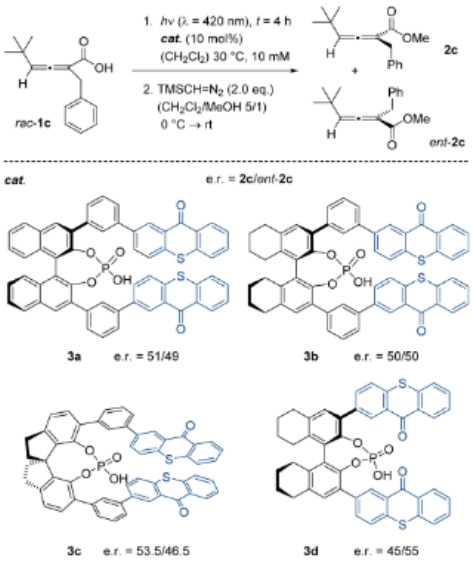

Scheme 2 Photochemical deracemization attempts performed with 2,3-allenoic acid *rac*-**1c** and known catalysts **3a–3d**. The acid was methylated to determine the enantiomeric ratio (e.r.) by chiral HPLC analysis.

backbone. In catalysts **3a–3c**, a *meta*-substituted phenyl group acts as a hinge connecting the chromophore with the phosphoric acid, while the chromophore is directly attached to the chiral backbone in catalyst **3d**. The results indicated that it might be beneficial to prepare new spinol-based catalysts to which thioxanthone was directly attached at the 6- and 6′-positon of the biindane skeleton.

The synthesis of the spinol derivatives commenced with the respective mono- or diiodinated precursors **4a**[20] and **4b**,[21] the hydroxy groups of which were protected by methoxymethyl (MOM) substituents (Fig. 1). Subsequent Pd-catalysed cross-coupling with known boronates **5a**[17c] and **5b**[22] was immediately followed by removal of the MOM protecting groups and formation of the respective phosphates **3e–3g**.

Catalyst **3e** was obtained in an overall yield of 52%. The reaction to the 6,6′-disubstituted catalysts **3f** (48% overall) and **3g** (72% overall) turned out to be equally efficient, but the separation from impurities proved tedious in all cases. The performance of the catalysts notably improved when compared to the previous results obtained with catalysts **3a–3d** in the photochemical deracemization. Particularly, the two-fold thioxanthone-substituted catalyst **3f** combined a good enantiodiscrimination in the reaction of chiral acid *rac*-**1c** (e.r. = 76/24) with good availability on larger scale. Further optimisation experiments were consequently performed with the latter catalyst (Table 1). By choosing different reaction times (entries 1–4), it was confirmed that the photostationary state was

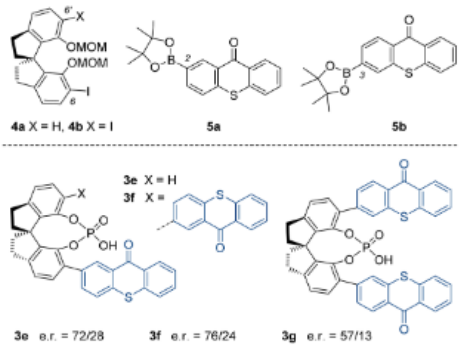

Fig. 1 Starting materials **4–5** (top) required for the synthesis of spinol-based chiral phosphoric acids **3e–3g**. The e.r. refers to the enantiomeric ratio obtained with the respective catalyst in the photochemical deracemization of 2,3-allenoic acid *rac*-**1c** (*cf.* Scheme 2).

Table 1 Reaction optimisation for the photochemical deracemization of 2,3-allenoic acid *rac*-**1c** catalyzed by chiral Brønsted acid **3f** (*cf.* Scheme 2 and Fig. 1)

entry[a]	3f [mol%]	Solvent	T [°C]	t [h]	Yield	e.r.[b]
1	10	CH_2Cl_2	30	4	Quant	76/24
2	10	CH_2Cl_2	30	2	Quant	74/26
3	10	CH_2Cl_2	30	6[c]	Quant	75/25
4	10	CH_2Cl_2	30	22	78%	70/30
5[c]	10	CH_2Cl_2	30	4	88%	74/26
6[d]	10	CH_2Cl_2	30	4	93%	76/24
7	5	CH_2Cl_2	30	4	Quant	73/27
8	20	CH_2Cl_2	30	4	96%	74/26
9	10	CH_2Cl_2	−10	4	97%	82/18
10	10	CH_2Cl_2	−40	4	Quant	80/20
11[e]	10	CH_2Cl_2	−10	4	97	79/21
12	10	DCE[f]	30	4	96%	58/42
13	10	Toluene	30	4	Quant	65/35
14	10	Acetone	30	4	97%	51/49
15	10	TFT[g]	30	4	89%	72/28
16	10	HFX[h]	30	4	87%	75/25

[a] Unless otherwise noted, the reactions were performed at a substrate concentration of $c = 10$ mM. The product was isolated as its methyl ester **2c**/*ent*-**2c**. [b] The enantiomeric ratio (e.r.) was determined after methylation by chiral-phase HPLC analysis. [c] $c = 5$ mM. [d] $c = 20$ mM. [e] The irradiation was performed at $\lambda = 440$ nm. [f] 1,2-Dichloroethane. [g] Trifluorotoluene. [h] 1,3-Bis(trifluoromethyl)benzene.

reached after an irradiation time of four hours. There was no improvement of the e.r. at longer reaction times.

The influence of the substrate concentration (c) was probed by changing the concentration to $c = 5$ mM (entry 5) and $c = 20$ mM (entry 6), respectively. There was no notable change which is why a concentration of $c = 10$ mM was routinely chosen. Likewise the catalyst loading (entries 7, 8) had little influence on the reaction outcome and the loading was kept at 10 mol%. The most significant parameter leading to an improvement of the enantioselectivity was the reaction temperature. At −10 °C, the e.r. increased to 82/18 (entry 9) but there was no further increase upon lowering the temperature to −40 °C (entry 10). Since the fluorescent light bulbs display a relative broad emission spectrum, other light sources with a narrower emission band were tested. One example is included in Table 1 (entry 11). Here, a light emitting diode (LED) with an emission maximum at $\lambda = 440$ nm was used. The outcome was somewhat inconsistent, possible due to the little overlap between emission and absorption by the catalyst (*vide infra*). On average, neither yield nor e.r. improved notably when choosing other light sources (see the SI for details). The choice of solvent was limited by the solubility of the chiral Brønsted acid. All tested solvents (entries 12–16) turned out to be inferior to dichloromethane, and we selected the conditions of entry 9 to study different substrates in photochemical deracemization reactions mediated by catalyst **3f**.

Initial substrate modifications concerned primarily the substituent in 2-position. Diversely substituted phenyl groups were probed at the benzylic position and it was shown that the protocol was compatible with alkyl (**1g**, **1i**, **1j**), fluoro (**1d**), chloro (**1o**), bromo (**1e**), iodo (**1f**), alkylsulfanyl (**1h**), phenyl (**1k**), cyano (**1l**) and alkoxy (**1m**) substituents (Scheme 3). In some cases, the ratio of the acid enantiomers could not be directly assessed, and the acid was converted into the respective methyl ester. Yields were consistently high but decreased for strongly electron deficient (**1p**) and electron rich (**1n**) substituents.

Although steric bulk at the 2-benzyl substituent did not change the enantioselectivity of the deracemization, as seen for example in the reaction of *rac*-**1j**, the 1-naphthyl group led to a notable decrease in e.r. (product **1q**). It was possible to scale-up the reaction, and an improved yield was recorded when running the reactions on larger scale. For instance, acid **1f** was obtained in 94% yield when the reaction was run on 0.5 mmol scale while the small-scale reaction (50 μmol) gave only a yield of 76%. Catalyst recovery was feasible, and 70% of the catalyst was re-isolated in the mentioned 0.5 mmol scale reaction.

In general, the free acids elute relatively slowly from column, and some product was likely lost because it was too diluted for detection in late fractions or it remained on column. The issue was particularly relevant on small scale, and the lower yields for cases in which the acids were isolated are partially due to their high polarity. For example, product **1l** was obtained in only 64% as the acid, but the yield was 95% for the methyl ester **2l** under otherwise identical reaction conditions.

Expectedly, the size of the substituents in 2- and 4-position plays a significant role in the enantiomer discrimination by the catalyst. If the size of the substituent R^1 at C4 was decreased, the e.r. of the product acid was lower than for standard substrate **1c** (R^1 = *tert*-butyl). The methyl-substituted acid **1r** (R^1 = methyl) was obtained in a comparably low e.r. of 65/35. When increasing the steric bulk of R^1, the e.r. improved as seen for **1s**, **1t**, and **1u**. Likewise, small groups R at position C2 led to relatively low enantioselectivity (Scheme 4).

For R = H (**1v**) and R = methyl (**1w**), the e.r. was lower than for the standard substrate **1c** with R = benzyl. A dimethylallyl group at C2, however, seems to mimic the benzyl group well, and acid **1x** was successfully deracemized in good yield (85%,

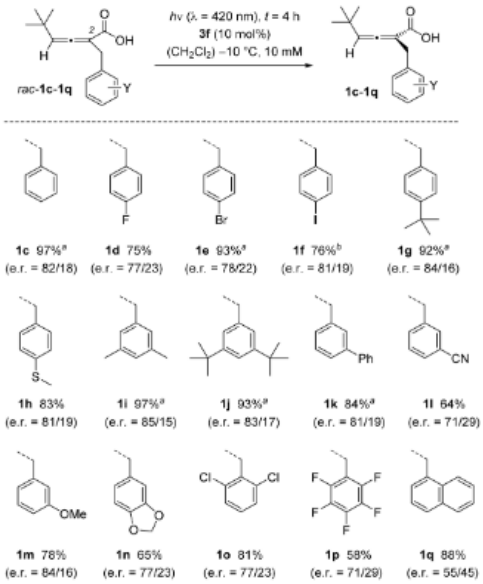

Scheme 3 Photochemical deracemization of 2,3-allenoic acids *rac*-**1c** to *rac*-**1q** as catalysed by chiral Brønsted acid **3f** (50 μmol scale). [a] Yield and e.r. of the product were obtained after methyl ester formation as described in Scheme 2. [b] When performed on 0.5 mmol scale the yield was 94% (e.r. = 80/20).

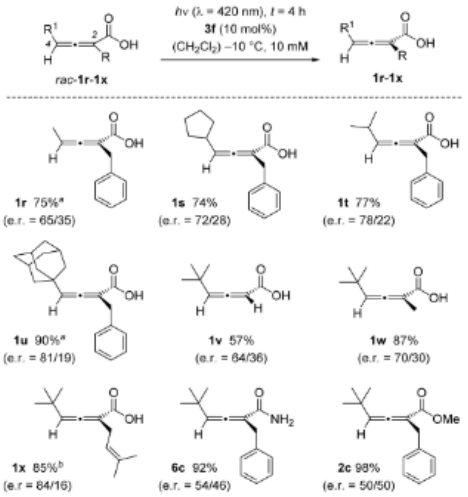

Scheme 4 Influence of substitution and binding motif on the outcome of the photochemical deracemization of 2,3-allenoic acids *rac*-**1r** to *rac*-**1x** and of allenoic acid derivatives *rac*-**6c** and *rac*-**2c**. [a] Yield and e.r. of the product were obtained after methyl ester formation as described in Scheme 2. [b] Yield of the isolated carboxylic acid, the e.r. was determined after primary amide formation.

e.r. = 84/16). Phenyl groups in position C2 or C4 of the allene lead to a bathochromic shift of the UV/Vis absorption which likely invites a direct excitation and hampers the enantioselectivity in an attempted deracemization reaction (see the SI for details). Although an association of the carboxylic acid to the catalyst by hydrogen bonding was assumed to be an integral part of the mode of action, we confirmed the critical influence of the binding site by subjecting other allenoic acid derivatives to the deracemization conditions. Both amide *rac*-**6c** and ester *rac*-**2c** resulted in low or no enantioselectivity.

The absolute configuration of the products was established by comparison with authentic material of known configuration. Enantioenriched acid **1f** was converted to amide **6f** which was shown by chiral HPLC analysis to exist as an 80/20 mixture of enantiomers **6f**/*ent*-**6f**. The absolute configuration of minor enantiomer *ent*-**6f** was known from previous work.[12c] On chiral HPLC, the enantiomers are baseline separated which allowed to assign the absolute configuration of the stereogenic axis as (*R*). The same exercise was performed for acid **1h** confirming the assignment. All other configuration assignments were based on analogy with the major enantiomer being (*R*)-configured (Scheme 5).

Mechanistically, the configurational instability of allenes **1** seems to be the result of a sensitized excitation leading to an achiral triplet intermediate.[23] Experiments with enantioenriched (scalemic) substrate **1f** (e.r. = 80/20) performed at λ = 440 nm and at $T = -10$ °C showed the compound to be configurationally stable. If achiral thioxanthen-9-one was added and the reaction was performed under otherwise unchanged conditions (Scheme 6) a slight but clearly detectable racemization was observed. The most likely scenario to account for the racemization is a sensitization by thioxanthen-9-one, the triplet energy [$E(T_1)$] of which has been determined as $E(T_1)$ = 274 kJ mol^{-1} (77 K, methylcyclohexane-isopentane).[24] The intermediate allene-derived diradical **7f**[25] is achiral and reforms statistically either one of the two product enantiomers **1f** and *ent*-**1f**. The only small e.r. change is attributed to the low absorption coefficient ε of thioxanthen-9-one at $\lambda = 440$ nm ($\varepsilon \leq 1$ L mol^{-1} cm^{-1} in CH_2Cl_2).

At shorter wavelength, employing fluorescent lamps emitting at $\lambda = 420$ nm, the racemization was more extensive (e.r. = 66/34) under otherwise identical conditions. However, it was

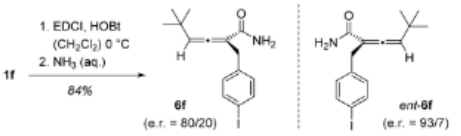

Scheme 5 Proof of absolute configuration: Enantioenriched carboxylic acid was converted into amide **6f** (EDCI = 1-ethyl-3-(3-dimethylaminopropyl)carbodiimide, HOBt = 1-hydroxybenzotriazole) which was compared on chiral HPLC with a sample of amide *ent*-**6f**,[12c] the absolute configuration of which was known.

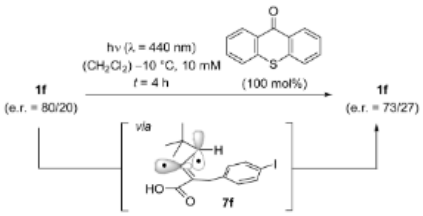

Scheme 6 2,3-Allenoic acid **1f** is not configurationally stable upon excitation. In the presence of thioxanthen-9-one, irradiation at λ = 440 nm leads to a decrease in the enantiomeric ratio, presumably *via* achiral triplet intermediate **5**.

surprisingly found, that substrate **1f** undergoes a detectable racemization (e.r. = 76/24) even in the absence of the catalyst. We ascribe this observation to a minor emission band of the fluorescent lamps occurring at $\lambda = 365$ nm (for the spectral data see the SI). In the deracemization experiments, this emission should be inconsequential, since catalyst **3f** has a far more extensive absorption at this wavelength than substrate *rac*-**1f** and it should be almost exclusively excited. The allenoic acid absorbs minimally at $\lambda = 365$ nm with $\varepsilon \leq 1$ L mol^{-1} cm^{-1} (CH_2Cl_2) while the absorption coefficient for **3f** is $\varepsilon = 5630$ L mol^{-1} cm^{-1} (CH_2Cl_2). In fact, the photophysical properties of catalyst **3f** (Fig. 2) are similar to parent thioxanthen-9-one.[26]

The energy of the lowest lying singlet state was determined from the crossing point of the absorption and fluorescence emission as $E(S_1) = 295$ kJ mol^{-1}. The compound shows an intense luminescence at 77 K which is mostly due to phosphorescence. The triplet energy was calculated from the point of inflection in the phosphorescence spectrum as $E(T_1) = 260 \pm 2$ kJ mol^{-1} (77 K, CH_2Cl_2).

The most coherent explanation for the observed enantiomer differentiation is based on a preferred energy transfer to one substrate enantiomer of allenoic acid. The situation is depicted for the parent compound *rac*-**1c** in Scheme 7 and was further corroborated by quantum-chemical calculations. Dexter energy transfer[27] is strongly distance dependent, and proximity of the triplet energy donor and the respective acceptor facilitate energy transfer.[28] We propose that enantiomer *ent*-**1c** is more readily processed by photoexcited catalyst **3f*** because the

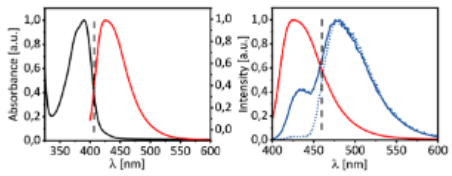

Fig. 2 Photophysical properties of catalyst **3f**: Normalized absorption and emission spectra at ambient temperature in CH_2Cl_2 solution (left). Emission spectra recorded at r.t. (red solid line) and 77 K (blue solid line) in CH_2Cl_2 ($\lambda_{exc} = 385$ nm). The blue dotted line shows the phosphorescence spectrum at 77 K ($\lambda_{exc} = 385$ nm, $t_{delay} = 100$ µs) in CH_2Cl_2.

thioxanthone and the allene chromophore are spatially closer in complex **3f**·*ent*-**1c** than in the diastereomeric complex **3f**·**1c**. If this is correct the catalytic cycle involving the former complex is preferred and the rate of racemization *via* achiral intermediate **7c** is higher for allenoic acid enantiomer *ent*-**1c**. In the photostationary state, the enantiomer **1c**, which is more slowly processed, prevails and is isolated in excess.

For theoretical investigations, minimum energy conformers were computed using conformational sampling[29–31] of complexes **3f**·*ent*-**1c** and **3f**·**1c** with the GFN2-xTB[32,33] method, followed by subsequent geometry optimization and frequency calculation to confirm the correct minimum energy structures. Therefore, the PBEh-3c[34–37] composite method including implicit solvation[38,39] was used. In addition, thermodynamic corrections[33,40,41] were included to the electronic energies that were computed using the PW6B95-D3(BJ)/def2-QZVP[35,36,42,43] level of theory. The most stable minimum energy conformers of both complexes are visualized in Scheme 7. The Gibbs free enthalpy of both diastereomeric complexes is almost identical with a calculated ΔG of only 0.473 kJ mol^{-1}. Subsequent analyses were based on all sampled ground-state minimum energy conformers (40 for **3f**·*ent*-**1c** and 24 for **3f**·**1c**) that were weighted by a Boltzmann distribution. Computational details on the sampling procedure, energy calculations, and analyses can be found in the SI.

As Dexter-type triplet energy transfers are strongly distance dependent, we analysed the interatomic distances of the two distinct diastereomeric complexes as previous investigations of similar allene deracemizations have shown that distances observed in the ground-state equilibrium geometries are similar to those in the triplet manifold.[12c] Analysis revealed that the distance between the thioxanthone moiety and the conjugated atoms in the allene is smaller in case of complex **3f**·*ent*-**1c** compared to complex **3f**·**1c**, both for the lowest minimum energy conformer as well as in the Boltzmann-weighted average. To avoid dependencies on arbitrary reference points and the resulting introduction of a bias, we used the overlap of scaled van der Waals radii[44] as a measure for the proximity of the relevant groups. A larger volume indicates a better overlap of the radii and a greater proximity of the two components within the assembly. The resulting volumes obtained for the minimum structures, 2.98 Å^3 for **3f**·**1c** and 3.81 Å^3 for **3f**·*ent*-**1c**, are plotted in addition to the structures in Scheme 7 (green areas). The Boltzmann-weighted averages, 2.97 Å^3 for **3f**·**1c** and 3.72 Å^3 for **3f**·*ent*-**1c**, confirm the observation obtained from the lowest minimum energy conformers. The differences in the volumina are clearly visible and are additionally supported by the distances of each atom in the allene moiety to the thioxanthone plane that are plotted in the SI. These results confirm previously observed trends that shorter distances are in correlation with lower barriers in Dexter-type triplet-energy transfers.[28]

Since the distance difference for the diastereomeric complexes **3f**·**1** *vs.* **3f**·*ent*-**1** is relatively low, the achieved enantioselectivity is not as high as in previous cases.[12] While the enantioselectivities obtained with spinol-derived catalyst **3f** are moderate, our computational analysis shows that the selectivity correlates with differences in Dexter energy transfer efficiency between diastereomeric complexes, quantified by Boltzmann-

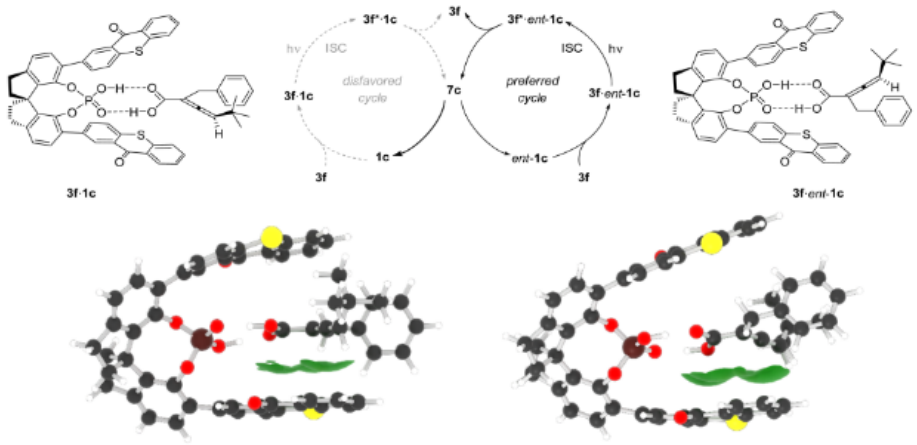

Scheme 7 Mechanistic scenario for the deracemization of racemic allenoic acid *rac*-**1c** upon irradiation in the presence of catalyst **3f**. Triplet energy transfer is faster in complex **3f**·*ent*-**1c** than in complex **3f**·**1c** because the average distance of the thioxanthone chromophore to the allene is smaller. Triplet energy transfer from excited **3f*** to the allene leads to formation of achiral triplet intermediate **5c** (*cf.* Scheme 6) which dissociates from the phosphoric acid and forms either one of the two enantiomers **1c** or *ent*-**1c** of the allenoic acid. The lowest minimum energy conformations of each enantiomer with catalyst **3f** are shown below, in addition to the overlap of scaled van der Waals radii (green areas) to visualize the proximity of the allenoic acids to the catalyst.

weighted proximity/overlap descriptors. This mechanistic handle suggests avenues for optimization, such as closer or asymmetric placement of the thioxanthone unit, tuning of the chromophore's triplet energy, or reinforcement of the hydrogen-bonding network. These strategies, together with data-driven screening based on the computed descriptors[45] or machine learning optimization techniques,[46] provide a roadmap for future improvements in enantioselectivity.

An interesting twist of the Dexter energy transfer mechanism relates to the fact that a dual catalytic system is conceivable, in which achiral thioxanthen-9-one and a chiral phosphoric acid with a suitable chromophore act synergistically. Preliminary results showed the approach to be viable but the enantioselectivities remained lower than with the sensitizing phosphoric acid **3f** (see the SI for details).

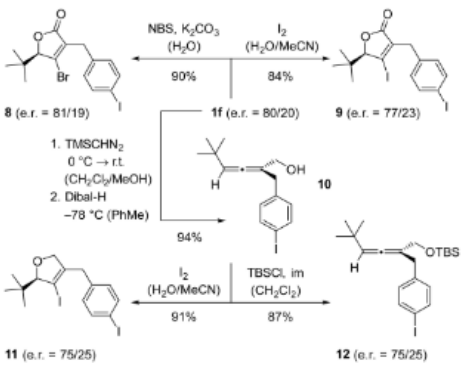

Scheme 8 Consecutive reactions of scalemic allenoic acid **1f**. Abbreviations: Dibal-H = diisobutylaluminium hydride; im = imidazole; NBS = *N*-bromosuccinimide; TBS = *tert*-butyldimethylsilyl.

The transformation of axially chiral allenes to products with a stereogenic center has been studied extensively in prior work. In particular, the Diels–Alder reaction has been broadly utilized and was shown to occur with high chirality transfer.[47] In the present study, we have mainly investigated a consecutive halolactonization[48] or haloesterification (Scheme 8).[49] We found the bromolactonization of scalemic allenoic acid **1f** to occur with perfect chirality transfer generating lactone **8** in high yield. The absolute configuration of the major enantiomer was assigned based on the assumption that the temporarily formed bromonium ion is substituted intramolecularly by the carboxylic acid.[48,50] The iodolactonization to product **9** proceeded smoothly but the enantiomeric purity was not fully retained. Upon reduction of the acid to alcohol **10**, the iodoetherification delivered the desired ether **11** in an e.r. of 75/25. Since the e.r. of alcohol **10** could not be determined by chiral HPLC, it was transformed into silyl ether **12**. Based on the fact that its e.r. was identical to the e.r. of the iodoetherification product, it seems most likely that the observed loss of enantiomeric purity is due to the reduction step while the absolute configuration is retained in the two consecutive reactions.

Conclusions

In summary, we have successfully shown that a chiral phosphoric acid can be employed as a single photocatalyst for a photochemical deracemization reaction. The catalyst operates

likely by triplet energy transfer to the allenoic acid, inducing a racemization *via* the triplet state of the substrate. Proper positioning of the thioxanthone chromophore in the catalyst is crucial for the differentiation of the two substrate enantiomers. The relatively high flexibility of catalyst and allenoic acid precludes the catalyst from recruiting a single allene enantiomer in the energy transfer step. Although there is a preference for processing one enantiomer over the other, the degree of differentiation and consequently the enantioselectivity are yet not as optimal as previously seen for azabicyclo[3.1.1]nonan-2-one-based energy transfer catalysts. Still, the results provide an excellent starting point for further catalyst optimization and design.

Author contributions

M. S. and T. B. developed the project. Funding was acquired by T. B. and J. W.; M. S. designed and performed the synthetic experiments. M. S. generated and validated the experimental data, D. B. the computational data. T. B. and J. W. administered the project and supervised the research. All authors wrote, reviewed, and edited the manuscript.

Conflicts of interest

There are no conflicts to declare.

Data availability

The data that supports the findings of this study are available in the supplementary material (SI) of this article. Primary research data are openly available in the repository RADAR4Chem at https://doi.org/10.22000/14d69n7httd5f1yw.[51] Supplementary information: synthetic procedures and full characterization for all starting materials and products (**1c–1x, 2c, 2e, 2g, 2i, 2j, 2k, 2r, 2u, 3e–3g, 6c, 6f, 6x, 8–12**), spectroscopic and computational data. See DOI: https://doi.org/10.1039/d5sc05356k.

Acknowledgements

Financial support by the Deutsche Forschungsgemeinschaft (DFG, German Research Foundation) – TRR 325 (project B2 and seed funding for JW) – 444632635 is gratefully acknowledged. Computations for this work were done using resources of the Leipzig University Computing Center, the NHR Center at TU Dresden, and Paderborn Center for Parallel Computing (PC2). We thank O. Ackermann, J. Kudermann, P. Freund, and N. Pflaum (all TU Munich) for their help with the GLC and HPLC analyses. We are grateful to Dr S. Breitenlechner (TU Munich) for his help with the preparation of the repository. M. Reichel and J.-J. Schneider are acknowledged for synthetic assistance. Toni Oestereich is acknowledged for initial quantum chemical calculations.

Notes and references

1 (*a*) H. Lorenz and A. Seidel-Morgenstern, *Angew. Chem., Int. Ed.*, 2014, **53**, 1218–1250; (*b*) J. Sui, N. Wang, J. Wang, X. Huang, T. Wang, L. Zhou and H. Hao, *Chem. Sci.*, 2023, **14**, 11955–12003.

2 For recent reviews on enzyme catalysis, see:(*a*) M. T. Reetz, G. Qu and Z. Sun, *Nat. Synth.*, 2024, **3**, 19–32; (*b*) A. O'Connell, A. Barry, A. J. Burke, A. E. Hutton, E. L. Bell, A. P. Green and E. O'Reilly, *Chem. Soc. Rev.*, 2024, **53**, 2828–2850; (*c*) E. J. Hossack, F. J. Hardy and A. P. Green, *ACS Catal.*, 2023, **13**, 12436–12444; (*d*) M. T. Reetz, *Adv. Synth. Catal.*, 2022, **364**, 3326–3335; (*e*) R. A. Sheldon, D. Brady and M. L. Bode, *Chem. Sci.*, 2020, **11**, 2587–2605.

3 (*a*) A. Ghanem and H.-Y. Aboul-Enein, *Chirality*, 2005, **17**, 1–15; (*b*) P. D. de María, C. A. García-Burgos, G. Bargeman and R. W. van Gemert, *Synthesis*, 2007, 1439–1452; (*c*) E. Fernández-Álvaro, R. Kourist, J. Winter, D. Böttcher, K. Liebeton, C. Naumer, J. Eck, C. Leggewie, K. E. Jaeger, W. Streit and U. T. Bornscheuer, *Microb. Biotechnol.*, 2010, **3**, 59–64; (*d*) A. Brodzka, D. Koszelewski, M. Zysk and R. Ostaszewski, *Catal. Commun.*, 2018, **106**, 82–86; (*e*) K. Okuno, Y. Furuya and S. Shirakawa, *Eur. J. Org Chem.*, 2024, **27**, e202300985; (*f*) Z. Dou, X. Chen, L. Zhu, X. Zheng, X. Chen, J. Xue, S. Niwayama, Y. Ni and G. Xu, *Nat. Commun.*, 2024, **15**, 9057.

4 Selected reviews:(*a*) H. Pellissier, *Eur. J. Org Chem.*, 2022, e202101561; (*b*) L.-C. Yang, H. Deng and H. Renata, *Org. Process Res. Dev.*, 2022, **26**, 1925–1943; (*c*) O. Verho and J.-E. Bäckvall, *J. Am. Chem. Soc.*, 2015, **137**, 3996–4009; (*d*) H. Pellissier, *Tetrahedron*, 2003, **59**, 8291–8327.

5 (*a*) N. Krause and S. Hashmi, *Modern Allene Chemistry*, Wiley-VCH, Weinheim, 2004; (*b*) S. Yu and S. Ma, *Angew. Chem., Int. Ed.*, 2012, **51**, 3074–3112.

6 S. Ramaswamy, R. A. H. F. Hui and J. B. Jones, *J. Chem. Soc., Chem. Commun.*, 1986, 1545–1546.

7 (*a*) M. Pietzsch, O. Vielhauer, D. Pamperin, B. Ohse and H. Hopf, *J. Mol. Catal. B: Enzym.*, 1999, **6**, 51–57; (*b*) B. Skrobo, J. D. Rolfes and J. Deska, *Tetrahedron*, 2016, **72**, 1257–1275.

8 J. D. Carballeira, P. Krumlinde, M. Bocola, A. Vogel, M. T. Reetz and J.-E. Bäckvall, The absolute configuration of the major enantiomer is not provided in the paper, but it is said to be the (+)-allenoic acid, *Chem. Commun.*, 2007, 1913–1915.

9 A. Horváth and J. E. Bäckvall, *Chem. Commun.*, 2004, 964–965.

10 (*a*) J. Nyhlén, L. Eriksson and J.-E. Bäckvall, *Chirality*, 2008, **20**, 47–50; (*b*) J. Yu, W.-J. Chen and L.-Z. Gong, *Org. Lett.*, 2010, **12**, 4050–4053; (*c*) Y.-F. Ao, D.-X. Wang, L. Zhao and M.-X. Wang, *J. Org. Chem.*, 2014, **79**, 3103–3110.

11 For the preparation of enantiopure 2,3-allenoic acids, see: (*a*) W. Runge, G. Kresze and E. Ruch, *Liebigs Ann. Chem.*, 1975, 1361–1378; (*b*) S. Ma and S. Wu, *Chem. Commun.*, 2001, 5, 441–442; (*c*) J. Nyhlén, L. Eriksson and J.-E. Bäckvall, *Chirality*, 2008, **1**, 47–50; (*d*) W.-F. Zheng, W. Zhang,

C. Huang, P. Wu, H. Qian, L. Wang, Y.-L. Guo and S. Ma, *Nat. Catal.*, 2019, **2**, 997–1005; (*e*) J. Wang, W.-F. Zheng, Y. Li, Y.-L. Guo, H. Qian and S. Ma, *Org. Chem. Front.*, 2024, **11**, 2477–2484.

12 (*a*) A. Hölzl-Hobmeier, A. Bauer, A. V. Silva, S. M. Huber, C. Bannwarth and T. Bach, *Nature*, 2018, **564**, 240–243; (*b*) M. Plaza, C. Jandl and T. Bach, *Angew. Chem., Int. Ed.*, 2020, **59**, 12785–12788; (*c*) M. Plaza, J. Großkopf, S. Breitenlechner, C. Bannwarth and T. Bach, *J. Am. Chem. Soc.*, 2021, **143**, 11209–11217; (*d*) T. Kratz, P. Steinbach, S. Breitenlechner, G. Storch, C. Bannwarth and T. Bach, *J. Am. Chem. Soc.*, 2022, **144**, 10133–10138.

13 For a different approach towards the photochemical deracemization of allenes, see:(*a*) C. Song, X. Bai, B. Li, Y. Dang and S. Yu, *J. Am. Chem. Soc.*, 2024, **146**, 21137–21146; (*b*) C. Song and S. Yu, *ACS Catal.*, 2024, **14**, 15997–16002.

14 Selected reviews:(*a*) M. Huang, T. Pan, X. Jiang and S. Luo, *J. Am. Chem. Soc.*, 2023, **145**, 10917–10929; (*b*) J. Großkopf and T. Bach, *Angew. Chem., Int. Ed.*, 2023, **62**, e202308241; (*c*) J. Wang, X. Lv and Z. Jiang, *Chem.–Eur. J.*, 2023, **6**, e202204029; (*d*) Q. Shi and J. Ye, *Angew. Chem., Int. Ed.*, 2020, **59**, 4998–5001.

15 For the use of thioxanthone in photocatalysis, see: N. F. Nikitas, P. L. Gkizis and C. G. Kokotos, *Org. Biomol. Chem.*, 2021, **19**, 5237–5253.

16 For key references on the use of phosphoric acids in enantioselective photocatalysis, see:(*a*) L. J. Rono, H. G. Yayla, D. Y. Wang, M. F. Armstrong and R. R. Knowles, *J. Am. Chem. Soc.*, 2013, **135**, 17735–17738; (*b*) R. S. J. Proctor, H. J. Davis and R. J. Phipps, *Science*, 2018, **360**, 419–422; (*c*) K. Cao, S. M. Tan, R. Lee, S. Yang, H. Jia, X. Zhao, B. Qiao and Z. Jiang, *J. Am. Chem. Soc.*, 2019, **141**, 5437–5443; (*d*) Y.-Z. Cheng, Q.-R. Zhao, X. Zhang and S.-L. You, *Angew. Chem., Int. Ed.*, 2019, **58**, 18069–18074; (*e*) N. Y. Shin, J. M. Ryss, X. Zhang, S. J. Miller and R. R. Knowles, *Science*, 2019, **366**, 364–369; (*f*) E. M. Sherbrook, M. J. Genzink, B. Park, I. A. Guzei, M.-H. Baik and T. P. Yoon, *Nat. Commun.*, 2021, **12**, 5735; (*g*) Z. C. Girvin, L. F. Cotter, H. Yoon, S. J. Chapman, J. M. Mayer, T. P. Yoon and S. J. Miller, *J. Am. Chem. Soc.*, 2022, **144**, 20109–20117; (*h*) T. Uchikura, N. Kamiyama, T. Mouri and T. Akiyama, *ACS Catal.*, 2022, **12**, 5209–5216; (*i*) G. Liu and Y. Cao, *Adv. Synth. Catal.*, 2023, **365**, 3044–3062.

17 For work on chiral phosphoric acid-based thioxanthone catalysts by other groups, see: (*a*) J. Lyu, A. Claraz, M. R. Vitale, C. Allain and G. Masson, *J. Org. Chem.*, 2020, **85**, 12843–12855; (*b*) R. Takagi and C. Tabuchi, *Org. Biomol. Chem.*, 2020, **18**, 9261–9267; (*c*) R. Takagi and T. Tanimoto, *Org. Biomol. Chem.*, 2022, **20**, 3940–3947.

18 (*a*) F. Pecho, Y.-Q. Zou, J. Gramüller, T. Mori, S. M. Huber, A. Bauer, R. M. Gschwind and T. Bach, *Chem.–Eur. J.*, 2020, **26**, 5190–5194; (*b*) F. Pecho, Y. Sempere, J. Gramüller, F. M. Hörmann, R. M. Gschwind and T. Bach, *J. Am. Chem. Soc.*, 2021, **143**, 9350–9354.

19 M. Stierle, C. Jaschke, D. J. Grenda, M. T. Peschel, T. Pickl, N. Gessner, P. Nuernberger, B. P. Fingerhut, C. Ochsenfeld, R. de Vivie-Riedle and T. Bach, *Angew. Chem., Int. Ed.*, 2025, **64**, e202501433.

20 X. Xiong, T. Zheng, X. Wang, Y.-L. S. Tse and Y.-Y. Yeung, *Chem*, 2020, **6**, 919–932.

21 Y. Yang, S.-F. Zhu, H.-F. Duan, C.-Y. Zhou, L.-X. Wang and Q.-L. Zhou, *J. Am. Chem. Soc.*, 2006, **129**, 2248–2249.

22 X. Dong, S. Shen, Y. Qin, X. Hu, H. Gao, G. Liu, T. Gao, Z. Pang, P. Wang and Y. Wang, *Chin. Chem. Lett.*, 2023, **34**, 108331.

23 For early precedence, see:(*a*) O. Rodriguez and H. Morrison, *J. Chem. Soc., Chem. Commun.*, 1971, 679; (*b*) C. S. Drucker, V. G. Toscano and R. G. Weiss, *J. Am. Chem. Soc.*, 1973, **95**, 6482–6484.

24 W. G. Herkstroeter, A. A. Lamola and G. S. Hammond, *J. Am. Chem. Soc.*, 1964, **86**, 4537–4540.

25 For the structure of a related diradical, see: G. Bucher, A. A. Mahajan and M. Schmittel, *J. Org. Chem.*, 2009, **74**, 5850–5860.

26 A. Iyer, A. Clay, S. Jockusch and J. Sivaguru, *J. Phys. Org. Chem.*, 2017, **30**, e3738.

27 (*a*) D. L. Dexter, *J. Chem. Phys.*, 1953, **21**, 836–850; (*b*) N. J. Turro, V. Ramamurthy and J. C. Scaiano, *Modern Molecular Photochemistry of Organic Molecules*; University Science, Sausalito, 2010, pp. 383–413.

28 J. Großkopf, T. Kratz, T. Rigotti and T. Bach, *Chem. Rev.*, 2022, **122**, 1626–1653.

29 P. Pracht, F. Bohle and S. Grimme, *Phys. Chem. Chem. Phys.*, 2020, **22**, 7169–7192.

30 S. Grimme, *J. Chem. Theory Comput.*, 2019, **15**, 2847–2862.

31 P. Pracht, S. Grimme, C. Bannwarth, F. Bohle, S. Ehlert, G. Feldmann, J. Gorges, M. Müller, T. Neudecker, C. Plett, S. Spicher, P. Steinbach, P. A. Wesołowski and F. Zeller, *J. Chem. Phys.*, 2024, **160**, 114110.

32 C. Bannwarth, S. Ehlert and S. Grimme, *J. Chem. Theory Comput.*, 2019, **15**, 1652–1671.

33 S. Ehlert, M. Stahn, S. Spicher and S. Grimme, *J. Chem. Theory Comput.*, 2021, **17**, 4250–4261.

34 S. Grimme, J. G. Brandenburg, C. Bannwarth and A. Hansen, *J. Chem. Phys.*, 2015, **143**, 054107.

35 S. Grimme, J. Antony, S. Ehrlich and H. Krieg, *J. Chem. Phys.*, 2010, **132**, 154104.

36 S. Grimme, S. Ehrlich and L. Goerigk, *J. Comput. Chem.*, 2011, **32**, 1456–1465.

37 H. Kruse and S. Grimme, *J. Chem. Phys.*, 2012, **136**, 154101.

38 M. Garcia-Ratés and F. Neese, *J. Comput. Chem.*, 2020, **41**, 922–939.

39 V. Barone and M. Cossi, *J. Phys. Chem. A*, 1998, **102**, 1995–2001.

40 S. Grimme, *Chem.–Eur. J.*, 2012, **18**, 9955–9964.

41 C. Bannwarth, E. Caldeweyher, S. Ehlert, A. Hansen, P. Pracht, J. Seibert, S. Spicher and S. Grimme, *Wiley Interdiscip. Rev.: Comput. Mol. Sci.*, 2021, **11**, e1493.

42 F. Weigend and R. Ahlrichs, *Phys. Chem. Chem. Phys.*, 2005, **7**, 3297–3305.

43 Y. Zhao and D. G. Truhlar, *J. Phys. Chem. A*, 2005, **109**, 5656–5667.
44 S. Alvarez, *Dalton Trans.*, 2013, **42**, 8617–8636.
45 J. P. Reid and M. S. Sigman, *Nature*, 2019, **571**, 343–348.
46 F. Häse, L. M. Roch, C. Kreisbeck and A. Aspuru-Guzik, *ACS Cent. Sci.*, 2018, **4**, 1134–1145.
47 F. M. Harvey, A. H. Heidecker, C. Merten and T. Bach, *Org. Biomol. Chem.*, 2023, **21**, 4422–4428.
48 (*a*) G. B. Gill and M. S. H. Idris, *Tetrahedron Lett.*, 1985, **26**, 4811–4814; (*b*) S. Ma, Z. Shi and Z. Yu, *Tetrahedron*, 1999, **55**, 12137–12148; (*c*) S. Ma, B. Wu and Z. Shi, *J. Org. Chem.*, 2004, **69**, 1429–1431; (*d*) G. Nemecek, R. Thomas, H. Goesmann, C. Feldmann and J. Podlech, *Eur. J. Org Chem.*, 2013, 6420–6432.
49 (*a*) J. Li, C. Fu, G. Chen, G. Chai and S. Ma, *Adv. Synth. Catal.*, 2008, **350**, 1376–1382; (*b*) J. Deska and J.-E. Bäckvall, *Org. Biomol. Chem.*, 2009, **7**, 3379–3381.
50 K. Shingu, S. Hagishita and M. Nakagawa, *Tetrahedron Lett.*, 1967, **8**, 4371–4374.
51 M. Stierle, D. Bitterlich, J. Westermayr and T. Bach; 2025, *Dataset for Publication "Photochemical deracemization of 2,3-allenoic acids mediated by a sensitizing chiral phosphoric acid catalyst" RADAR4Chem*, DOI: 10.22000/14d69n7httd5f1yw.

7. Summary

Based on previous reports by our group[57,58] and others[60,62], a new generation of structurally diverse PACPAs was synthesized in this thesis. Two novel enantioselective reaction modes were thereby unlocked. Figure 4 aims to give a chronological overview of some of the prepared PACPAs and the reactions they were employed for.

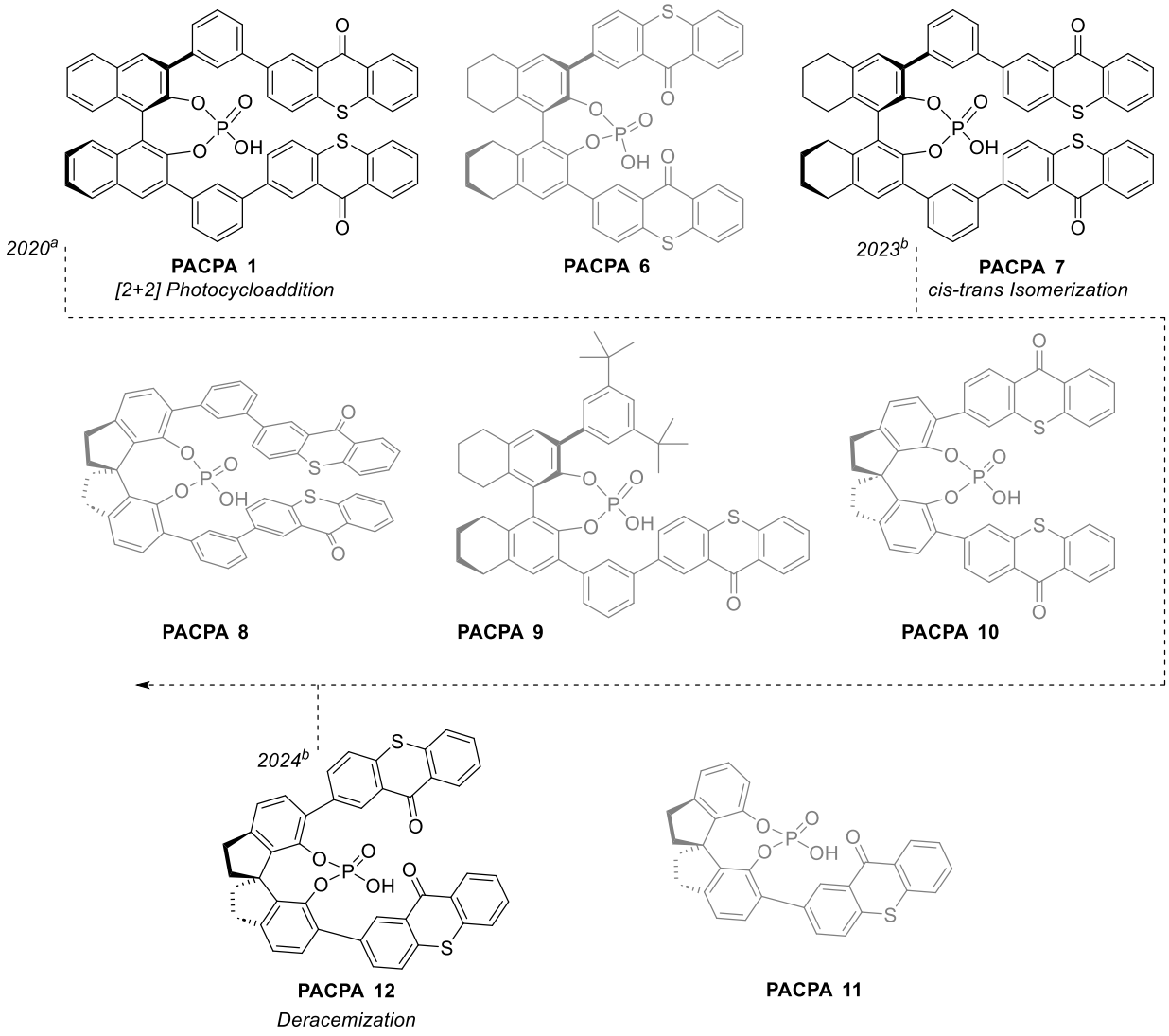

Figure 4. *Chronological selection of some in this work prepared* ***PACPAs 6-12*** *and the reactions they were used for.* [a]*Prepared by Pecho and Zou, year of publication is stated.* [b]*Year of first synthesis is stated.*

We identified carboxylic acid **66** from a selection of possible compounds as the most suitable model substrate for an enantioselective *cis-trans* isomerization (Scheme 15).[71] Because the photochemically generated, chiral *cis*-alkene (*rac*)-**67** is too reactive to be isolated, we studied racemic trapping reactions under direct irradiation conditions (14 diene examples, up to 98% yield). Finally, we were able to show how the utilization of **PACPA 7** as catalyst, under visible-light irradiation, lead to *Diels-Alder* products **68** with a notable degree of enantiodifferentiation.

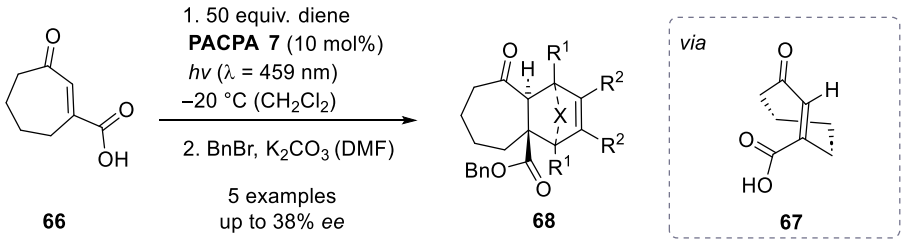

Scheme 15. *Enantioselective, visible-light mediated cis-trans isomerization of acid* ***66*** *towards the highly strained alkene* ***67****. Thermal Diels-Alder reaction with a suitable diene and benzylation lead to the isolated products* ***68.***

A detailed computational analysis by our collaboration partners suggests EnT from the thioxanthene-9-one units of the chiral catalysts towards the coordinated substrate. The calculations propose that the overall observed enantioselectivity is induced in the isomerization step.

In a second synthetic study, we were able to show how tuning the exact nature of the PACPA catalyst leads to an improved deracemization reaction (Scheme 16).[72]

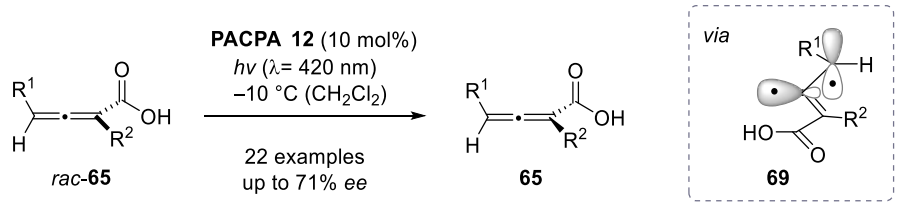

Scheme 16. *Photochemical deracemization of allenoic acids rac-****65*** *mediated by* ***PACPA 12*** *under irradiation with visible-light.*

By employing **PACPA 12** we were able to deracemize the 2,4-disubstituted 2,3-allenoic acids *rac*-**65** under irradiation with visible light, leading to the enantioenriched allene carboxylic acids **65**. Computational input by our collaboration partners, as well as mechanistic experiments suggest different sensitization rates for the two enantiomers of *rac*-**65** in the two different diastereomeric complexes formed by coordination to the phosphoric acid catalyst. Thereby, *ent*-**65** is processed faster by the catalyst to form achiral diradical intermediate **69**, leading to enantiomeric enrichment of **65** in the reaction solution.

In summary, this work contains the first example of the enantioselective *cis-trans* isomerization of an enone ever reported, although the obtained enantioselectivities stayed on a proof-of-principle level (up to 38% *ee*). Furthermore, a pioneering contribution to the still relatively young field of photochemical deracemization was made by efficient catalyst design (up to 71% *ee*). Thereby, previous limitations were surpassed and the reaction scope of photochemically active chiral phosphoric acids was expanded.

8. Licenses

9. References

[1] Michael J. R. Desborough, David M. Keeling, *Br. J. Haematol.* **2017**, *177*, 674–683.

[2] H. Beck, M. Härter, B. Haß, C. Schmeck, L. Baerfacker, *Drug Discov. Today* **2022**, *27*, 1560–1574.

[3] NobelPrize.org, "The Nobel Prize in Chemistry 2001 - NobelPrize.org", can be found under https://www.nobelprize.org/prizes/chemistry/2001/summary/, last accessed on 28.09.25.

[4] NobelPrize.org, "The Nobel Prize in Chemistry 2005 - NobelPrize.org", can be found under https://www.nobelprize.org/prizes/chemistry/2005/summary/, last accessed on 28.09.25.

[5] NobelPrize.org, "The Nobel Prize in Chemistry 2010 - NobelPrize.org", can be found under https://www.nobelprize.org/prizes/chemistry/2010/summary/, last accessed on 28.09.25.

[6] NobelPrize.org, "The Nobel Prize in Chemistry 2021 - NobelPrize.org", can be found under https://www.nobelprize.org/prizes/chemistry/2021/summary/, last accessed on 28.09.25.

[7] NobelPrize.org, "The Nobel Prize in Chemistry 2022 - NobelPrize.org", can be found under https://www.nobelprize.org/prizes/chemistry/2022/summary/, last accessed on 28.09.25.

[8] D. C. Blakemore, L. Castro, I. Churcher, D. C. Rees, A. W. Thomas, D. M. Wilson, A. Wood, *Nat. Chem.* **2018**, *10*, 383–394.

[9] F. Lovering, J. Bikker, C. Humblet, *J. Med. Chem.* **2009**, *52*, 6752–6756.

[10] D. G. Brown, J. Boström, *J. Med. Chem.* **2016**, *59*, 4443–4458.

[11] M. K. P. Jayatunga, W. Xie, L. Ruder, U. Schulze, C. Meier, *Nat. Rev. Drug Discov.* **2022**, *21*, 175–176.

[12] a) J. Tsien, C. Hu, R. R. Merchant, T. Qin, *Nat. Rev. Chem.* **2024**, *8*, 605–627; b) R. Pellicciari, M. Raimondo, M. Marinozzi, B. Natalini, G. Costantino, C. Thomsen, *J. Med. Chem.* **1996**, *39*, 2874–2876.

[13] a) V. V. Levterov, Y. Panasiuk, K. Sahun, O. Stashkevych, V. Badlo, O. Shablykin, I. Sadkova, L. Bortnichuk, O. Klymenko-Ulianov, Y. Holota, L. Lachmann, P. Borysko, K. Horbatok, I. Bodenchuk, Y. Bas, D. Dudenko, P. K. Mykhailiuk, *Nat. Commun.* **2023**, *14*, 5608; b) D. Dibchak, M. Snisarenko, A. Mishuk, O. Shablykin, L. Bortnichuk, O. Klymenko-Ulianov, Y. Kheylik, I. V. Sadkova, H. S. Rzepa, P. K. Mykhailiuk, *Angew. Chem. Int. Ed.* **2023**, *62*, e202304246; c) V. V. Levterov, Y. Panasiuk, O. Shablykin, O. Stashkevych, K. Sahun, A. Rassokhin, I. Sadkova, D. Lesyk, A. Anisiforova, Y. Holota,

P. Borysko, I. Bodenchuk, N. M. Voloshchuk, P. M. Mykhailiuk, *Angew. Chem. Int. Ed.* **2024**, *63*, e202319831; d) V. V. Levterov, Y. Panasyuk, V. O. Pivnytska, P. K. Mykhailiuk, *Angew. Chem. Int. Ed.* **2020**, *59*, 7161–7167; e) Y. Liang, F. Paulus, C. G. Daniliuc, F. Glorius, *Angew. Chem. Int. Ed.* **2023**, *62*, e202305043; f) Y. Liang, R. Kleinmans, C. G. Daniliuc, F. Glorius, *J. Am. Chem. Soc.* **2022**, *144*, 20207–20213.

[14] S. M. Mennen, C. Alhambra, C. L. Allen, M. Barberis, S. Berritt, T. A. Brandt, A. D. Campbell, J. Castañón, A. H. Cherney, M. Christensen, D. B. Damon, J. E. de Diego, S. García-Cerrada, P. García-Losada, R. Haro, J. Janey, D. C. Leitch, L. Li, F. Liu, P. C. Lobben, D. W. C. MacMillan, J. Magano, E. McInturff, S. Monfette, R. J. Post, D. Schultz, B. J. Sitter, J. M. Stevens, I. I. Strambeanu, J. Twilton, K. Wang, M. A. Zajac, *Org. Process Res. Dev.* **2019**, *23*, 1213–1242.

[15] F.-P. Wu, J. L. Tyler, F. Glorius, *Acc. Chem. Res.* **2025**, *58*, 893–906.

[16] L. Candish, K. D. Collins, G. C. Cook, J. J. Douglas, A. Gómez-Suárez, A. Jolit, S. Keess, *Chem. Rev.* **2022**, *122*, 2907–2980.

[17] F. Lévesque, P. H. Seeberger, *Angew. Chem. Int. Ed.* **2012**, *51*, 1706–1709.

[18] A. Denisenko, P. Garbuz, S. V. Shishkina, N. M. Voloshchuk, P. K. Mykhailiuk, *Angew. Chem. Int. Ed.* **2020**, *59*, 20515–20521.

[19] W. H. Brooks, W. C. Guida, K. G. Daniel, *Curr. Top. Med. Chem.* **2011**, *11*, 760–770.

[20] R. Brimioulle, D. Lenhart, M. M. Maturi, T. Bach, *Angew. Chem. Int. Ed.* **2015**, *54*, 3872–3890.

[21] M. J. Genzink, J. B. Kidd, W. B. Swords, T. P. Yoon, *Chem. Rev.* **2022**, *122*, 1654–1716.

[22] G. Balavoine, S. Jugé, H. B. Kagan, *Tetrahedron Lett.* **1973**, *14*, 4159–4162.

[23] A. Hölzl-Hobmeier, A. Bauer, A. V. Silva, S. M. Huber, C. Bannwarth, T. Bach, *Nature* **2018**, *564*, 240–243.

[24] J. Großkopf, M. Plaza, A. Seitz, S. Breitenlechner, G. Storch, T. Bach, *J. Am. Chem. Soc.* **2021**, *143*, 21241–21245.

[25] M. Plaza, C. Jandl, T. Bach, *Angew. Chem. Int. Ed.* **2020**, *59*, 12785–12788.

[26] R. Brimioulle, T. Bach, *Science* **2013**, *342*, 840–843.

[27] A. Bauer, F. Westkämper, S. Grimme, T. Bach, *Nature* **2005**, *436*, 1139–1140.

[28] E. Arceo, I. D. Jurberg, A. Álvarez-Fernández, P. Melchiorre, *Nat. Chem.* **2013**, *5*, 750–756.

[29] N. Vallavoju, S. Selvakumar, S. Jockusch, M. P. Sibi, J. Sivaguru, *Angew. Chem. Int. Ed.* **2014**, *53*, 5604–5608.

[30] H. Guo, E. Herdtweck, T. Bach, *Angew. Chem. Int. Ed.* **2010**, *49*, 7782–7785.

[31] a) H. Huo, X. Shen, C. Wang, L. Zhang, P. Röse, L.-A. Chen, K. Harms, M. Marsch, G. Hilt, E. Meggers, *Nature* **2014**, *515*, 100–103; b) C. Onneken, T. Morack, J. Soika, O. Sokolova, N. Niemeyer, C. Mück-Lichtenfeld, C. G. Daniliuc, J. Neugebauer, R. Gilmour, *Nature* **2023**, *621*, 753–759.

[32] W. Ding, L.-Q. Lu, Q.-Q. Zhou, Y. Wei, J.-R. Chen, W.-J. Xiao, *J. Am. Chem. Soc.* **2017**, *139*, 63–66.

[33] J. Guo, Y.-Z. Fan, Y.-L. Lu, S.-P. Zheng, C.-Y. Su, *Angew. Chem. Int. Ed.* **2020**, *59*, 8661–8669.

[34] J. S. Trimble, R. Crawshaw, F. J. Hardy, C. W. Levy, M. J. B. Brown, D. E. Fuerst, D. J. Heyes, R. Obexer, A. P. Green, *Nature* **2022**, *611*, 709–714.

[35] L. J. Rono, H. G. Yayla, D. Y. Wang, M. F. Armstrong, R. R. Knowles, *J. Am. Chem. Soc.* **2013**, *135*, 17735–17738.

[36] C. Brenninger, A. Pöthig, T. Bach, *Angew. Chem. Int. Ed.* **2017**, *56*, 4337–4341.

[37] E. M. Sherbrook, H. Jung, D. Cho, M.-H. Baik, T. P. Yoon, *Chem. Sci.* **2020**, *11*, 856–861.

[38] E. M. Sherbrook, M. J. Genzink, B. Park, I. A. Guzei, M.-H. Baik, T. P. Yoon, *Nat. Commun.* **2021**, *12*, 1–7.

[39] M. J. Genzink, M. D. Rossler, H. Recendiz, T. P. Yoon, *J. Am. Chem. Soc.* **2023**, *145*, 19182–19188.

[40] E. F. Plachinski, R. Z. Qian, R. Villanueva, D. L. Poole, T. Rosenthal, T. P. Yoon, *J. Am. Chem. Soc.* **2024**, *146*, 31400–31404.

[41] T. Uchikura, K. Takahashi, T. Oishi, T. Akiyama, *Org. Biomol. Chem.* **2023**, *21*, 9138–9142.

[42] J. Großkopf, T. Kratz, T. Rigotti, T. Bach, *Chem. Rev.* **2022**, *122*, 1626–1653.

[43] S. J. Chapman, W. B. Swords, C. M. Le, I. A. Guzei, F. D. Toste, T. P. Yoon, *J. Am. Chem. Soc.* **2022**, *144*, 4206–4213.

[44] Z. C. Girvin, L. F. Cotter, H. Yoon, S. J. Chapman, J. M. Mayer, T. P. Yoon, S. J. Miller, *J. Am. Chem. Soc.* **2022**, *144*, 20109–20117.

[45] S. B. Cahoon, S. J. Chapman, T. A. Fiala, M. J. Genzink, T. P. Yoon, *J. Org. Chem.* **2024**, *89*, 17615–17620.

[46] D. Tian, W. Shi, X. Sun, X. Zhao, Y. Yin, Z. Jiang, *Nat. Commun.* **2024**, *15*, 1–9.

[47] F. Liu, Y. Guo, W. Lu, X. Zhao, Y. Yin, Z. Jiang, *Chem. Sci.* **2025**, *16*, 10555–10562.

[48] X. Sun, Y. Liu, Y. Yin, X. Ban, X. Zhao, Z. Jiang, *Nat. Chem.* **2024**, *16*, 1169–1176.

[49] G. Zeng, W. Shi, Z. Wang, X. Zhao, Y. Yin, Z. Jiang, *J. Am. Chem. Soc.* **2025**, *147*, 26079–26088.

[50] N. A. Romero, D. A. Nicewicz, *Chem. Rev.* **2016**, *116*, 10075–10166.

[51] R. S. J. Proctor, H. J. Davis, R. J. Phipps, *Science* **2018**, *360*, 419–422.

[52] a) K. Okada, K. Okamoto, N. Morita, K. Okubo, M. Oda, *J. Am. Chem. Soc.* **1991**, *113*, 9401–9402; b) G. Pratsch, G. L. Lackner, L. E. Overman, *J. Org. Chem.* **2015**, *80*, 6025–6036; c) T. Qin, J. Cornella, C. Li, L. R. Malins, J. T. Edwards, S. Kawamura, B. D. Maxwell, M. D. Eastgate, P. S. Baran, *Science* **2016**, *352*, 801–805.

[53] a) C. Müller, A. Bauer, T. Bach, *Angew. Chem. Int. Ed.* **2009**, *48*, 6640–6642; b) R. Alonso, T. Bach, *Angew. Chem. Int. Ed.* **2014**, *53*, 4368–4371; c) F. Mayr, L.-M. Mohr, E. Rodriguez, T. Bach, *Synthesis* **2017**, *49*, 5238–5250; d) A. Böhm, T. Bach, *Synlett* **2016**, *27*, 1056–1060.

[54] T. Rigotti, A. Casado-Sánchez, S. Cabrera, R. Pérez-Ruiz, M. Liras, V. A. de La Peña O'Shea, J. Alemán, *ACS Catal.* **2018**, *8*, 5928–5940.

[55] D. Parmar, E. Sugiono, S. Raja, M. Rueping, *Chem. Rev.* **2014**, *114*, 9047–9153.

[56] a) M. R. Monaco, B. Poladura, M. Diaz de Los Bernardos, M. Leutzsch, R. Goddard, B. List, *Angew. Chem. Int. Ed.* **2014**, *53*, 7063–7067. For more recent photocatalytic work by the same group: b) S. Das, C. Zhu, D. Demirbas, E. Bill, C. K. De, B. List, *Science* **2023**, *379*, 494–499.

[57] F. Pecho, Y.-Q. Zou, J. Gramüller, T. Mori, S. M. Huber, A. Bauer, R. M. Gschwind, T. Bach, *Chem. Eur. J.* **2020**, *26*, 5190–5194.

[58] F. Pecho, Y. Sempere, J. Gramüller, F. M. Hörmann, R. M. Gschwind, T. Bach, *J. Am. Chem. Soc.* **2021**, *143*, 9350–9354.

[59] R. Takagi, C. Tabuchi, *Org. Biomol. Chem.* **2020**, *18*, 9261–9267.

[60] R. Takagi, T. Tanimoto, *Org. Biomol. Chem.* **2022**, *20*, 3940–3947.

[61] J. Lyu, A. Claraz, M. R. Vitale, C. Allain, G. Masson, *J. Org. Chem.* **2020**, *85*, 12843–12855.

[62] J. Lyu, M. Leone, A. Claraz, C. Allain, L. Neuville, G. Masson, *RSC Adv.* **2021**, *11*, 36663–36669.

[63] A. B. Rolka, N. Archipowa, R. J. Kutta, B. König, F. D. Toste, *J. Org. Chem.* **2023**, *88*, 6509–6522.

[64] D. Liang, J.-R. Chen, L.-P. Tan, Z.-W. He, W.-J. Xiao, *J. Am. Chem. Soc.* **2022**, *144*, 6040–6049.

[65] Q. Fu, S. Cao, J. Wang, X. Lv, H. Wang, X. Zhao, Z. Jiang, *J. Am. Chem. Soc.* **2024**, *146*, 8372–8380.

[66] M. Plaza, J. Großkopf, S. Breitenlechner, C. Bannwarth, T. Bach, *J. Am. Chem. Soc.* **2021**, *143*, 11209–11217.

[67] E. J. Corey, M. Tada, R. LaMahieu, L. Libit, *J. Am. Chem. Soc.* **1965**, *87*, 2051–2052.

[68] P. E. Eaton, K. Lin, *J. Am. Chem. Soc.* **1965**, *87*, 2052–2054.

[69] D. P. Schwinger, M. T. Peschel, C. Jaschke, C. Jandl, R. de Vivie-Riedle, T. Bach, *J. Org. Chem.* **2022**, *87*, 4838–4851.

[70] a) J. Y. Wang, E. Villalona, R. R. Knowles, *J. Am. Chem. Soc.* **2025**, *147*, 15307–15317; b) F. Zhong, R. Li, B. K. Mai, P. Liu, G. C. Fu, *Nature* **2025**, *640*, 107–113.

[71] M. Stierle, C. Jaschke, D. J. Grenda, M. T. Peschel, T. Pickl, N. Gessner, P. Nuernberger, B. P. Fingerhut, C. Ochsenfeld, R. de Vivie-Riedle, T. Bach, *Angew. Chem. Int. Ed.* **2025**, *64*, e202501433.

[72] M. Stierle, D. Bitterlich, J. Westermayr, T. Bach, *Chem. Sci.* **2025**, DOI: 10.1039/D5SC05356K.